

Multi-Axes CNC Turn-Mill-Hob Machining Center and Its Applications in Biomedical Engineering

CHEN, Xianshuai

A Thesis Submitted in Partial Fulfillment
of the Requirements for the Degree of
Doctor of Philosophy
in
Mechanical and Automation Engineering

The Chinese University of Hong Kong
September 2012

UMI Number: 3538901

All rights reserved

INFORMATION TO ALL USERS

The quality of this reproduction is dependent upon the quality of the copy submitted.

In the unlikely event that the author did not send a complete manuscript and there are missing pages, these will be noted. Also, if material had to be removed, a note will indicate the deletion.



UMI 3538901

Published by ProQuest LLC (2013). Copyright in the Dissertation held by the Author.

Microform Edition © ProQuest LLC.

All rights reserved. This work is protected against unauthorized copying under Title 17, United States Code



ProQuest LLC.
789 East Eisenhower Parkway
P.O. Box 1346
Ann Arbor, MI 48106 - 1346

Abstract

With the ever increasing demand for reduced size and increased complexity and accuracy, traditional machine tools have become ineffective for machining miniature components. A typical example is the dental implant and the other is the pinion used mechanical watch movement. With complex geometry and tight tolerance, few machine tools are capable of making these parts. We designed and built a CNC Turn-Mill-Hob Machining Center that is capable of machining various complex miniature parts. The machining center has 8 axes, an automatic bar feeder, an automatic part collection tray, and a custom-made CNC controller. In particular, the CNC controller gives not only higher accuracy but also ease of use. In addition, to improve the accuracy, a software based volumetric error compensation system is implemented. Based on the experiment testing, the machining error is $\pm 4 \mu\text{m}$ for turning, $\pm 7 \mu\text{m}$ for milling, and the maximum profile error is less than $\pm 7.5 \mu\text{m}$ for gear hobbing.

Many biomedical parts are axial asymmetric parts. While these parts can be machined using conventional CNC machining methods, the efficiency is low and the cost is high. We proposed a new CNC machining method based on polar coordinate interpolation, which is better than the Cartesian coordinate interpolation when rotational axes are involved. To facilitate the use the polar coordinate interpolation module, a special G code is developed. This module is integrated into our CNC Turn-Mill-Hob Machining Center.

Another important development is the use of hobbing method for machining axial symmetric / asymmetric parts. Invented some 100 years ago, hobbing is the most efficient method for machining gears. Its efficiency lies on multiple teeth simultaneous cutting. Presently, gear hobbing is a standard manufacturing process making millions of gears every day. Though, no one has used it for machining axial asymmetrical parts. After carefully examining the gear hobbing, it is found that the profile of the gear tooth is determined by a combination of the profile of the hob tooth and the relative position

and motion between the hob and the workpiece. Therefore, by tuning the hob tooth profile and controlling the relative position and motion between the hob and the workpiece, it is possible to machine various axial symmetrical and asymmetrical parts, such as a star, a hexagon and etc. This method is efficient to machine continuously changed axial asymmetrical parts. This is validated by means of experiments. The experiments also indicate that the new method is much more efficient than the conventional milling method.

Our machining center and new machining methods have many practical applications. Dental implant is a typical example. It is estimated that 10% of the people will need dental implants in their life time. Presently, there are a number of brands in the market, though these implants may not fit for patients who have special oral conditions. In this case, custom-made implants are necessary. The key problem of the custom-made dental implant is manufacturing. Our multi-axes CNC Turn-Mill-Hob Machining Center and the new machining method can effectively machine the custom-made dental implants. Moreover, the efficient is good.

摘 要

随着对减小零件尺寸和增加其复杂性和准确性的日益增加的需求，传统机床已经不能有效的加工微型元件了。一个典型的例子是牙科种植体（生物医学设备）和用于机械手表机芯的齿轮轴。由于这些零件的复杂几何形状和严格的公差要求，市面上只有很少一部分机床有能力加工它们。我们设计的多轴数控“车削-铣削-滚齿”加工中心对加工精密复杂工程零件是非常有效的。此机器为 8 轴机床，除了执行加工的 8 轴外，还有一个自动上料机构和一个自动收集机构，可以实现自动上料，加工，收集等整条生产线的运作。运用电子齿轮技术以保证精密滚齿功能；运用先进控制技术（深层交叉耦合技术）以保证多轴的同步控制，实现加工的高效，高精度，并且容易使用。另外，为了保障机床精度，我们研发了多轴数控机床几何误差的软件补偿技术。根据实验测试，此加工中心的车削精度为 0.003 毫米，铣削精度为 0.005 毫米，滚齿误差小于 0.0075 毫米。

众多的生物医学零件是轴不对称零件。虽然这些零件可以用传统的数控加工方法进行加工，但是效率极低且成本高。而基于我们加工中心的新型铣削方法可以有效、高精度的加工这些零件。这种方法是运用极坐标的插值原理，比利用笛卡尔直角坐标系加工的原理更加优越，特别是当需要一个线性轴和旋转轴插值生成曲线时。为了方便使用这个极坐标插值模块，我们开发了一系列特殊的极坐标加工 G 代码。整个开发的程序模块最终融入我们多轴数控“车削-铣削-滚齿”加工中心。

另外一个重要的发现是运用滚齿方法加工轴对称和轴不对称零件。从滚齿方法被发明出来的这 100 年中，其一直是最有效的加工齿轮的方式。它的高效是由于多个刀齿同时切削工件。现在，滚齿是一种标准的加工方式并且每天运用这种方法加工几百万个零件。但是，没有人用这种方法加工轴不对称零件。经过仔细研究滚齿原来，可以得出以下观点：一）齿轮的齿形是与滚刀的齿形一样的；

二) 齿轮轮廓是由工件和滚刀的相对位置确定的。把滚刀设计和控制工件和滚刀的相对位置结合起来，我们发现运用滚齿的方法是可以加工各种轴对称和非对称部分，例如：星形零件和多边形零件。特别是，该方法可以有效的加工不断变化的轴不对称零件。最后，我们比较其的加工效率和传统的铣削加工，结果验证运用这种方法的加工时间远小于采用铣削方法。

我们设计的加工中心和新型加工方法在生物医学工程有很多的应有。牙科种植体就是一个典型的例子。具权威机构统计，约有 10%的人会在一生中选用种植牙技术对牙齿进行修复。但是不幸的是，没有人研究个性化种植体。目前，市面上的种植体并不能精确的适合病人牙根情况，完成特殊口腔环境的牙齿修复。所以，对个性化种植体的研究是迫切并具有市场效益的。关于个性化种植体研制的一个难点是其的制造。个性化种植体之所以难加工是由于它的复杂形状及所用材料（钛）。但是，我们设计的多轴数控“车削-铣削-滚齿”加工中心和基于此机床的新型加工方法可以有效、高精度的加工此种植体。

Acknowledgement

First, I would like to express my sincere gratitude to my supervisor, Prof. Ruxu Du, for his great support and patient guidance through all these four years. From him I have learned a lot of knowledge, research methodology, and skills as well as positive attitude towards life, which are very helpful in my future career. I really appreciate him for giving me the opportunity to study in CUHK.

I also want to say thanks to other people who played vital roles in completing this thesis. Special thanks go to Prof. Charlie C. L. Wang, Prof. Hui, Kin-chuen and Prof. YH Chen who took the time to serve on my dissertation committee and provided insightful comments and ideas to further improve this dissertation.

I am grateful to all the people who have helped me through the process, especially Dr. Tom Kong, Mr. Chan Ngai Shing, Dr. Longhan Xie, Dr. Kai He and Dr. Yuanxin Luo for their encouragement and valuable advice thought the process. I wish to thank Dr. Peng Zhang for his suggestions on the mechanics model, Mr. Lei Man Cheong for FEA simulation results, Dr. Dailin Zhang for his help to develop the control system. I am also grateful to other colleagues at Institute of Precision Engineering, CUHK. I enjoy the study and life in IPE. I will treasure the wonderful time and the friendship forever.

Finally, with great love and respect, I would like to deeply appreciate the continuous and strong support from my family and my girlfriend, Miss Bai Yinghua.

The research presented in this thesis is partially supported by a direct grant from the Faculty of Engineering at the Chinese University of Hong Kong under the grant number 2050469, as well as a Major Project of the Science and Technology Ministry in China under the grant number is 2010ZX04014-052.

Table of Contents

Abstract	I
摘要	III
Acknowledgement	V
Table of Contents	VI
List of Tables	VIII
List of Figures	IX
Acronym	XIII
Chapter 1: Introduction	1
1.1 Background	1
1.2 Overall Literature Review	3
1.3 Objectives	17
Chapter 2: The Multi-Axes CNC Turn-Mill-Hob Machining Center	18
2.1 A Brief Review	18
2.2 The Design and Prototype	20
2.3 The CNC Controller	26
2.4 The Calibration	32
2.5 Cutting Tests	35
2.6 Summary	43
Chapter 3: Hobbing Gears and Axial Asymmetric Parts	45
3.1 A Brief Review	45
3.2 The Theory	47
3.3 Computer Simulation	54
3.4 Cutting Tests	68
3.5 Summary	78
Chapter 4: Millining Axial Asymmetric Parts	80
4.1 A Brief Review	80
4.2 The Theory	81
4.3 Cutting Tests	89
4.4 Summary	94
Chapter 5: Machining Dental Implants	95

5.1 A Brief Review	95
5.2 The Database of Custom-made Dental Implant	98
5.3 The Design and FEA	103
5.4 Cutting Tests	108
5.5 Summary	110
Chapter 6: Concluding Remarks and Future Work	111
6.1 Concluding Remarks	111
6.2 Future Work	113
Bibliography	116
Publication Record	127

List of Tables

- Table 2-1: Key design parameters of our CNC turn-mill machining center
- Table 2-2: Measurement results of the ten samples machined by the system
- Table 2-3: Measurement results of the ten samples machined by Deco 10a
- Table 2-4: Preliminary comparison of Deco 10a with our machining center
- Table 2-5: The measurement results of our machining pinion
- Table 2-6: The measurement results of our machining Ureteroscope part
- Table 3-1: The simulation procedure
- Table 3-2: The parameters for cutting an eccentric part
- Table 3-3: The parameters of cutting the elliptical section
- Table 3-4: The parameters of cutting the angular section
- Table 4-1: Measurement results of the machined Date Corrector Pinions
- Table 4-2: The comparison of our machining center and Deco10a in program module
- Table 5-1: A list of manufacturers of dental implants
- Table 5-2: The best-fit parameters in this case
- Table 5-3: The measurement results of our machining dental implant

List of Figures

- Figure 1-1: Dental implants and the pinion used mechanical watch movement
- Figure 1-2: The first palm-top micro-lathe
- Figure 1-3: Micro-lathe developed by Loffler
- Figure 1-4: Micro-lathe in a SEM chamber
- Figure 1-5: Micro machine tool prototype machined by E. Kussul
- Figure 1-6: Precision turning machine for machining flexible Polyamide composites
- Figure 1-7: NC milling machine
- Figure 1-8: Micro/Meso-scale machine tool
- Figure 1-9: 4-axes machine tool
- Figure 1-10: Micro-factory
- Figure 1-11: Miniature bearing assembly
- Figure 1-12: Some precision machine tool in market
- Figure 1-13: Gear with diameter of 5m made by gear hobbing
- Figure 1-14: Gear with diameter of 1.2 mm also machined by gear hobbing
- Figure 1-15: A traditional gear hobbing machine
- Figure 1-16: Working principle of a traditional gear hobbing machine
- Figure 1-17: Five-freedom hobbing machine
- Figure 1-18: 3D linear interpolation
- Figure 1-19: NCPP prototype
- Figure 2-1: Typical micro parts, their diameters are about 1 mm and requirement tolerance is 10 μm
- Figure 2-2: The CAD model of our CNC Turn-Mill-hob Machining Center
- Figure 2-3: The photo of our CNC Turn-Mill Machining Center
- Figure 2-4: Turning and hobbing function
- Figure 2-5: Milling and grinding function
- Figure 2-6: The turning operation
- Figure 2-7: The Hobbing part of the machine
- Figure 2-8: The milling and grinding operation
- Figure 2-9: Relative speed strategy of our machining center

- Figure 2-10: Cross coupling technology of our machining center
- Figure 2-11: Hardware Architecture of the control system
- Figure 2-12: Mitsubishi servomotor HF-KP23 and amplifier MR-J3-20A
- Figure 2-13: The photo of our machine control system
- Figure 2-14: Jog Motion and G code Interface
- Figure 2-15: The working principle of mechanically decoupled gear hobbing
- Figure 2-16: Synchronization error of the spindles
- Figure 2-17: The position accuracy of our machining center
- Figure 2-18: Minimum error for every sample point on hobbing
- Figure 2-19: Designation of dimension for the balance staff
- Figure 2-20: Balance staff samples machined by the system
- Figure 2-21: The drawing of Date Corrector Pinion
- Figure 2-22: The comparison between Deco 10a and our machine
- Figure 2-23: The hob from Swiss company Diametal
- Figure 2-24: The drawing of reduction pinion
- Figure 2-25: The magnified reduction pinion sample machined by our machine
- Figure 2-26: The drawing and samples of Ureteroscope part
- Figure 3-1: Two typical dental implants
- Figure 3-2: Illustration of a gear hob
- Figure 3-3: The gear hobbing process
- Figure 3-4: The coordinate systems in the hobbing process
- Figure 3-5: The process of hobbing an axial asymmetric part
- Figure 3-6: The cutter path when hobbing a gear
- Figure 3-7: Illustration of hobbing an asymmetric part
- Figure 3-8: The cutter path when changing the synchronization ratio
- Figure 3-9: The tool path when changing the helix angle
- Figure 3-10: The hob used in the simulation
- Figure 3-11: Extracted cutter profile in MATLAB
- Figure 3-12: Illustration of the hobbing process
- Figure 3-13: Simulation result of Case 1
- Figure 3-14: Zoom up views of the simulated gear profile

- Figure 3-15: Some polygon parts
- Figure 3-16: An eccentric part
- Figure 3-17: Simulation result of Case 2
- Figure 3-18: A continuously changing axial asymmetric part
- Figure 3-19: Simulation of cutting the elliptic section
- Figure 3-20: Simulation of cutting the angular section
- Figure 3-21: Simulation result of Case 3
- Figure 3-22: 3D Simulation result of master gear
- Figure 3-23: Simulation process of eccentric part
- Figure 3-24: The magnified sample gear machined by our machine
- Figure 3-25: Comparison between the machined profile and the design profile
- Figure 3-26: The machined profile enclosed by the error $\pm 7.5 \mu\text{m}$ bound
- Figure 3-27: The CAD model of Case 2
- Figure 3-28: The tool path of part
- Figure 3-29: A sample experiment result
- Figure 3-30: The CMM measurement result
- Figure 3-31: The comparison in 2D
- Figure 3-32: The CAD model of the elliptical part
- Figure 3-33: The tool path of the part
- Figure 3-34: A sample experiment result
- Figure 3-35: The CMM measurement result
- Figure 3-36: The comparison in 2D
- Figure 3-37: The CAD model of the part
- Figure 3-38: The tool path of the part
- Figure 3-39: An experiment result
- Figure 3-40: The CMM measurement of the part
- Figure 3-41: The comparison in 2D
- Figure 4-1: The difference between using Polar coordinate interpolation and Cartesian coordinate interpolation to machine parts
- Figure 4-2: Architecture of motion control table for milling and grinding
- Figure 4-3: The circular interpolation principle

- Figure 4-4: The linear interpolation principle
- Figure 4-5: Hardware Architecture of the control system
- Figure 4-6: The drawing of the Date Corrector Pinion
- Figure 4-7: Simulation result
- Figure 4-8: The milling operation
- Figure 4-9: The machined Date Corrector Pinions
- Figure 5-1: Drilling hole in patient's alveolar bone
- Figure 5-2: The design and production process
- Figure 5-3: The parameters of implant
- Figure 5-4: Parameter optimization
- Figure 5-5: Feature-based design of dental implant
- Figure 5-6: The database of custom-made dental implant
- Figure 5-7: One example of 'best-fit' condition
- Figure 5-8: Dual-tread design
- Figure 5-9: The plastic model
- Figure 5-10: The 3D drawing of this custom-made dental implant
- Figure 5-11: The model of FEA
- Figure 5-12: The material properties and boundary conditions
- Figure 5-13: $\theta = 0$, Max. Equivalent Stress = 93.999MPa
- Figure 5-14: $\theta = 0$, Max. Total Deformation = 0.0060133mm
- Figure 5-15: $\theta = 15^\circ$, Max. Equivalent Stress = 341.85MPa
- Figure 5-16: $\theta = 15^\circ$, Max. Total Deformation = 0.061912mm
- Figure 5-17: The RP prototype
- Figure 5-18: Machined sample by using our machining center
- Figure 5-19: Machined sample by SLM
- Figure 6-1: The CAD drawing of the new machining center
- Figure 6-2: The design of main spindle and sub-spindle

Acronym

CAD	computer-aided design
CAM	computer-aided manufacturing
CNC	computer numerical controlled
CST	constant strain triangular
FEA	finite element analysis
FEM	finite element modeling
NC	numerical control
PC	personal computer
PLC	programmable logic controller
SPM	stroke per minute
3D	three dimensional
MMR	material removal rate
NCPP	numerical control program processor
RP	rapid prototyping
DDA	digital differential analyzer

Chapter 1:

Introduction

1.1 Background

With the ever increasing demand for reduced sizes and increased complexity and accuracy, traditional machine tools have become ineffective for machining miniature components. A typical example is dental implant (Biomedical equipment) and the other is the pinions used mechanical watch movement, as shown in Figure 1-1. With complex geometry and tight tolerance, few machine tools are capable of making them.



Fig. 1-1: Dental implants and the pinion used mechanical watch movement

The thesis describes the works I have done as one of the members of the manufacturing team of IPE during the four-year period from September 2008 to July 2012. As opposed to a conventional thesis in which a particular problem is studied intensively to order to derive new algorithms or methods in solving the problem, the nature of this thesis is different. Instead of focusing on a very specific scientific or mathematical problem, this thesis is project-oriented in which the ultimate goal is to consolidate a series of technical knowledge gained in the process of designing, building and using Multi-Axes CNC Turn-Mill-Hob Machining Center. This thesis describes some methods for hobbing and machining axial asymmetric parts, especially in Biomedical Engineering. It is also the intention that this thesis will serve as a recipe for the engineer should he/she would like to replicate the system or to develop other similar precision machining systems.

Although the readers of this thesis are encouraged to read the chapters in the order they are organized as this provides the most synergy, the chapters can still be read independently with good understanding. The following paragraphs briefly describe the main contributions of each chapter.

The rest of this introductory chapter presents background information, overall literature review and our objectives which prepare the readers for the core of this thesis. The overall literature review of the presented research will first be explained to the readers followed by a brief introduction on the traditional precision machines and how to machining complex parts.

Chapter 2 presents the actual development of the hardware and software of Multi-Axes CNC Turn-Mill-Hob Machining Center. Details such as the actual design, control system, choices of components, operation parameters, calibration accuracy and unique features are presented to the readers. Also, the performance of the system is compared to a commercially available system in terms of cutting accuracy. Turning experiment, milling experiment and gear hobbing experiments are also conducted and results are provided.

Chapter 3 will present a study on the mechanics of gear hobbing as a diagnostic tool to increase the profile accuracy of the gears machined by Multi-Axes CNC Turn-Mill-Hob Machining Center. Detail such as the hobbing theory (including hobbing gear and non-gear profile), key parameters analysis and actual hobbing simulation are provided. In particular, the hobbing process is investigated by means of computer simulation. Realistic manufacture situations are considered in which process defects are taken into account and the simulated profiles are also studied to observe the effects of the process defects. Also, some typical experiments results, which are including hobbing axial symmetric parts and asymmetric parts, are provided.

Chapter 4 presents the method for milling axial asymmetric parts. Based on the basic interpolation principles, the polar coordinate interpolation module is developed and then based on the module; the special G codes are developed to facilitate the polar coordinate programming. The developed programming module is finally integrated into the programming system of our Multi-Axes CNC Turn-Mill-Hob Machining Center. Details such as the special algorithm, simulation and experiments results are provided.

Chapter 5 shows the design and machining of custom-made dental implants. With the ever increasing demand for tight tolerance, complexity, and accuracy, traditional machine tools have become ineffective for machining these parts. But, the presented Multi-Axes CNC Turn-Mill-Hob Machining Center can machine this implants accurately and efficiently. Details such as the custom-made design of dental implants, FEA analysis and automatic machining samples are provided.

Finally, Chapter 6 contains the conclusions and the future work.

1.2 Overall Literature Review

1.2.1 Literature review of precision machining tool

The idea of using small machine tools to manufacture miniature parts have been exploited recently by researchers and this section presents the works of these researchers. The first realization of a MMT dated back to 1996 where Okazaki and Kitahara of Mechanical Engineering Laboratory of Kanazawa University developed the famous palm-top machine tool as a component of a micro-factory [1]. With a weight of merely 100 g, the footprint of this micro-lathe is 32 x 28 x 30 mm and Figure 1-2 is a photo of the micro-lathe [2].



Fig. 1-2: The first palm-top micro-lathe [2]

The main spindle of the micro-lathe is driven by a small 1.5W DC motor and the linear stages are driven by two sets of embedded PZT actuators. Although this micro-lathe is capable of machining brass material to very small diameter such as $50\ \mu\text{m}$ with fine surface finish such as $0.5\ \mu\text{m } R_y$ and $60\ \text{nm } R_a$, this micro-lathe is not applicable in real manufacturing environment as it lacks chip handling, tool change and machine throughput capability.

In 1998, Lu and Yoneyama [3] also developed a micro-lathe measuring 200 mm in length and investigated cutting forces during cutting with a single point diamond tool. Using a 15000 RPM, they successfully turned $300\ \mu\text{m}$ brass wires to $10\ \mu\text{m}$ in diameter with a surface roughness of $R_{max} = 1\ \mu\text{m}$. Besides from simple turning, they also attempted other kinds of operations such as contour cutting, micro-grooving, micro-boring and micro-threading with their MMT. However, the adoption of the MMT to real manufacturing environment is still a distance away.

More Japanese researchers followed the trend in building miniaturized machine tools. For example, Ito in [4] described another micro-lathe with machine base size of 150 x 100 mm with similar specifications and performances to the one developed by Lu and Yoneyama. Loffler developed another micro-lathe that is small enough to be used in the chamber of a scanning electron microscope (SEM) to investigate micro cutting process

in vacuum condition [5]. Figure 1-3 is a photo of the developed micro-lathe by Loffler and Figure 1-4 shows the machine itself in a Visitec SEM chamber.

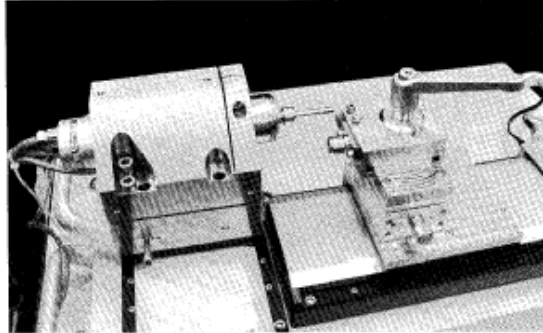


Fig. 1-3: Micro-lathe developed by Loffler [5]

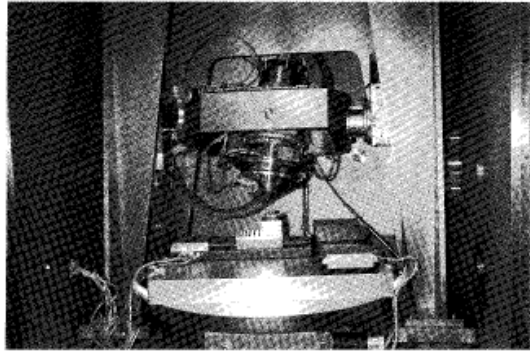


Fig. 1-4: Micro-lathe in a SEM chamber [5]

Also, Bae *et al.* in [6] carried out high aspect ratio turning with aluminum on their micro-lathe and in particular, a part with diameter of 65 μm and length of 1 mm was turned.

In [7][8], Kussul, Baidyk, Ruiz-Huerta and Caballero-Ruiz took a more theoretical approach in developing and analyzing micro machine tool. In particular, he suggested that sources of error such as thermal expansion and vibration of a machine tool decrease at least linearly with its size and it is beneficial to decrease machine tool sizes down to sizes comparable to the workpieces. The MMT developed measures 130 x 160 x 85 mm in size and its photo is shown in Figure 1-5. The tool rack can accommodate multiple turning tools.

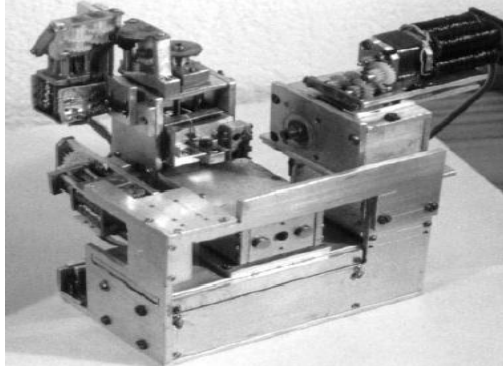


Fig. 1-5: Micro machine tool prototype machined by E. Kussul

In recently years, Davim [9] developed a precision turning machine, which can machine flexible Polyamide composites, as shown in Figure 1-6.

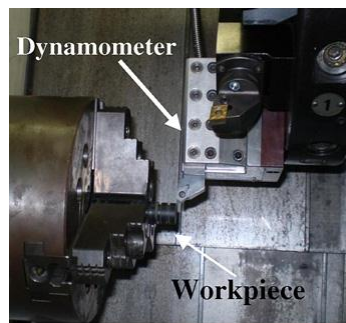


Fig. 1-6: Precision turning machine for machining flexible Polyamide composites

Besides from micro-lathes, several researchers also attempted to build micro-milling machines. The first realization of micro milling machine is done by Okazaki in 2000 [10]. It is called NC milling machine, as shown in Figure 1-7.



Fig. 1-7: The NC milling machine made by Okazaki [10]

In 2003, Vogler built Micro/Meso-scale machine tool with high position accuracy [11], as shown in Figure 1-8.

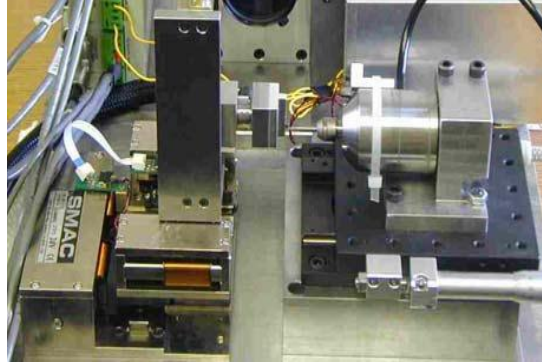


Fig. 1-8: The Micro/Meso-scale machine tool made by Vogler [11]

Kurita in [12] reported their efforts in building a miniaturized machine tool with hybrid capabilities. Their machine is capable of performing various machining operations such as milling, EDM and ECM. Also, this hybrid machine is highly modularized; for example, a milling spindle can be installed on the machined to machine a workpiece of certain geometry and this resulting workpiece itself can be used as the electrode when the machine is operating in EDM or ECM mode. However, Kurita did not focused on obtaining very accurate or very smooth surface of the resulting workpieces as the purpose of the research was to develop energy efficient and environmental friendly machine tools.

Takeuchi *et al.* in [13][14] reported their efforts in developing an ultra-precise 5-axes milling machine. In particular, they employed aerostatic technology onto the linear bearings and leadscrews of the machine tools such that no Coulomb friction existed within the machine tool itself. They performed experiments using high speed air turbine spindle and diamond milling tool to machine tiny 3-dimensional workpieces and microstructures.

In recently year, Axinte built a micro milling machine. It has 4 axes, and the accuracy is within $1\ \mu\text{m}$ [15]. The 3D model of this machine is shown in Figure 1-9.

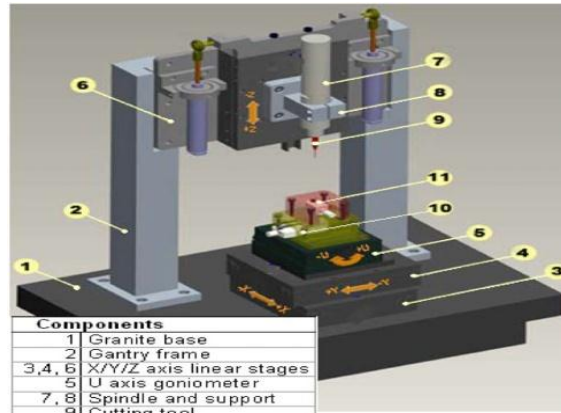


Fig. 1-9: 4-axes machine tool [15]

Besides from individual machine tools, researchers also consider the integration of multiple machine tools to form a miniaturized production system known as a “micro-factory.” In his technical brief, Okazaki [16] presented a survey on the field of micro-factory and micro machine tools around the world. In particular, in one of Okazaki’s referenced literatures, Tanaka and *et al.* [17][18][19][20] developed a micro-factory prototype which consists of a micro milling machine, a micro-lathe, a micro press, a micro transfer arm and a two-fingered manipulator. Figure 1-10 is a photo of Tanaka’s microfactory. Furthermore, as a trial product, his microfactory was used to fabricate a miniature ball bearing assembly with a 0.9 mm outside diameter and 3 mm shaft length. Figure 1-11 shows the individually fabricated parts and the assembled product.

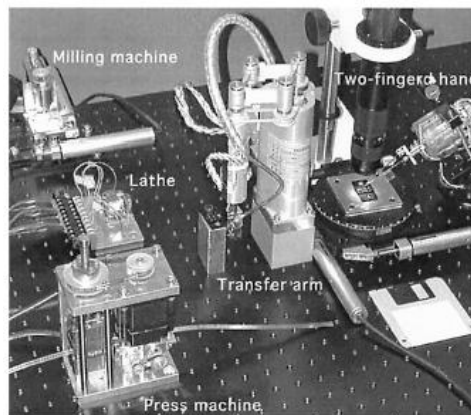


Fig. 1-10: Micro-factory [17]

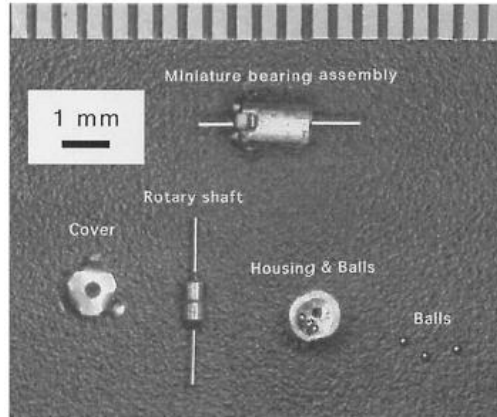


Fig. 1-11: Miniature bearing assembly [17]

Similarly, Ehman *et al.* in [21] supported the use of meso-scale machine tools to manufacture complex 3D mechanical microstructures as an alternative to conventional macro-scale ultra-precision CNC machine tools. It is also suggested that meso-scale manufacturing is facing scientific, technological and commercialization barriers [22][11]. Ishikawa in [23] also argued that meso or micro-sized machine tools are facing problems such as accuracy, nano-scale effects and limited applications.

Besides from developing miniaturized machine tools and factories, researchers also focused on issues such as the micro-machining process, control algorithms and stage designs as attempts in further improve the accuracy of the miniaturized machine tools and factories. Masuzawa in [24] provided a survey on the state of the art of micromachining from a general perspective. He introduced processes such as micro-EDM, micro LBM (laser beam machining), micro-USM (ultrasonic machining), LIGA, micro-ECM, micro-grinding, micro-punching, micro-molding and micro-casting with great details.

In commercial market, there are a number of companies have the ability to make multi-function machine tools for precision engineering. Some precision machine tools show in Figure 1-12 [25] [26] [27].



Koepfer MZ120 [25]



Tornos Deco 20a [26]



Mazak 6100 [27]

Fig. 1-12: Some precision machine tool in market

Based on our investigation, it is believed that the major challenges of micro or meso-scale machines are as follows:

- a) The need of application: while many micro or meso-scale machine tools are being developed, few have been used in the industry. So far, there have been few applications that can only be handled by these machines but not the conventional precision machines.
- b) The lack of functionality: Most laboratory machines are single-function machine. For example, none of the existing micro or meso-scale machine tools can conduct gear hobbing.
- c) The need of automation: Most of the existing micro or meso-scale machines, if not all, lack basic automation features, such as automatic workpiece loading, automatic tool changer and alignment features. This limitation makes them impractical for adoption in industry.
- d) The need for Biomedical Engineering: no one research on design and built a professional machine tool for machining biomedical parts.

1.2.2 Literature review of machining methods

With the ever increasing demand for reduced sizes and increased complexity and accuracy, traditional machining method has become ineffective for machining miniature components. A typical example is dental implant (Biomedical equipment) and the other is the pinions used mechanical watch movement. The following are some investigation of traditional gear hobbing method and milling method.

It is known that gears can be manufactured using a wide variety methods such as milling, hobbing, grinding, broaching, shaping and forming just a name a few. Among all of these methods, gear hobbing is the most preferred by the industry because of its continuous nature and efficiency. Also, gear hobbing can be deployed in very diverse applications in terms of size; as shown in Figure 1-13 [28] and Figure 1-14, a large gear as tall as 5 meters and a miniature watch gear as small as 1.2 mm can both be machined using gear hobbing given the appropriate cutter tool. Furthermore, by adjusting the appropriate process parameters, spur gears and non-circular gears can be machined using gear hobbing.



Fig. 1-13: Gear with diameter of 5m made by gear hobbing [28]

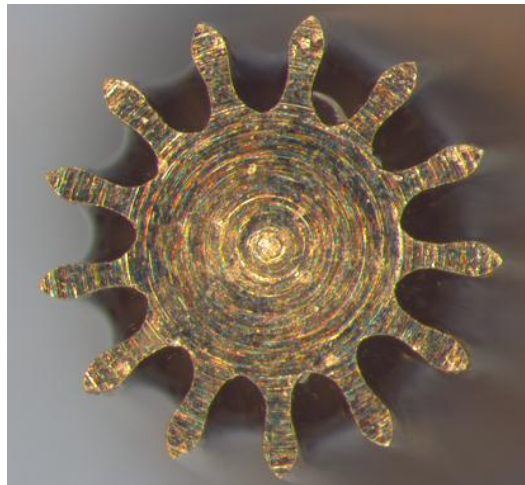


Fig. 1-14: Gear with diameter of 1.2 mm also machined by gear hobbing

Figure 1-15 [29] is a typical traditional gear hobbing machining and its working principle of is shown in Figure 1-16 [30][31]. The main spindle motor of the machine

will be directly coupled to the tool spindle, providing rotational motion and torque for the cutter hob. The main spindle motor will also simultaneously drive the workpiece axis through a gear train that realizes speed reduction. Therefore, the workpiece spindle and the tool spindle are mechanically synchronized by the gear train and the synchronization ratio is the gear reduction ratio of the gear train.



Fig. 1-15: A traditional gear hobbing machine [29]

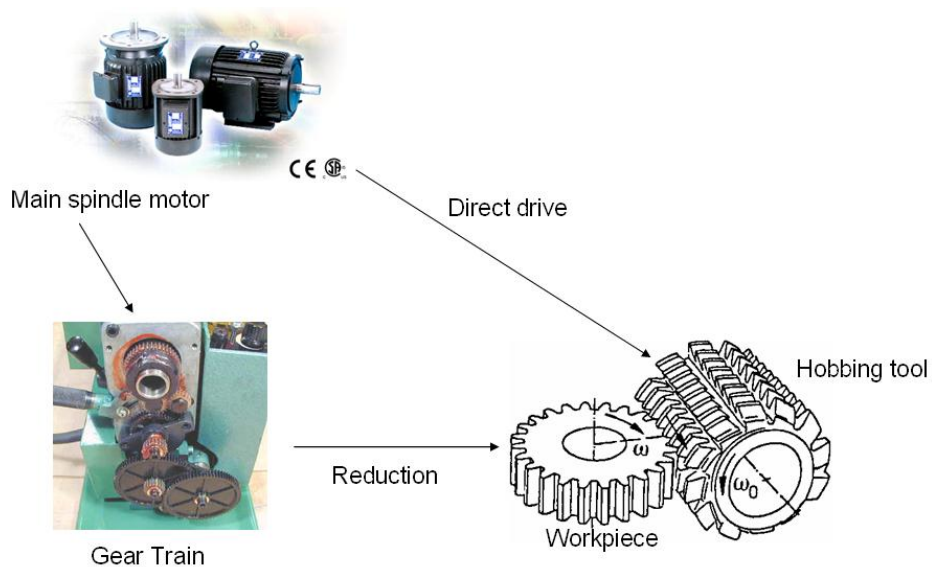


Fig. 1-16: Working principle of a traditional gear hobbing machine [30][31]

In recently years, Claudin and Rech [32] built a new hobbing machine, as shown in Figure 1-17. It can achieve 5 DOF hobbing, and it is also relied on the traditional gear hobbing method.



Fig. 1-17: Five-freedom hobbing machine [32]

There are several advantages for traditional gear hobbing machine. First, as the workpiece and the tool spindle are mechanically linked, the synchronization is deterministic if the tolerance of the gear train is known. Also, traditional gear hobbing machine is an open-loop system in which the main spindle motor needs not to be controlled under any circumstances, thus simplifying the design of electronics. Furthermore, as traditional gear hobbing machine is only capable of executing simple feeding motion, the process of hobbing planar gears becomes very efficient.

Although traditional gear hobbing machine has its advantages in manufacturing simple planar gears, there are limitations of the machine that make it not extensively applicable the field of precision engineering and watch components manufacturing. The first problem of traditional gear hobbing machine is the inflexibility of the synchronization ratio. Although deterministic synchronization between the tool and workpiece spindle is achieved by the reduction gear train, a change in the synchronization ratio will require the entire gear train to be replaced; thus posing inconvenience and extra setup time on the shop floor. Also, in order to achieve rotational synchronization and the relative linear feeding motion between the workpiece and tool spindle, the mechanical design of traditional gear hobbing machine is rather complex and involves a multitude of

mechanical components. Therefore, the machine itself will be more vulnerable for manufacture errors and it is only reasonable that these errors will appear in the components made by the machine. Finally, traditional gear hobbing machine is not capable of machining non-planar gears or gears with any 3-D features. In order to machine gears with 3-D features, the raw material must first be turned to the required diameters and then transferred to the gear hobbing machine where special fixtures are used to hold the part during gear hobbing. If the fixture is not accurate enough, the transfer of the part will likely cause excessive concentricity error on the resulting gear profile.

Examining the cause of inefficiency of the existing technologies, it is found that the main reason is the use of small tools chipping off materials a bit at a time. This is necessary since the curvatures of the part could be small and hence, large tools cannot get in. To solve this problem, the proposed idea is to use large multiple teeth tools similar to gear hobbing together with CNC technology.

Another important method for machining complex parts is micro milling. Now, many machines use the Cartesian coordinate to machine parts. Only a few machines use the polar coordinate to machine parts. But, the interpolation in polar coordinate is better than in Cartesian coordinate when a linear axis and a rotational axis are interpolated to generate curves.

Qiu, Cheng and Li researched on interpolation for micro milling [33]. They presented a new algorithm of circular arc interpolation for planar curves. It is based on the principle of minimax approximation. This method uses the Cartesian coordinate for interpolation.

In 2000, Min-Yang Yang built a PC-NC milling machine. And in his machine, he used the Cartesian coordinate to achieve 3D linear interpolation, as shown in Figure 1-18. [34]

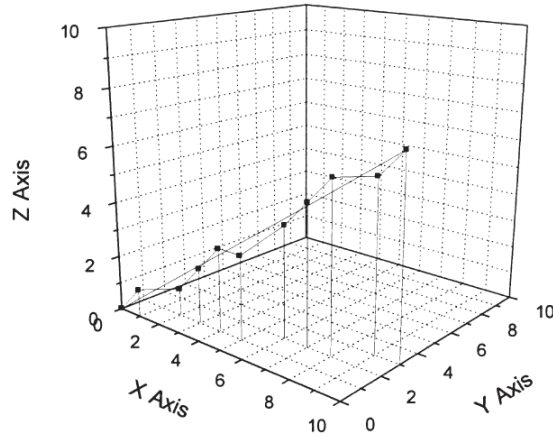


Fig. 1-18: 3D linear interpolation [34]

In last year, Guo developed a universal NC program processor for CNC systems [35]. This system is mainly for milling parts by used the Cartesian coordinate. Figure 1-19 shows his NCPP (NC program processor) prototype.

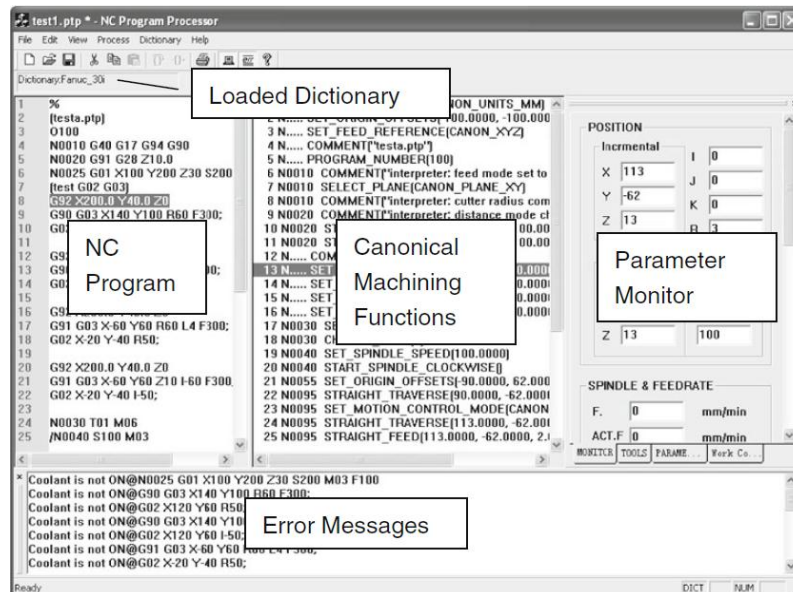


Fig. 1-19: NCPP prototype [36]

Young Joon Ahn presents a method for G^2 end-point interpolation of offset curves using rational Bézier curves [36]. The method is based on a G^2 end-point interpolation of circular arcs using quadratic Bézier curves.

Based on our investigation, it is believed that the major challenges of machining method are as follows:

- a) The need of machining method: With the ever increasing demand for reduced sizes and increased complexity and accuracy, traditional machining method has become ineffective for machining miniature components, no matter hobbing method or milling method.
- b) The limitation of hobbing method: traditional gear hobbing method is not extensively applicable the field of precision engineering and biomedical engineering manufacturing.
- c) The limitation of milling method: traditional milling method uses Cartesian coordinate to machine parts. But now, it is not capable of machining precise axial asymmetric parts. For example, when a linear axis and a rotational axis are interpolated to generate curves.
- d) The need for developing new machining method: now, no one research on developing new machining method, especially, using hobbing method to machine axial symmetric and asymmetric part, except gear. Hobbing is the most efficient method lies on multiple teeth simultaneous cutting.

1.3 Objectives

The objectives of this thesis include:

- Design and built a Multi-Axes CNC Turn-Mill-Hob Machining Center for machining complex parts. The machining center shall
 - Be capable of turning, milling, grinding, gear hobbing and conducting other precision machining operations
 - Have high precision
 - Be cost effective
 - Be capable of adopting new methods to machine various complex parts
- Develop efficient methods for machining symmetric / asymmetric parts. These include

- Using hobbing method to machine symmetric / asymmetric parts
- Using polar coordinate interpolation method to machine asymmetric parts

Chapter 2:

The Multi-Axes CNC Turn-Mill-Hob Machining Center

2.1 A Brief Review

Machining is one of the oldest and yet most commonly used manufacturing processes. As a result, much research has been done and the basic theory of machining is well established, including metal cutting principles [37], machine tool dynamics [38], tool path generation [39], high speed machining and etc. Machining precision miniature parts is however still a challenge. For complex precision miniature parts, such as the dental implants, gears rack used in camera focusing system, as well as gears and pinions used in mechanical watch movements, few machine tools are capable of making them.

It is generally believed that smaller machine tools would be effective for machining miniature parts. In recently years, the so-called micro factory has become a hot research topic [40][41][42]. The idea of micro machine tool may be traced back to 1970s [43]. But the first realization was not found until 1996 in Japan [44]. In 2000, Okazaki and Kitahara built a micro-lathe measured 32 mm in length [45]. Though, it suffered from poor accuracy and limited shape generation capability. Lu and Yoneyama [46] developed a micro-lathe measuring 200 mm in length and successfully turned a 300 μm brass wire to 10 μm in diameter using diamond tools, but it has no other functions, such as CNC. Entering the 21st century, with the rapid advance of precision control technology, building a micro machine tool becomes much easier. Loffler [5] developed micro lathe that is small enough to be used in the chamber of a Scanning Electron Microscope (SEM) to investigate micro cutting process in vacuum condition. Sun, Liang and Du [47] developed a high speed micro lathe with its own CNC software. It can cut 3D sculptures on a bar of 2 mm in diameter. Vogler and et al [11] developed a meso-scale Machine Tool, called mMT. More recently, Davim and et al developed a precision turning machine and used it to machining flexible polyamide composites [48]. Axinte and et al built a 4-axes machine tool, which reached the accuracy about 1 μm [15].

Mecombera and et al worked on the micro milling [49]. These machine tools however are not meant for practical manufacturing. They have limited functions and can only make simple parts as tool changer; automatic workpiece loading / unloading, as well as side / end milling capability are not available.

In practice, miniature parts from the industry are complex. Figure 2-1 shows a number of sample micro parts, including dental implants, a camera gear rack, and a couple of parts used in mechanical watch movements. These parts are approximately 1 ~ 3 mm in diameter and the required tolerances are less 10 μ m. Moreover, they require multiple cutting steps and special functions such as gear hobbing. Because of the shapes of these parts, other processes, such as chemical milling and MEMS lithography, are imperative.



Fig. 2-1: Typical micro parts, their diameters are about 1 mm and required tolerance is about 10 μ m

According to market survey, there are a number of machine tools capable of machining these parts. An example is the Swiss made Tornos DECO machine tool [26]. It is effective in machining complex micro parts with high accuracy. Though, it is rather expensive costing approximately US\$250,000. Moreover, it is evolved from the Swiss lathe relying on mechanical means to set up. As a result, changing a part may require changing the gear train of the machine.

From the brief review above, it is seen that there are still many unsolved problems in micro machining. This motivates us to design and build a low cost precision CNC turning milling machining center with gear hobbing capability.

2.2 The Design and Prototype

This section presents the development of the hardware as well as the testing results of the proposed Multi-Axes CNC Turn-Mill-Hob Machining Center. The readers are reminded that the major qualitative requirements for the system are as follows:

1. Capable of high speed turning, milling, grinding, gear hobbing and manufacturing complex precision components.
2. Accurate and precise.
3. Comparable to similar commercially available machine tools in terms of performance.
4. Cost effective.

It should be noted to the readers that the reason for stating the requirements qualitatively is to account for project agility. For example, a particular number is not associated to the term accurate and precise which could have been easily done. However, simply by stating the required accuracy of the center to be either $\pm 1 \mu\text{m}$, $\pm 0.1 \mu\text{m}$ or even the accuracy required by mechanical watch components would be meaningless if the resources available for development are not taken into account. On the other hand, stating a required accuracy that is too loose would make the system incapable. Therefore, the strategy is to swiftly establish a system prototype and measure its limiting capabilities. By measuring how far the status of the system is from the ultimate goal, that is, to manufacture mechanical watch components and biomedical parts, appropriate upgrades to the system can be done. This process is iteratively performed until the required mechanical watch components and biomedical parts can be manufactured by the system with close tolerances.

Our Multi-Axes CNC Turn-Mill-Hob Machining Center is very effective for machining miniature precision engineering components, such as the bending head of the ureteroscope, pinion of the mechanical watch movement and dental implant. The machine has 8 axes, an automatic bar feeder, an automatic part collection tray. It can do turning, milling, gear hobbing and other precision machining operations.

2.2.1 Specifications of the Machining Center

The CAD model of our Multi-Axes CNC Turn-Mill Machining Center is shown in Figure 2-1. It has three spindles: W_1 , W_2 , W_3 , and five axes: Z_1 , X_2 , Y_2 , X_3 , Z_3 , as well as an auxiliary axis θ (for setting the gear hob). The overall dimension of the machine is $480 \times 580 \times 1500$ (L \times W \times H) mm and the work volume is $100 \times 100 \times 100$ (L \times W \times H) mm. The key design parameters of the machine are listed in Table 2-1. The main spindle (W_1) is equipped with a guide bush and hence, can automatically feed the workpiece. The angular position accuracy of the main spindle (W_1) and the 2nd spindle (W_2) is 0.036 degrees when the resolution of the encoder is 10,000 counts per revolution. The angular position accuracy of the 3rd spindle (W_3) is 0.03 degrees when the resolution of the encoder is 10,000 counts per revolution. The position resolution of the tables is 1 μ m. The tables sit on a marble base for low thermal expansion. The photo of the machine is shown in Figure 2- 3.

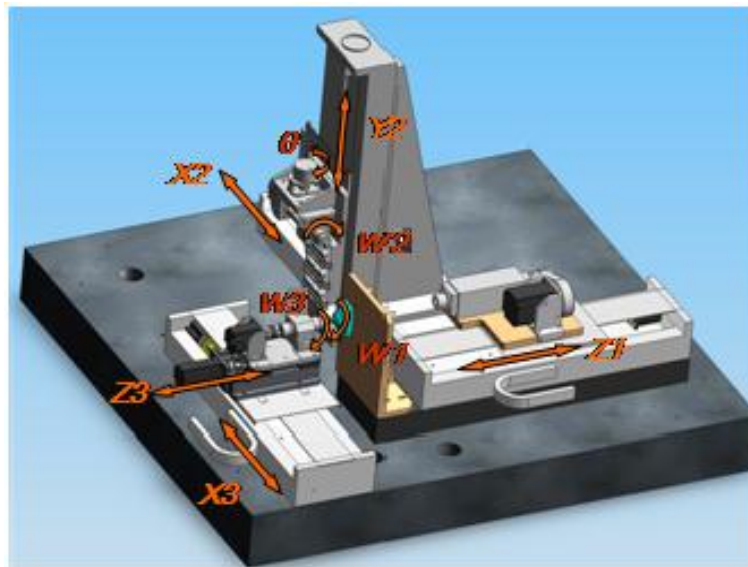


Fig. 2-2: The CAD model of our CNC Turn-Mill-hob Machining Center

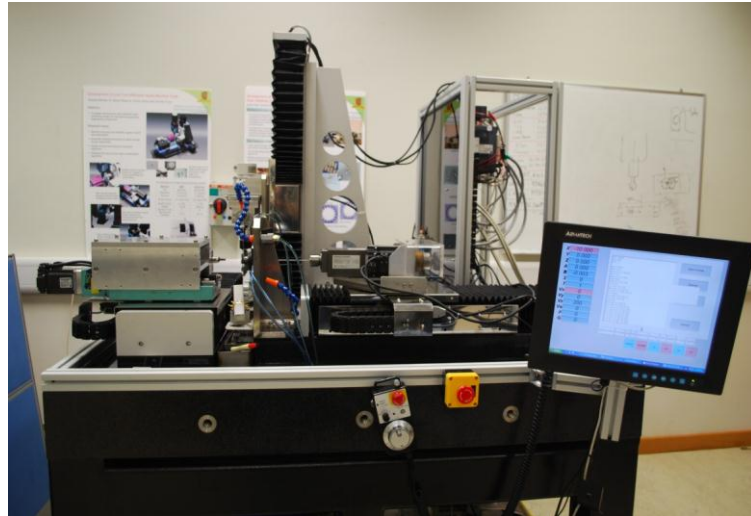


Fig. 2-3: The photo of our CNC Turn-Mill Machining Center

Table 2-1: Key design parameters of our CNC turn-mill machining center

Name	Parameters	Value
Main spindle (W_1)	Power	0.75KW
	Speed	10 ~ 10,000 RPM
	Maximum workpiece diameter	10 mm
2 nd spindle (W_2)	Power	0.2 KW
	Speed	10 ~ 6,000 RPM
	Maximum workpiece diameter	10 mm
3 rd spindle (W_3)	Power	0.4 KW
	Speed	10 ~ 12,000 RPM
	Maximum workpiece diameter	10 mm
1 st table travel	Z_1	600 mm
2 nd table travel	X_2	400 mm
	Y_2	400 mm
3 rd table travel	X_3	400 mm
	Z_3	200 mm

2.2.2 Overall Configuration*

From the function point of view, the machine can be divided into two parts: one for turning and gear hobbing as shown in Figure 2-4, and the other for milling and grinding as shown in Figure 2-5.

(* In this section, I wish to thank Dr. Dailin Zhang and Mr. Chan Ngai Shing, because they built the mechanism for turning and hobbing function, which is shown in Figure 2-4. And based on this design, I built mechanism for milling and grinding function and developed the control system.)

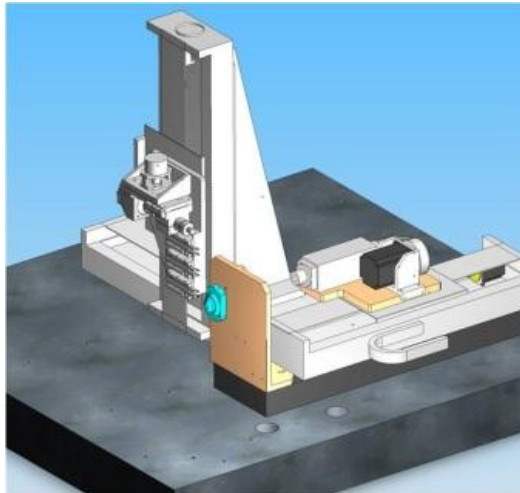


Fig. 2-4: Turning and hobbing function

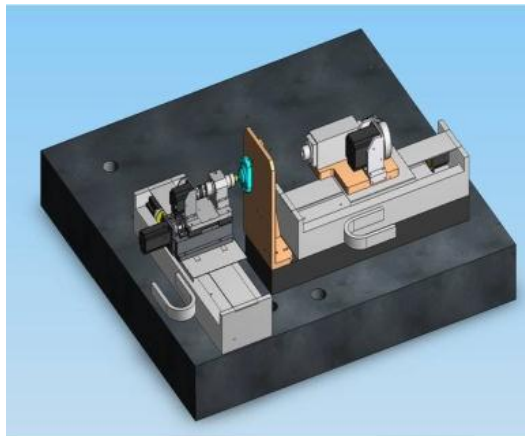


Fig. 2-5: Milling and grinding function

Turning

The turning operation is shown in Figure 2-6. The turning tool rack can accommodate up to five turning tools and the tool change is done by aligning the 2nd table, X_2 and Y_2 , and the workpiece table, Z_1 . The gap between the tools is 12 mm and therefore, can accommodate 8 mm or 10 mm tool holders. In particular, we use 710 and 740 series of Applitec turning tools [50].



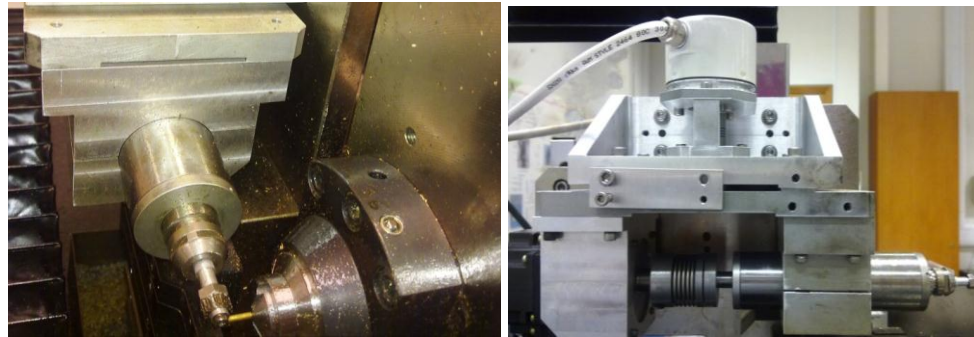
Fig. 2-6: The turning operation

Hobbing

Invented some 100 years ago, gear hobbing is very efficient for gear production [51]. The gear hobbing principle is as follows: as the hob rotates, the so-called basic rack is generated. Furthermore, with a synchronized workpiece motion, the gear profile is produced. Thus, from geometric point of view, it is the relative motion between the gear hob and the workpiece generates the gear profile as the image of the gear hob. Note that at any time, a number of teeth of the hob are engaged in the cut making the operation very efficient.

Gear hobbing is done through the 2nd spindle, as shown in Figure 2-7(a). Hobbing is a rather complicated process in which the gear teeth are formed by a series of synchronized engagement between the workpiece and the hob. The key parameter of hobbing is helix pitch, because there is the angle between hob axes and workpiece axes [52]. So, we use encoder to make a mechanism for controlling hobbing angle, as shown in Figure 2-7(b). In practice gear hobs can be purchased from a number of companies,

such as Diametal [53].



(a) The hobbing operation

(b) The angle control mechanism

Fig. 2-7: The Hobbing part of the machine

Milling and Grinding

The milling and grinding function is done through the 3rd spindle, as shown in Figure 2-8. In order to achieve higher accuracy, the motions of the 3rd table and the 1st table can be synchronized with linear and circular interpolation.

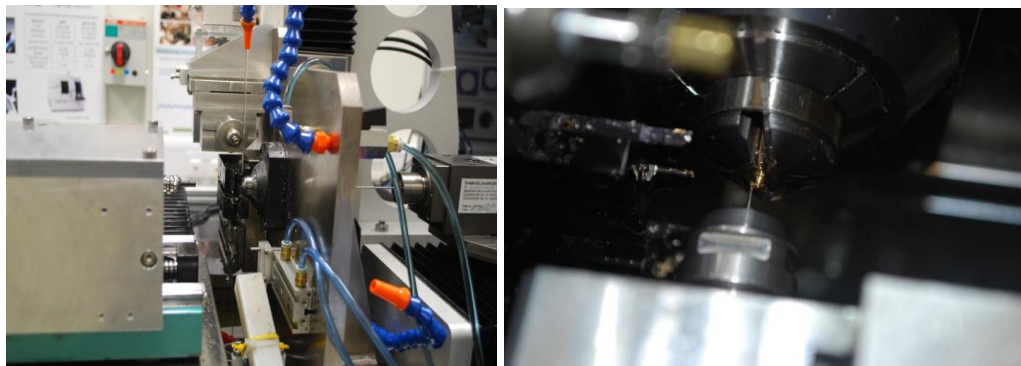


Fig. 2-8: The milling and grinding operation

2.2.3 Axes Characterization

As above mentioned, our Multi-Axes CNC Turn-Mill Machining Center has three spindle (W_1, W_2, W_3) and five linear axes (Z_1, X_2, Y_2, X_3, Z_3), as well as an auxiliary axis θ (for setting the gear hob). The following is detail setting information:

Linear Axes

All linear axes are controlled in a semi-closed loop manner based on the feedbacks from the servomotors. The theoretical resolution is 0.04 μm per count. The servo period for the linear axes controller card is set at 200 μs .

Spindle Axes

Since the control resolution for the main spindle is set at 80000 counts per revolution, closed-loop control is impossible when the center is operating in the turning mode where speeds ranging from 5000-8000 RPM are needed since the maximum allowable speed is limited by the sampling frequency of 2 MHz. Therefore, the main spindle will be operated in open-loop manner when the center is operating in turning mode. On the other hand, speeds ranging from 10-200 RPM are needed during the gear hobbing mode and closed-loop control will be used.

For the tool spindle, speeds ranging from 1000-3000 RPM are needed in the gear hobbing mode and therefore, it is operated in closed-loop manner under any circumstance. The servo period for the spindle controller card is set at 100 μs .

2.3 The CNC Controller

This section presents our effort in control system of Multi-Axes CNC Turn-Mill-Hob Machining Center. The readers are reminded that the major application of technology is following [124, 125]:

1. To ensure the accuracy, a software based volumetric error compensation system has been implemented. For example, Figure 2-9 shows our relative speed strategy.

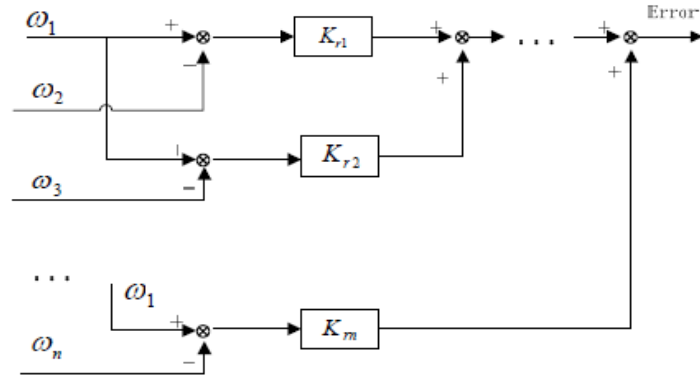


Fig. 2-9: Relative speed strategy of our machining center

- The machine uses advanced motion control technology (cross coupling) for multi-axes synchronized motion; this ensures the accuracy, as shown in Figure 2-10.

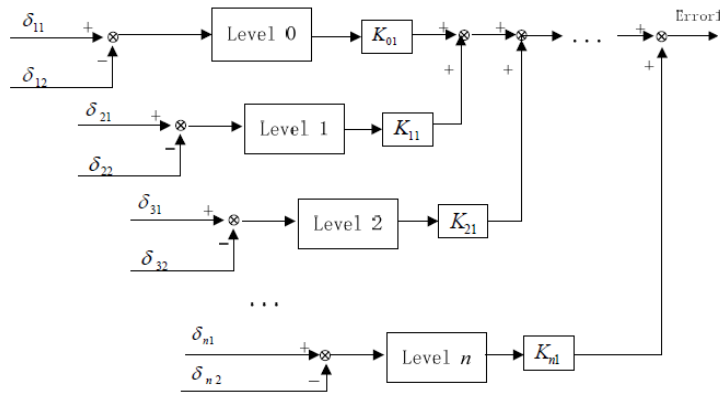


Fig. 2-10: Cross coupling technology of our machining center

- The machine uses the electronic gearing method for gear hobbing control; this gives not only higher accuracy but also ease of use, the detail of this method will be described in Section 2.3.2.

2.3.1 Hardware

The hardware includes an industrial control computer (Manufacturer: Advantech Technology Ltd.; Model: IPC-610-L) [54], two multi-axis controllers (Manufacturer: Googoltech Technology Ltd, Model: GT-400-SV) [55] and 8 axis servo drivers (Manufacturer: Mitsubishi, Model: Mr-J3series) [56]. The hardware architecture of the control system is shown in Figure 2-11 [127].

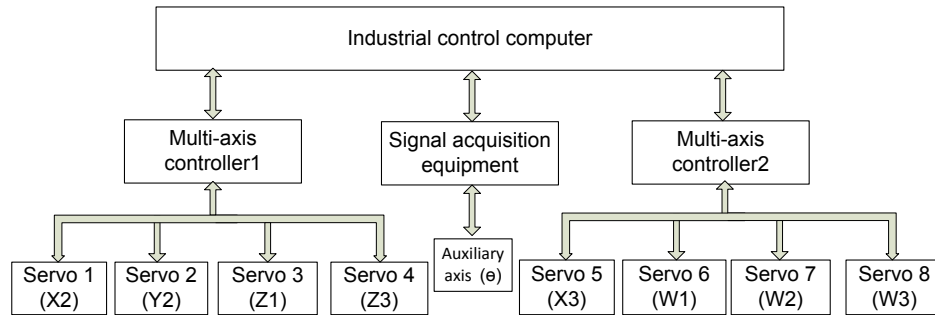


Fig. 2-11: Hardware Architecture of the control system

Two PC-based motion controller cards are used to manipulate the machine system. Both cards are manufactured by Googoltech Technology Ltd., and the model number is GT-400-SV [55]. Each card is capable of controlling up to four axes during independent motion and up to three axes during coordinated motion. For the system, one card is allocated to control the four linear axes and the other is used to control the three rotational spindle axes and one linear axis. Besides, the signal acquisition equipment is used for setting hobbing angle (θ). The maximum encoder sampling rate for each axis is 2 MHz. All linear axes are controlled in a semi-closed loop manner based on the feedbacks from the servomotors. All servomotors are Mitsubishi [56]. The theoretical resolution is 0.04 μm per count. The servo period for the linear axes controller card is set at 200 μs .

All Mitsubishi J3 series servomotors HF-KP23 and amplified by the corresponding drivers MR-J3-20A. Figure 2-12 is a photo of the servomotor and the amplifier [56]. The choice for using the J3 series is supported by its compactness and high performance feedback. The linear motion of each axis is realized by the conventional ball-screw and linear guide combination. Each axis consists a pair of linear rails and each rail has two sliding block and they are purchased from the Taiwanese company HIWIN with model number of HGN20. The ball-screw, which is also manufactured by HIWIN with model number FSV, is directly coupled to the servomotor via a DKN series flexible coupling manufactured by the German company Gerwah and the model number is DKN-10-14 with H7 fittings on both bores.

Each servomotor is equipped with a high resolution 18-bit serial encoder and it is configured to output 100000 counts per revolution. Since the pitch of the chosen ball-screw is 4 mm, a theoretical resolution of 0.04 μm is obtained. Also, the ball-screw is properly preloaded such that backlash is guaranteed to be within 5 μm along the entire stroke. Our center is setup as a semi-closed loop system and the system is controlled entirely based on feedbacks from the servomotors.



Fig. 2-12: Mitsubishi servomotor HF-KP23 and amplifier MR-J3-20A [56]

Since the control resolution for the main spindle is set at 80000 counts per revolution, closed-loop control is impossible when the machine is operating in the turning mode where speeds ranging from 5000-10000 RPM are needed since the maximum allowable speed is limited by the sampling frequency of 2 MHz. Therefore, the main spindle will be operated in open-loop manner when the machine is operating in turning mode. On the other hand, speeds ranging from 10-200 RPM are needed during the gear hobbing mode and closed-loop control will be used. For the tool spindle, speeds ranging from 1000-3000 RPM are needed in the gear hobbing mode and speeds ranging from 5000-10000RPM are needed in the milling mode .Therefore, they are operated in closed-loop manner under any circumstance. The servo period for the spindle controller card is set at 100 μs . Figure 2-13 shows the photo of our machine control system.



Fig. 2-13: The photo of our machine control system

2.3.2 Software

The software part of the control system is developed using C++ language and objective-oriented design method. Also FLTK libraries are used to make the interface beautiful and user-friendly. As an example, Figure 2-14 shows the jog motion and G code interfaces, respectively. The user interface can easily realize position and velocity display, tool management, automatic loading /unloading, home, jog running, spindle control, G code and so on [57].



Fig. 2-14: Jog motion and G code interface

One of the unique features of our machine is the capability to machine miniature gears. As opposed to traditional gear hobbing machines, the system does not use mechanically means to synchronize the axes but rather a technique called electronic gearing. Figure2-15 [58] shows the working principle of gear hobbing.

As the cutter hob axis is required to rotate much faster than the workpiece axis during gear hobbing, the driving servomotor that is directly coupled to the hobbing cutter is assigned to be the master axis and the driving servomotor is assigned to be the slave axis.

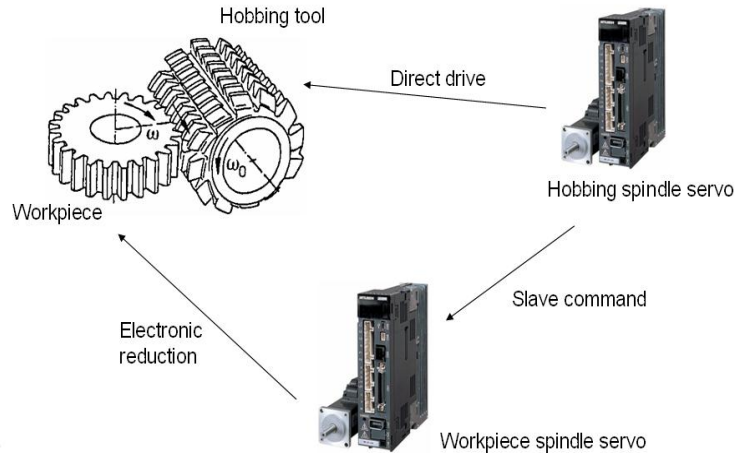


Fig. 2-15: The working principle of mechanically decoupled gear hobbing [58]

Since the two servomotors are not linked mechanically, synchronization is achieved entirely based on the motion control on the two closed-loop spindle axes [59]. Once the master axis is commanded to rotate at a given speed, the encoder feedback of the master axis will be continuously sampled and slave command will be generated to control the slave axis. Synchronization is achieved when the following position constraint is satisfied at any time instance:

$$C = \theta_m \cdot K - \theta_s \quad (2-1)$$

where θ_m is the angular position of the master axis, K is the required synchronization ratio, θ_s is the angular position of the slave axis and C is a constant synchronization bias. If C equals to zero, that is:

$$0 = \theta_m \cdot K - \theta_s \quad (2-2)$$

Then, total synchronization is achieved. The advantage of mechanically decoupled gear hobbing is obvious; that is, flexibility in changing and unlimited choice of synchronization ratio. However, the gains for both the position loop as the velocity loop of the two spindles must be carefully tuned in order to achieve accurate synchronization. More on the synchronization performance of our system is presented in Chapter 2-4. In summary, all functionalities can be written in G codes including the milling machining. Tuning, milling, gear hobbing and other machine processes can be realized through programming G codes. And based on RS274 standard, the developed G code can integrate with commercial CAM software.

2.4 The Calibration

2.4.1 Synchronization Performance

As mentioned in Chapter 2-3, the workpiece and tool spindle of the machine are mechanically coupled and synchronization is achieved by controlling the two closed-loop spindles electronically. This section will present the synchronization algorithm in details with experimental results reflecting the synchronization accuracy of our machine system.

Since the mechanical components used in the workpiece and the tool spindle are similar, it is reasonable to use an identical transfer function $G(s)$ to represent the two spindles [60]. Thus, the instantaneous position of the tool spindle θ_t can be expressed as:

$$\theta_t = G(s) \cdot \theta_i \quad (2-3)$$

where θ_i is the command position of the tool spindle. The instantaneous position of the tool spindle θ_t is used as the command position for the slave spindle, that is, the workpiece spindle. The instantaneous position of the workpiece spindle θ_w can be expressed as:

$$\theta_w = G(s) \cdot \theta_i \quad (2-4)$$

By introducing the synchronization ratio K , an expression relating the instantaneous position of the workpiece spindle θ_w and the command position of the tool spindle θ_i can be obtained:

$$\theta_w = G^2(s) \cdot \theta_i \cdot K \quad (2-5)$$

Equation (5) is the governing equation for the master-slave synchronization model used in the gear hobbing mode of our machine system. A data acquisition platform written in C is developed using a standard PC running in pure DOS environment. Sampling is triggered using the hard real-time interrupt function of the UCOS library. The angular positions of the tool spindle θ_i and the angular position of the workpiece spindle θ_w is sampled every 1 ms after the spindles are commanded to run. The following parameters are used in conducting this experiment: synchronization ratio $K = 0.0625$, master $Kp = 3$, slave $Kp = 2$, servo sample time $ST = 100 \mu s$, acceleration $a = 0.5 \text{ counts}/ST^2$ and velocity $v = 160 \text{ counts}/ST$. The time responses of the two spindles are shown in Figure 2-16.

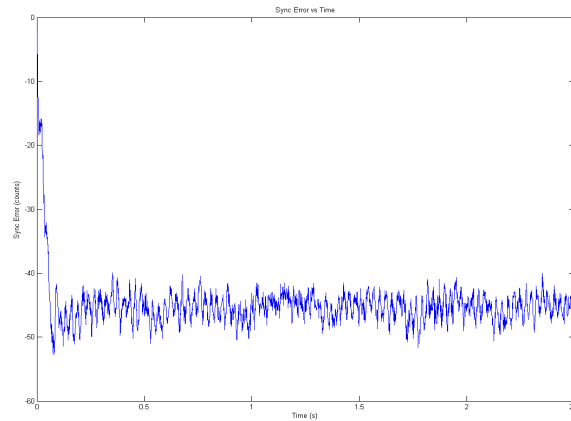
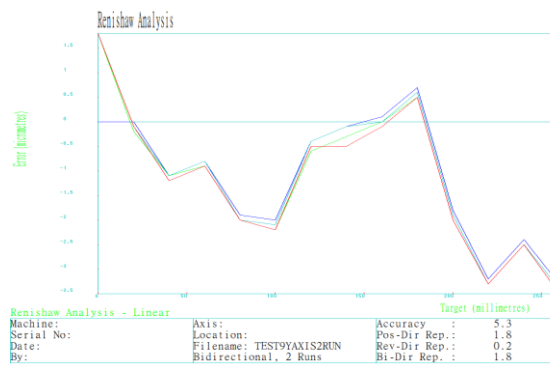


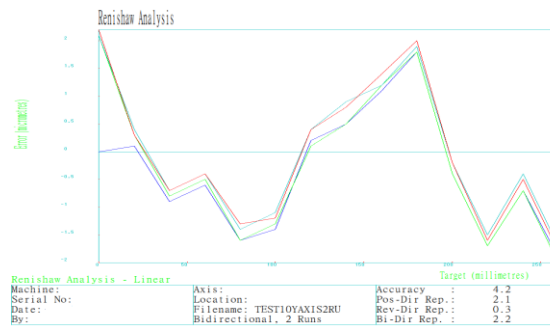
Fig. 2-16: Synchronization error of the spindles

2.4.2 Position Accuracy

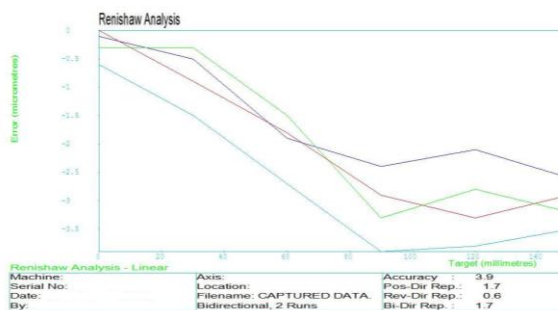
Figure 2-17 shows the position accuracy of our machining center by measured Renishaw Analysis Machine [61]. The results show that the position accuracy of X axis is $\pm 5.3/2 = \pm 2.65 \mu\text{m}$, Y axis is $\pm 4.2/2 = \pm 2.1 \mu\text{m}$, and the one of Z Axis is $\pm 3.9/2 = \pm 1.95 \mu\text{m}$. Besides, in order to reflect the average error along the entire machined profile by hobbing, the Euclidian distance between each extracted sample point to the corresponding closest point on the design profile is calculated [62]. It is found that the average error (Root Mean Squares) is $2.1 \mu\text{m}$. Figure 2-18 shows the errors for all sample point.



X axis



Y axis



Z axis

Fig. 2-17: The position accuracy of our machining center

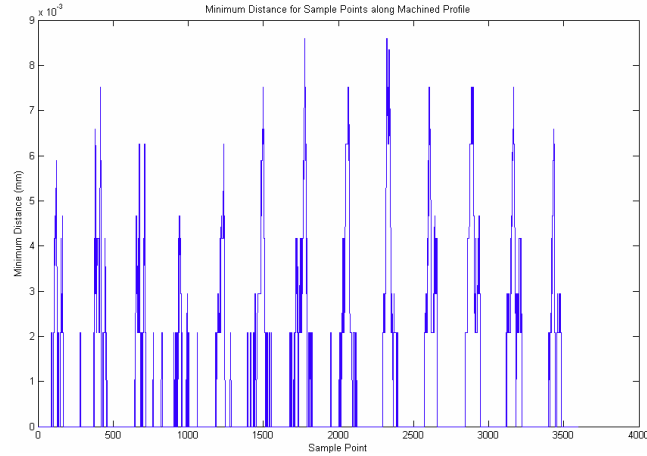


Fig. 2-18: Minimum error for every sample point on hobbing

2.5 Cutting test

For machining simple parts, as only using turning, milling functions, we use commercial CAM software to produce the tool path. On the other hand, for machining complex parts, as hobbing gear and non-gear parts, we developed a special program to produce the actual tool path. The detail is presented in Chapter 3.

2.5.1 Turning

A part known as the balance staff is used to benchmark the turning performance and it is a critical component with tight tolerances in a mechanical watch movement. Figure 2-19 shows the designations of dimension for the balance staff and the minimum dimension of this part is only 0.086mm (A and F). Figure 2-20 shows the samples of balance staff machined by the system with brass. Ten samples are chosen and the dimensions are measured using a micrometer. Table 2-2 shows the measurement results of the chosen samples.

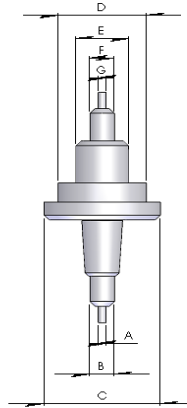


Fig. 2-19: Designation of dimension for the balance staff



Fig. 2-20: Balance staff samples machined by the system

Table 2-2: Measurement results of the ten samples machined by the system
(Material: AP20, Machining time: 15seconds/piece, in mm)

Sample# Design	A(mm)	B	C	D	E	F	G
1	0.085	0.276	1.302	0.999	0.600	0.281	0.085
2	0.085	0.279	1.297	0.996	0.600	0.282	0.088
3	0.082	0.281	1.301	0.998	0.597	0.284	0.087
4	0.081	0.281	1.299	0.997	0.598	0.285	0.090
5	0.083	0.283	1.299	0.997	0.598	0.284	0.090
6	0.085	0.282	1.303	1.000	0.599	0.282	0.088
7	0.082	0.282	1.303	0.996	0.597	0.285	0.088
8	0.082	0.281	1.302	0.998	0.600	0.281	0.087
9	0.083	0.283	1.299	0.999	0.597	0.285	0.089
10	0.083	0.283	1.300	0.999	0.596	0.284	0.088
Average	0.083	0.281	1.301	0.998	0.598	0.283	0.088
Average Error	-0.003	0.001	0.001	-0.002	-0.002	0.003	0.002
St Deviation	0.0015	0.0021	0.0020	0.0018	0.0014	0.0014	0.0017

It can be observed in Table 2-2 that the maximum error of the experiment occurs in dimension A and F in which both have an average error of 3 μm . The standard deviation for each dimension is also calculated and the repeatability of our system measured in this experiment is 2.18 μm .

The same experiment is also conducted on a commercially available turning center, namely, the Deco 10a manufactured by the Swiss company Tornos [26]. The cutting conditions and parameters are maintained the same as the ones used in our machining center experiment. Again, ten balance staff samples that are machined by the Deco 10a are chosen and the dimensions are measured using a micrometer. Table 2-3 shows the measurement results of the chosen samples machined by the Deco 10a. It can be observed that the maximum error of this experiment occurs in dimension A, F and G in which all of them have an average error of 10 μm . The repeatability of the Deco 10a measured in this experiment is 2.55 μm . Finally, Table 2-4 shows the preliminary comparison of our machining center with Deco 10a in terms of accuracy, repeatability and cost.

Table 2-3: Measurement results of the ten samples machined by Deco 10a
(Material: AP20, Machining time: 15seconds/piece, in mm)

Sample #	A (mm)	B	C	D	E	F	G
Design	0.086	0.280	1.300	1.000	0.600	0.280	0.086
1	0.077	0.270	1.310	0.993	0.594	0.270	0.077
2	0.078	0.272	1.311	0.995	0.598	0.273	0.073
3	0.078	0.271	1.304	0.993	0.591	0.270	0.078
4	0.077	0.271	1.304	0.990	0.592	0.269	0.078
5	0.072	0.272	1.309	0.992	0.595	0.269	0.077
6	0.076	0.271	1.305	0.993	0.590	0.269	0.076
7	0.075	0.270	1.309	0.992	0.594	0.270	0.077
8	0.077	0.270	1.306	0.992	0.594	0.270	0.075
9	0.075	0.270	1.308	0.993	0.594	0.269	0.076
10	0.074	0.270	1.309	0.993	0.594	0.270	0.077
Average	0.076	0.271	1.308	0.993	0.594	0.270	0.076
Average Error	-0.010	-0.009	0.007	-0.007	-0.006	-0.010	-0.010
St Deviation	0.00191	0.00082	0.00255	0.00126	0.00222	0.00120	0.00151

Table 2-4: Preliminary comparison of Deco 10a with our machining center

	Tornos Deco 10a	Our machining center
Cost (HK\$)	2,400,000	350,000
Overall accuracy (mm)	0.003	0.003
Repeatability (mm)	0.00255	0.00218

Although Table 2-4 shows our machining center is outperforming the Tornos' Deco 10a system under all criteria, it should be pointed out that this comparison is only preliminary and simply reflects the performances of our machining center and Deco 10a in this experiment rather than the performances under general manufacturing conditions. For example, the claimed cost of \$350,000 of our machining center is manufacturing cost of the system; on the other hand, the cost of \$2,400,000 of the Deco 10a is already the market value of system and therefore, the cost figures are not directly comparable. Instead, the figures simply present to the readers the magnitude of the cost in acquiring such systems. Also, the Deco 10a system is a much more complicated system than our machining center and has more subsystems that can be fine-tuned to achieve better accuracy. Whether the Deco 10a system is tuned optimally depends greatly on the skills and the experiences of the operator and it is believed that the accuracy of 0.010 mm in the previous comparison can be improved if the system is more carefully tuned and prepared. However, the accuracy of 0.004 mm of our machining center is obtained when the system is already optimally tuned and there is little room for further improvement in its accuracy. Therefore, the turning performance of our machine is better.

2.5.2 Milling

A part known as the Date Corrector Pinion is used to benchmark the milling performance and it is a critical component (non-axial component) with tight tolerances in a mechanical watch movement. Besides, it is difficult machined due to it has some concave features and the requirement of surface roughness on edges. Figure 2-21 shows the drawing of Date corrector pinion.

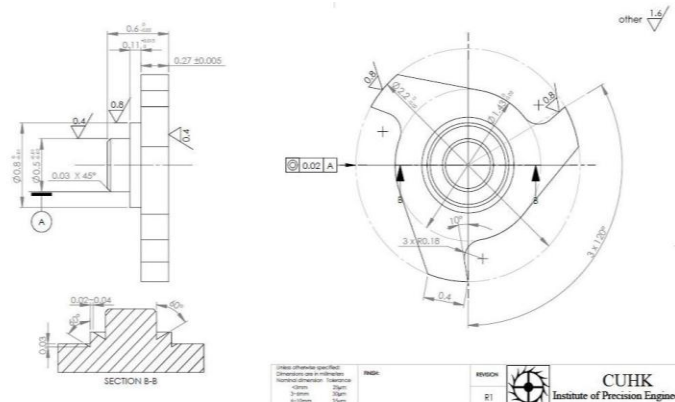


Fig. 2-21: The drawing of Date Corrector Pinion

There is a comparison of the part produced by Deco 10a [26] (Swiss, \$2,400,000 HK dollar, right) and our machine (left), as shown in Figure 2-22. We can see the profile of the part produced by our machine is much better than Deco 10a. Besides, the detail special algorithm for our milling function can be described in chapter 4.

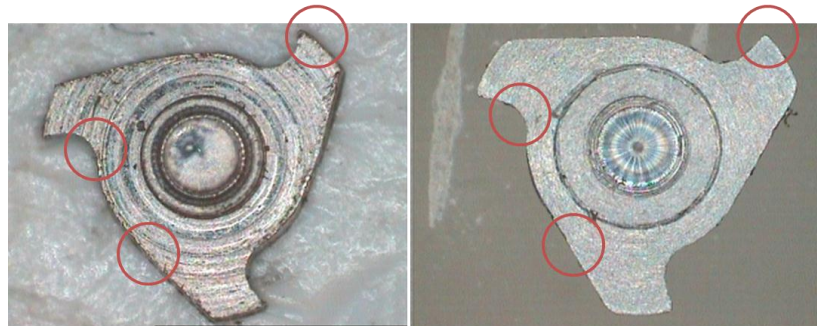


Fig. 2-22: The comparison between Deco 10a and our machine

2.5.3 Hobbing

With the synchronization accuracy measured, the gear hobbing performance of our system can be evaluated. In order to minimize error source during gear hobbing experiments, a high precision and custom-made gear hobbing tool is ordered from the Swiss company Diametal. Figure 2-23 shows the photos of the actual cutter and it is designated to machine a pinion with diameter of $\phi 0.971$ mm and module of 0.093. The drawing of reduction is shown in Figure 2-24 [53].

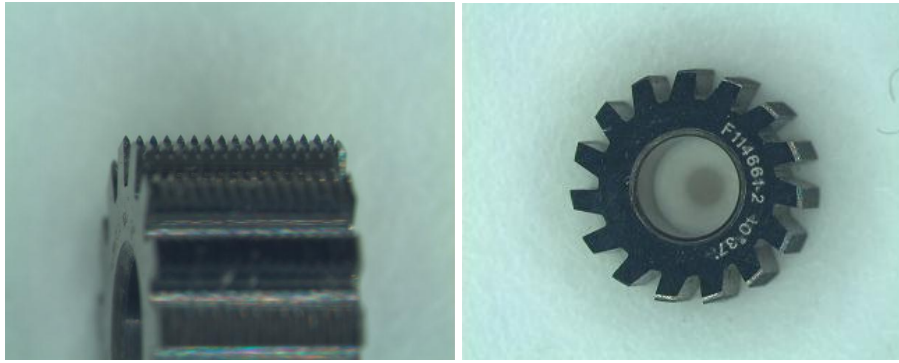


Fig. 2-23: The hob from Swiss company Diametal [53]

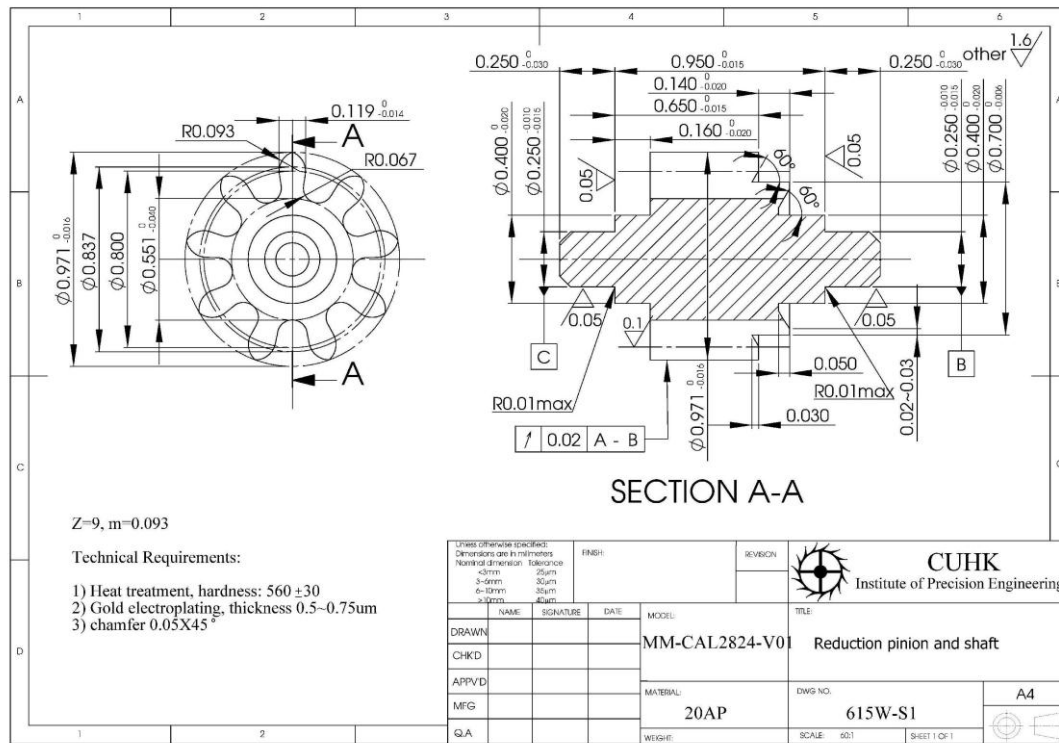


Fig. 2-24: The drawing of reduction pinion

Using brass as workpiece material, a gear sample is machined and it is magnified using a CMM system, namely, Mitutoyo's Quick Vision Pro. [64]. Figure 2-25 is the magnified image of the sample gear, which is machined by our machining center. Table 2-5 shows the measurement results of this pinion.



Fig. 2-25: The magnified reduction pinion sample machined by our machine

Table 2-5: The measurement results of our machining pinion
(Material: AP20, Machining time: 45seconds/piece, in mm)

	A	B	C	D	E
Nominal value	$\Phi 0.971$	0.950	$\Phi 0.250$	$\Phi 0.400$	$\Phi 0.700$
Tolerance	0 -0.016	0 -0.015	-0.010 -0.015	0 -0.020	0 -0.006
1	0.964	0.949	0.239	0.388	0.696
2	0.969	0.950	0.239	0.393	0.694
3	0.969	0.948	0.236	0.387	0.696
4	0.966	0.950	0.237	0.399	0.695
5	0.968	0.945	0.240	0.392	0.699
6	0.967	0.946	0.240	0.390	0.696
7	0.967	0.945	0.238	0.386	0.694
8	0.965	0.946	0.236	0.389	0.694
9	0.964	0.945	0.238	0.388	0.699
10	0.964	0.948	0.238	0.390	0.696
Max	0.966	0.950	0.240	0.399	0.699
Min	0.967	0.945	0.236	0.386	0.694
Mean	0.9663	0.9472	0.2381	0.3902	0.6959
STD	0.003327	0.002044	0.001449	0.003765	0.001853

The key demission of this pinion is A ($\Phi 0.971$) and E ($\Phi 0.700$), because they are gear shape parameters. From Table 2-5, we can know that the mean of our machined samples in A and E demission are 0.9663mm and 0.6959mm respectively. So, the maximum profile error is less than $\pm 7.5 \mu\text{m}$ in hobbing. Besides, the hobbing simulation and the detail experiment are shown in chapter 3.

2.5.4 Integration test

As above mentioned, Biomedical parts are much more complex [65]. So, we use the medicinal part to synthetically test our machining center. This part is used in Ureteroscope, the drawing and samples are shown in Figure 2-26. The part require multiple cutting steps and special functions [66]. For example, the front of this part, the side of this parts and the back of this parts are needed to machine. So, your machine should have multiple axes. Then, obviously, your machine should have turning, milling, grinding and other functions for machining this part. Finally, the tolerance of this part is tight. After testing, the maximum error of our machined samples is about $7 \mu\text{m}$ and the average error is only $4 \mu\text{m}$.

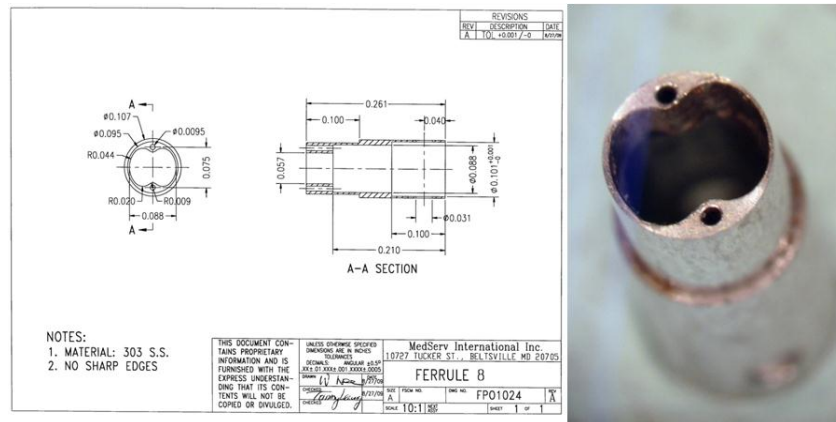


Fig. 2-26: The drawing and samples of Ureteroscope part

Table 2-6: The measurement results of our machining Ureterscope part
(Material: S303, Machining time: 10 minutes/piece, in inch)

	A	B	C	D	E	F	G	H	I	J
Nominal value	Φ0.107	Φ0.095	R0.044	R0.020	0.088	R0.009	0.075	Φ0.0095	0.057	0.261
Tolerance	+0.001 -0.001	+0.001 -0.001	+0.001 -0.001	+0.001 -0.001	+0.001 -0.001	+0.001 -0.001	+0.001 -0.001	+0.0005 -0.0005	+0.001 -0.001	+0.001 -0.001
1	0.108	0.0955	0.0432	0.0209	0.0882	0.0082	0.0746	0.0099	0.0571	0.2608
2	0.1079	0.0955	0.0435	0.0208	0.089	0.0084	0.0745	0.0100	0.0573	0.2609
3	0.108	0.0956	0.0432	0.021	0.0888	0.0084	0.0745	0.0100	0.0569	0.2609
4	0.1076	0.0952	0.0432	0.0209	0.0885	0.0082	0.0748	0.0100	0.0570	0.2608
5	0.1079	0.0952	0.0433	0.0208	0.0886	0.0085	0.0745	0.0098	0.0571	0.261
6	0.1079	0.0955	0.0435	0.0209	0.0884	0.0086	0.0746	0.0098	0.0570	0.261
7	0.1078	0.0953	0.0433	0.0209	0.0885	0.0085	0.0745	0.0099	0.0572	0.261
8	0.1076	0.0952	0.0436	0.0207	0.0885	0.0085	0.0748	0.0099	0.0571	0.2608
9	0.108	0.0955	0.0435	0.0209	0.0888	0.0082	0.0746	0.0097	0.0573	0.261
10	0.1075	0.0954	0.0435	0.0208	0.0889	0.0085	0.0745	0.0100	0.0570	0.2609
11	0.1079	0.0955	0.0432	0.0208	0.089	0.0086	0.0746	0.0099	0.0572	0.2608
12	0.1079	0.0953	0.0434	0.0209	0.0885	0.0087	0.0747	0.0099	0.0571	0.2609
13	0.1075	0.0952	0.0435	0.0206	0.0886	0.0084	0.0745	0.0100	0.0570	0.261
14	0.1076	0.0954	0.0432	0.0209	0.0884	0.0084	0.0746	0.0097	0.0571	0.2608
15	0.1075	0.0952	0.0433	0.0208	0.0887	0.0085	0.0745	0.0099	0.0573	0.261
Max	0.108	0.0956	0.0435	0.021	0.089	0.0087	0.0748	0.0100	0.0573	0.261
Min	0.1075	0.0952	0.0432	0.0206	0.0884	0.0082	0.0745	0.0097	0.0569	0.2608
Mean	0.107773	0.095367	0.04336	0.02084	0.088617	0.008441	0.074594	0.009888	0.057112	0.260906
STD	0.000198	0.000145	0.000145	0.000095	0.000195	0.00015	0.000106	0.000103	0.000125	0.000088

Table 2-6 shows the measurement results of our machining samples. From this table, we can find the maximum STD is only 0.000198 inch, about 0.005 mm.

2.6 Summary

As the demand for miniature components becomes higher as a consequence of the emerging trend of product miniaturization, the ability to manufacture these components accurately, swiftly and cost effectively becomes inevitable. In this chapter, the machining center developed by our institute is introduced. The machine has 8 axes, which can achieve turning, milling, grinding, hobbing and so on. With a flexible tool spindle and multiple cutting tools, the machine is able to machine parts with complex features such as gear profile and non-circular section in one single setup. Then, the machine uses the electronic gearing method for gear hobbing control; this gives not only

higher accuracy but also ease of use. Finally, the machine uses advanced motion control technology for multi-axes synchronized motion; this ensures the accuracy.

Based on experiments, the performance of the machine is found that: the machining error is $\pm 3 \mu\text{m}$ in turning, $\pm 7 \mu\text{m}$ in milling, and the maximum profile error is less than $\pm 7.5 \mu\text{m}$ in gear hobbing with excellent surface finish. The accurate is almost as the same as the precision machines in the market, but our machine is only cost \$350,000 HK dollar. It is seen that our machine is very competitive.

Chapter 3:

Hobbing Gears and Axial Asymmetric Parts

3.1 A Brief Review

Machining is one the oldest and most commonly used manufacturing processes. Every day, millions of parts are machined. As a result, much research has been done and the basic theory of machining is well established, including metal cutting principle [37], Computer Numeric Control (CNC) [67], tool path generation [68] and etc. Machining asymmetric parts is however still a challenge. According to literature and market survey, asymmetric parts are machined by either special form tools or by CNC milling. The former is efficient but inflexible as each part requires a set of form tools. Sometimes even special machines are needed. The later is flexible but time-consuming and expensive. A simple asymmetric part may take minutes to make. As a result, in applications such as biomedical engineering and MEMS, machining asymmetric parts often becomes a bottleneck.

As an example, Figure 3-1 shows a couple of typical dental abutment and implants. Making such parts are rather time consuming.



Fig. 3-1: Two typical dental implants

Examining the cause of inefficiency of the existing technologies, it is found that the main reason is the use of small tools chipping off materials a bit at a time. This is necessary since the curvatures of the part could be small and hence, large tools cannot get in. To solve this problem, the proposed idea is to use large multiple teeth tools similar to gear hobbing together with CNC technology. Figure 3-2 illustrates a gear hob, and Figure 3-3 shows the process of gear hobbing: As the hob rotates, the so-called basic rack is generated. Furthermore, with a synchronized workpiece motion, the gear profile is then produced. From geometric point of view, it is the relative motion between the gear hob and the workpiece generates the gear profile as the image of the gear hob. Note that at any time, a number of teeth of the hob may be engaged in the cut making the operation efficient.

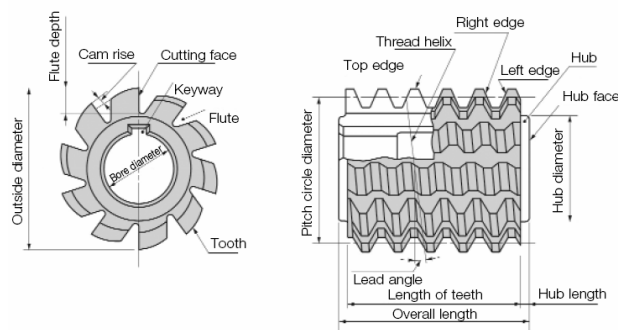


Fig. 3-2: Illustration of a gear hob [69]

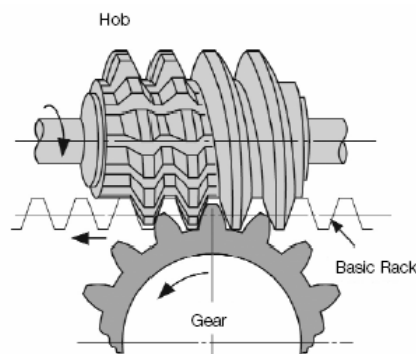


Fig. 3-3: The gear hobbing process [69]

The gear hobbing process is a complex process involving a large number of design and control parameters, but it has been well understood [69]. In recent years, the research also been extended to making of non-circular gears [70] and different gear profiles (such

as harmonic gears and cycloid gears) [71], as well as reducing manufacturing errors [72, 73]. There is no one however try to use the gear hobbing process to machine asymmetric parts.

This chapter presents a new method that uses hobbing to machine axial symmetric and asymmetric parts. The detail information is including: the theory, hobbing simulation and experiment validation.

3.2 The Theory

3.2.1 The basic principle

From a geometrical point of view, hobbing is done through the mesh movement between the hob and the workpiece in a 3D space [74]. In order to model the mesh movement, first, a set of coordinate systems are set up as shown in Figure 3-4. As shown in the figure, $O_h = (x_h, y_h, z_h)$ is the coordinate system of the hob; $O_g = (x_g, y_g, z_g)$ is the coordinate system of the workpiece; $O_0 = (x_0, y_0, z_0)$ is the global coordinate system, $O_1 = (x_1, y_1, z_1)$ and $O_2 = (x_2, y_2, z_2)$ are the reference coordinate systems of the hob and the workpiece in reference to the global coordinate system, respectively. The hob has Z_T blades and each blade has Z_C teeth. There are four important parameters: the helix angle of the hob (the angle between z_0 and z_h), λ ; the rotation angle of the hob (the angle between y_0 and y_h), θ ; the rotation angle of the workpiece (the angle between y_2 and y_g), φ ; and the feed of the workpiece, $f(\theta)$.

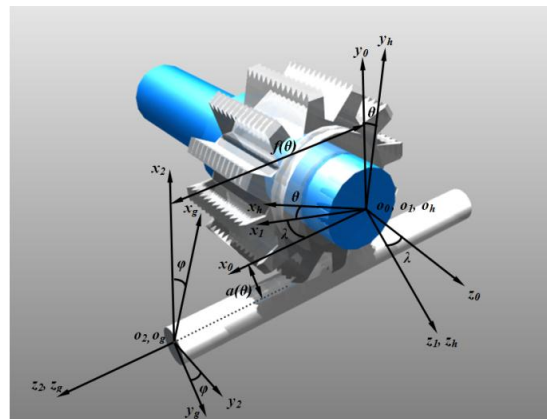


Fig. 3-4: The coordinate systems in the hobbing process

Figure 3-5 illustrates the process of hobbing an asymmetric part: The rotation speed of the workpiece is a constant (i.e., $V_w(\theta) = c \cdot \theta$, where c is a constant), while the rotation speed of the hob could be a function of θ (i.e., $V_h = V_h(\theta)$), and the center distance between the workpiece and the hob could also be a function of θ ($a = a(\theta)$). In general, asymmetric parts may take many shapes. Though, a part can always be decomposed into a series of convex and concave segments. In order to cut the part, the teeth of the hob must be able to cut the smallest concave segment of the part. Accordingly, the profile of the teeth is selected and denoted as $A(x, y)$. Moreover, the segments can be cut by controlling $V_h(\theta)$, $a(\theta)$ and the helix angle (or the helix pitch).

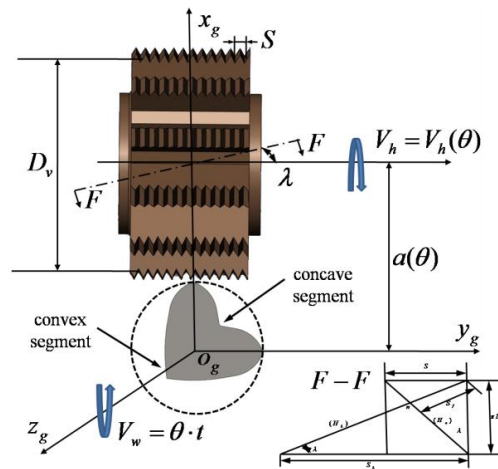


Fig. 3-5: The process of hobbing an axial asymmetric part

The mathematical expression for the mesh movement between the hob and the workpiece is rather complex [75]. A simplified model for hob a gear in 2D is shown below [74, 76]: Let R_g be the outer radius of the gear; m the module of the gear, and γ the synchronization ratio defined below:

$$\gamma = \frac{360 / Z_c}{V_h / V_w} \quad (3-1)$$

Accordingly, the gear profile is generated following the equations below:

$$\begin{cases} x' = -\sin\left(\arctan\left(-\frac{x}{y}\right) + \gamma\right) R_g - m \cdot n \lambda \cos(m\gamma) \\ y' = -\cos\left(\arctan\left(-\frac{x}{y}\right) + \gamma\right) R_g - m \cdot n \lambda \sin(m\gamma) \end{cases} \quad x < 0, \gamma < 0 \quad (3-2)$$

$$\begin{cases} x' = -\sin\left(\arctan\left(-\frac{x}{y}\right) + \gamma\right) R_g - m \cdot n \lambda \cos(m\gamma) \\ y' = \cos\left(\arctan\left(-\frac{x}{y}\right) + \gamma\right) R_g - m \cdot n \lambda \sin(m\gamma) \end{cases} \quad x < 0, \gamma > 0 \quad (3-3)$$

$$\begin{cases} x' = \sin\left(\arctan\left(\frac{x}{y}\right) + \gamma\right) R_g - m \cdot n \lambda \cos(m\gamma) \\ y' = \cos\left(\arctan\left(\frac{x}{y}\right) + \gamma\right) R_g - m \cdot n \lambda \sin(m\gamma) \end{cases} \quad x > 0 \quad (3-4)$$

where, $n = 0, 1, 2, \dots, Z_C$, denotes different blades. Note that equations above are a set of recursive equations, which describe the cutter path of a tooth cutting a small piece. For example, suppose the current blade is $A(x, y)$, then the next blade will be $A'(x', y')$, and the amount of cut will be $A'(x', y') - A(x, y)$. The combination of all the blade cuts will then form the gear as shown in Figure 3-6 [78]. Figure 3-6 shows an example, in which the hobbing parameters are as follows: the synchronization ratio is $\gamma = 1.846$, the helix angle is $\lambda = 0.0177$ and the center distance is $a = 1.276$.

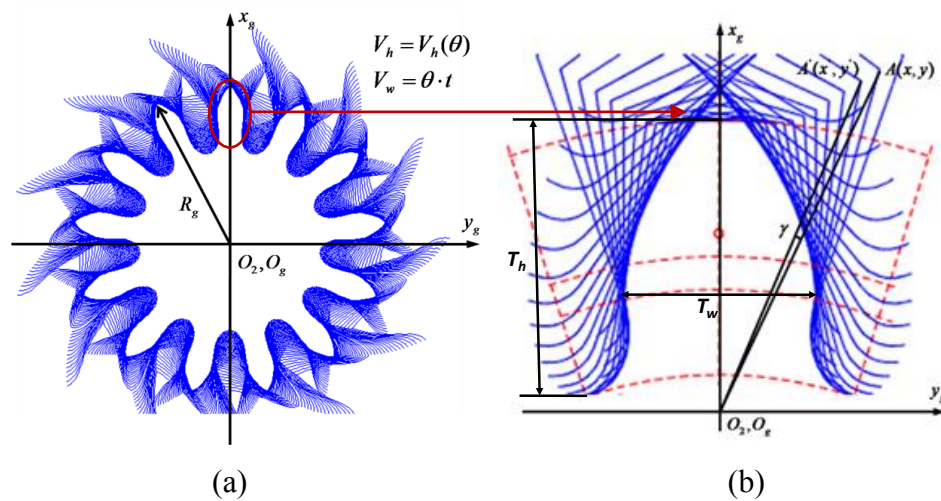


Fig. 3-6: The cutter path when hobbing a gear

where, $n = 0, 1, 2, \dots, Z_C$, denotes different blades. Note that equations above are a set of recursive equations, which describes the cutter path of a tooth cutting a small piece. For example, suppose the current blade is $A(x, y)$, then the next blade will be $A'(x', y')$, and the amount of cut will be $A'(x', y') - A(x, y)$. The combination of all the blade cuts will then form the gear.

The equations above also hint the principle of hobbing an asymmetric part. Examining Figure 3-5, it is seen that the process involves three control variables: V_h (which is equivalent to γ), a , and λ . By controlling these variables, we can get various shapes.

Figure 3-7 illustrates the process of hobbing an angular shaped part by varying $a(\theta)$. Note that at different time instance, different cutting teeth (and the blade) is engaged in cutting and the distance, $a(\theta)$, changes as well.

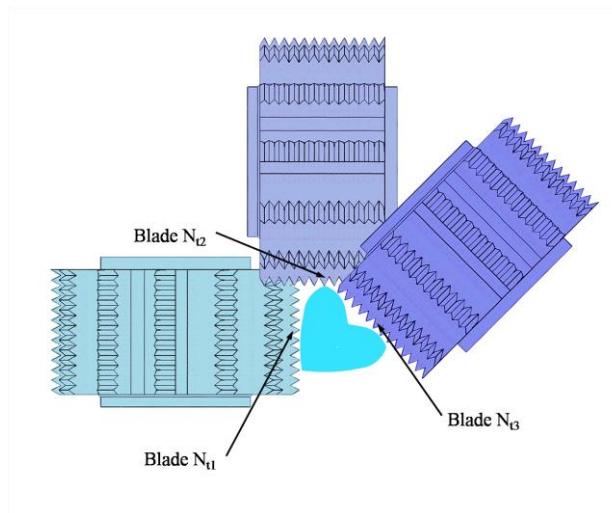


Fig. 3-7: Illustration of hobbing an asymmetric part

3.2.2 Key parameters analysis

From Figure 3-6(b), it is seen that a tooth of the gear is mainly characterized by two parameters, the height of the tooth, T_h , and the width of the tooth, T_w . According to [14], they can be determined by the following equations:

$$T_h = T_a + T_b = (2c_a + c_b)m \quad (3-5)$$

$$T_w = \frac{1}{2}\pi m \quad (3-6)$$

where, T_a , and T_b are the addendum and the dedendum of the gear respectively, $c_a = 1$ and $c_b = 0.25$ are the coefficient of the addendum and the coefficient of the bottom clearance respectively [79], and m is the modulus of gear. Based on Equation (3-1), the modulus of the gear can be written as follows:

$$m = \frac{2R_g Z_c V_w}{V_h} = \frac{R_g Z_c \lambda}{180} \quad (3-7)$$

Equations (3-2) ~ (3-4) also hint the principle of hobbing axial asymmetric parts: we can control the synchronization ratio, γ , the helix angle, λ , and the center distance between the hob and the workpiece, a , (which is proportional to R_g) to hob various kinds of “teeth”. First, let us examine the effect of the synchronization ratio while keep the helix angle and the center distance constant. Based on Equations (3-1), (3-5) (3-6) and (3-7), the height of the tooth, T_h , is:

$$T_h = (2c_a + c_b) \frac{R_g Z_c \gamma}{180} \quad (3-8)$$

The width of tooth:

$$T_w = \frac{\pi R_g Z_c \gamma}{180} \quad (3-9)$$

For instance, in the previous simulation example, changing the synchronization ratio from 1.846 to 0.75 while keeping the other parameters the same, the resulting part is a hexagon as shown in Figure 3-8.

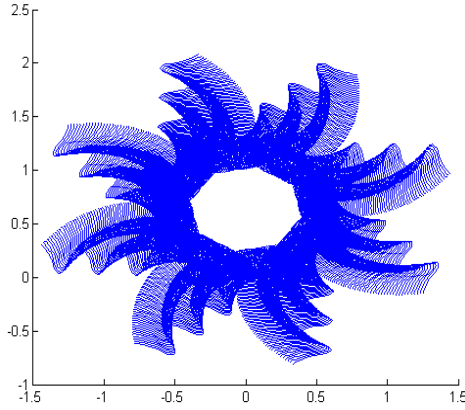


Fig. 3-8: The cutter path when changing the synchronization ratio

Next, let us consider the effect of the helix angle, λ , when keeping the synchronization ratio and the center distance the same, which will result in the change of the normal lead, S_f , [77]:

$$S_f = \pi D_v \sin \lambda \quad (3-10)$$

where, D_v the outer diameter of hob. From Figure 3-5, it is seen that the relationship between D_v and R_g is that:

$$a = \frac{D_v}{2} + R_g \quad (3-11)$$

$$R_g = \frac{1}{2} m (Z_c + 2c_a) = \frac{1}{2} m \left(\frac{V_h}{V_w} + 2c_a \right) \quad (3-12)$$

Hence, the resulting height of the part is:

$$T_h = \frac{V_w (2c_a + c_b) \left(2a - \frac{S_f}{\pi \sin \lambda} \right)}{V_h + 2V_w c_a} \quad (3-13)$$

The width of the tooth is:

$$T_w = \frac{\pi V_w \left(2a - \frac{S_f}{\pi \sin \lambda} \right)}{2V_h + 4c_a V_w} \quad (3-14)$$

Following the previous example, when changing the helix angle from 0.0177 to 0.0200 and keeping the other two parameters the same, the sides of this part become smoother, as shown in Figure 3-9.

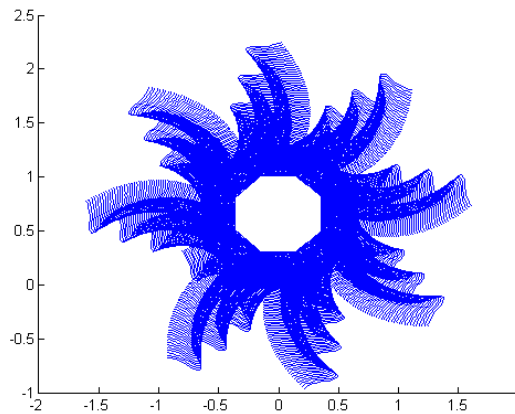


Fig. 3-9: The tool path when changing the helix angle

Similarly, we can find the effect of the centre distance when keeping the synchronization ratio and the helix angle constant. The resulting height of the part is:

$$T_h = \frac{2R_g V_w (2c_a + c_b)}{V_h} \quad (3-15)$$

The height of the tooth is:

$$T_w = \frac{\pi R_g V_w}{V_h} \quad (3-16)$$

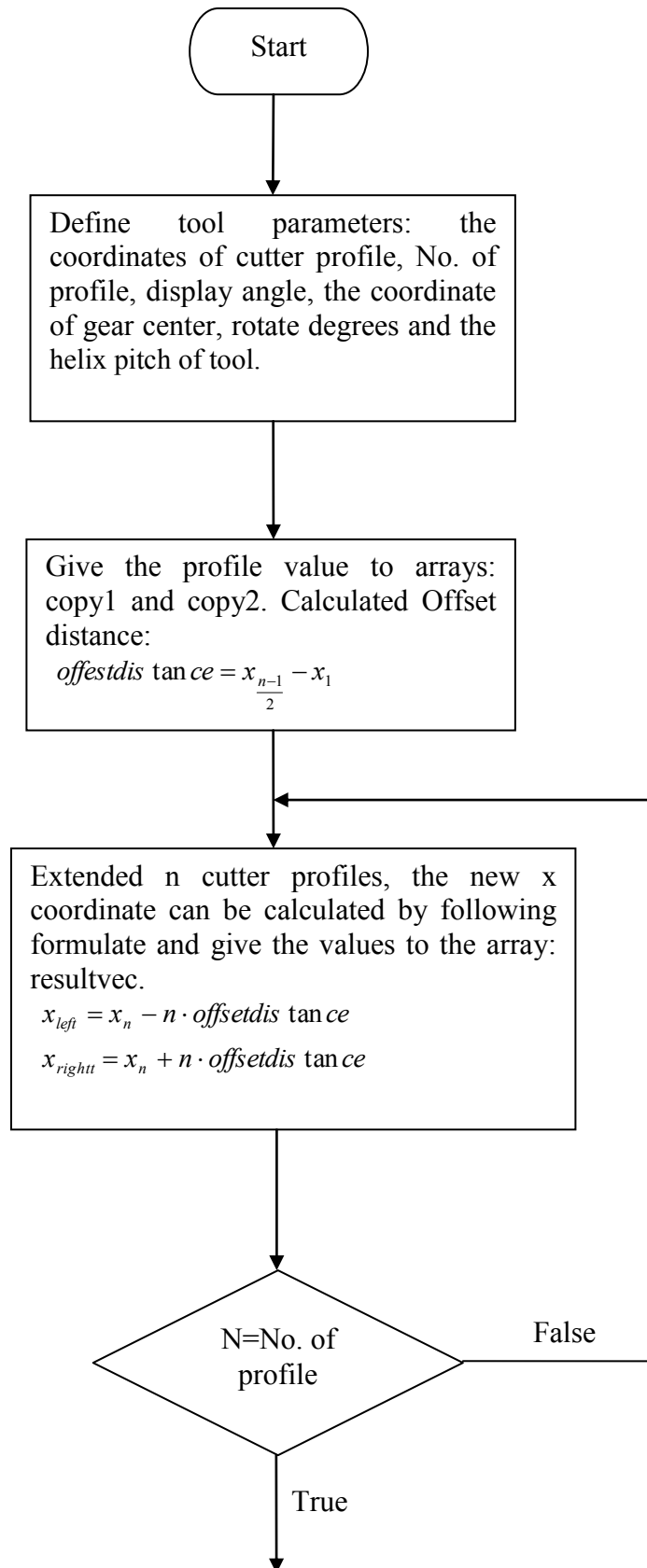
In summary, following observations can be made:

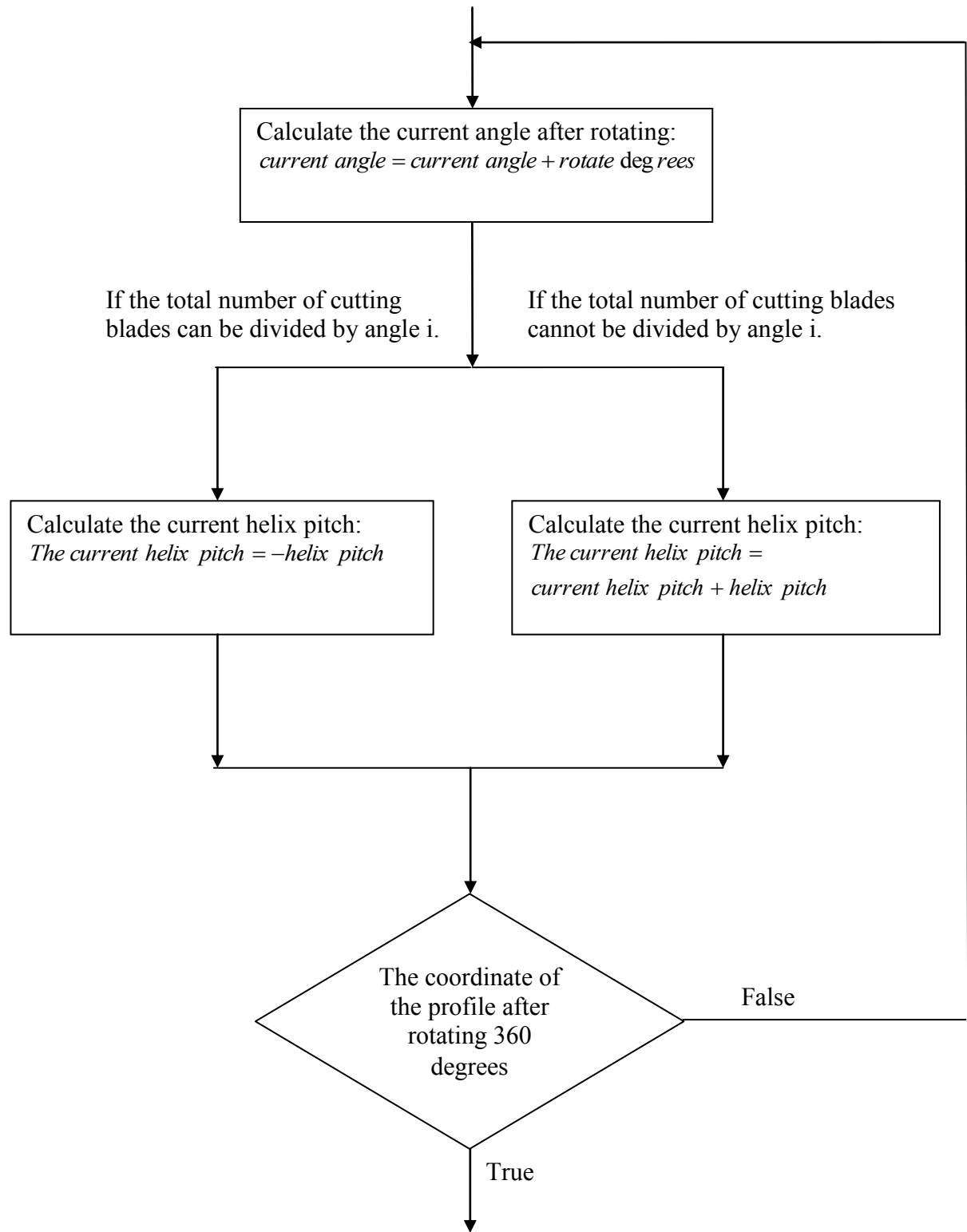
- (a) When the synchronization ratio increases, number of teeth becomes less;
- (b) When helix angle λ increases, the depth of the tooth decreases and the edges of the tooth become more smooth;
- (c) When center distance increases, the depth of the tooth decreases and the width of the tooth become smoother.

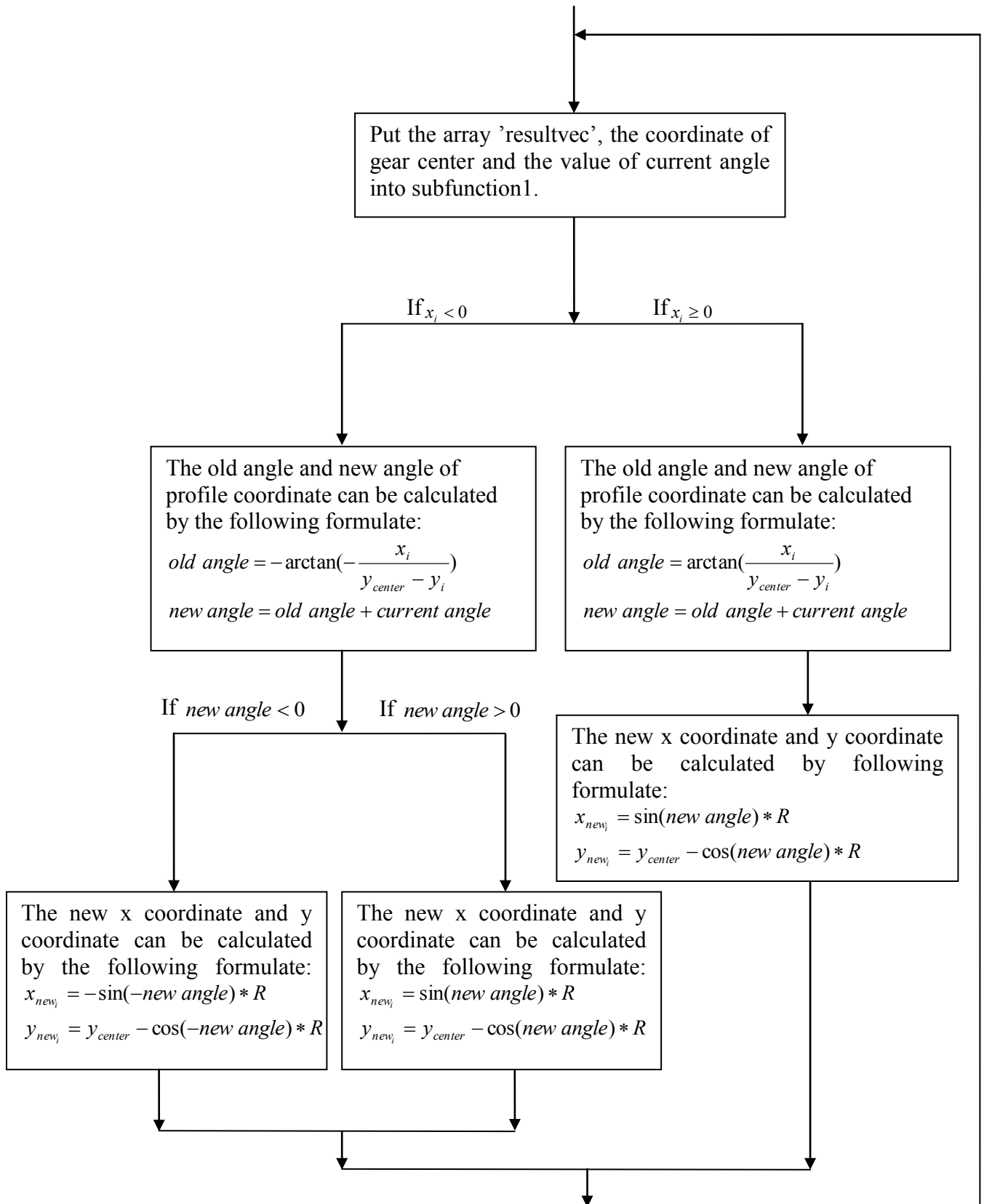
3.3 Computer Simulation

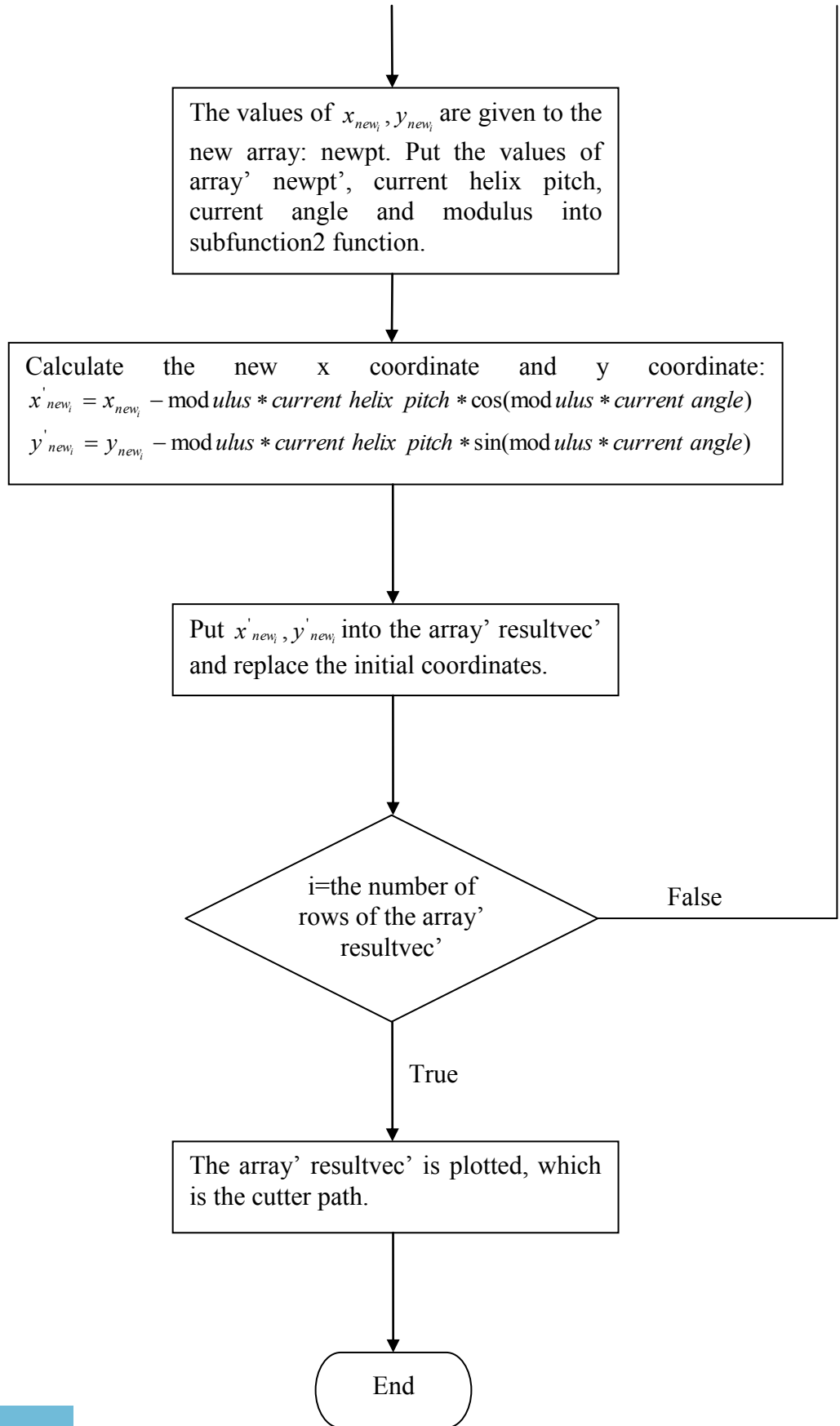
3.3.1 The process flow chart of simulation

As above mentioned, the hobbing simulation can be set up by using Equation (3-1) to Equation (3-16). The following is the process flow chart:









3.3.2 Simulation for machining axial symmetric / asymmetric parts

To demonstrate the presented idea, a number of computer simulations are carried out. For easy graphical interface and manipulation, MATLAB[®] is used as the simulation platform. In order to obtain consistent and comparable results, the same cutter tool will be used for all the simulations. Furthermore, in order to minimize error, a high precision and custom-made gear hobbing tool is ordered from the Swiss company Diametal [53]. We choose a 13 blade 15 teeth gear hob as shown in Figure 3-10. The photo of this gear hob is shown in Figure 2-20. It is designated to machine a pinion with diameter of $\Phi 1.284$ mm and module of 0.085. It is a cycloidal gear used in precision engineering [80][81]. We use this tool for all our simulation and cutting test.

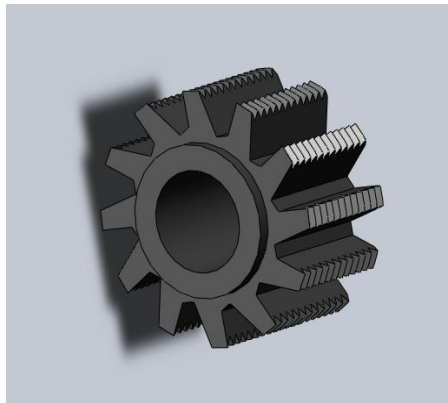


Fig. 3-10: The hob used in the simulation

The geometry of the cutter blade is first extracted using a CMM projector (Mitutoyo's QuickVision Pro), which has an extraction accuracy of $\pm 3 \mu\text{m}$. The sampling data points are $10 \mu\text{m}$ apart and then the data are linearly interpolated. Figure 3-11 shows the extracted cutter profile plotted in MATLAB[®].

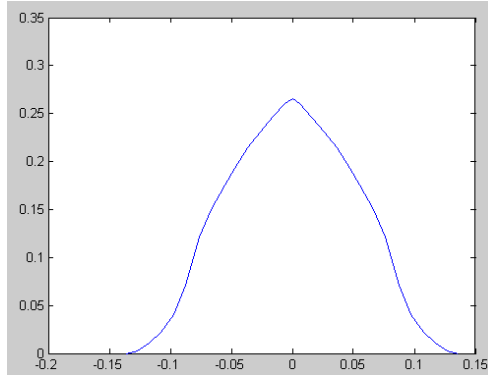


Fig.3-11: Extracted cutter profile in MATLAB

Table 3-1 shows the simulation procedure:

Table 3-1: The simulation procedure

Step 1:	Input the cutter parameters: number of teeth k , number of blades n , helix pitch γ
Step 2:	Calculate synchronization ratio $r = m/k$ and incremental angle $\theta = 360/(rn)$
Step 3:	Read cutter profile
Step 4:	For $i = 0$ to $rn - 1$
	Rotate profile axis to $i \cdot \theta$ degrees
	Plot cutter profiles along rotated profile axis
	Shift entire cutter profile array by $i\gamma$ along rotated profile axis

Three cases are studied in this chapter: (1) a 13 teeth gear; (2) an eccentric part; and (3) a continuous changing axial asymmetric part.

Case1: A 13 Teeth Gear

Gear is produced by the synchronized motion between the cutter and the workpiece. In this case, the helix angle λ , the synchronization ration γ , and the center distance a are all constants. The process is simulated by repeatedly plotting the teeth profile at different positions. Since the gear has 13 teeth, the γ is 13:1, and the helix pitch of the hob is set to be 0.0177 mm. The radius of the hob is 0.638 mm. Hence, for every 13 turns of the hob, the workpiece should undergo a single turn. As the cutter tool has 15 cutting blades, it implies that the tool will engage the workpiece for every $360 / 15 = 24$ degrees, and the workpiece axis must rotate $24 / 13 = 1.846$ degrees. Therefore, the simulation is conducted by plotting the cutter profile at intervals of 1.846 degrees with each profile

shifted by 0.0177 mm along its profile axis. Figure 3-12 demonstrates the simulation process graphically.

The simulation is completed when $360 / 1.846$ or 195 profiles are plotted and the result gear profile is obtained by extracting the envelope formed by all of the cutter profiles. Figure 3-13 shows the simulation results, from which the gear profile can be clearly seen.

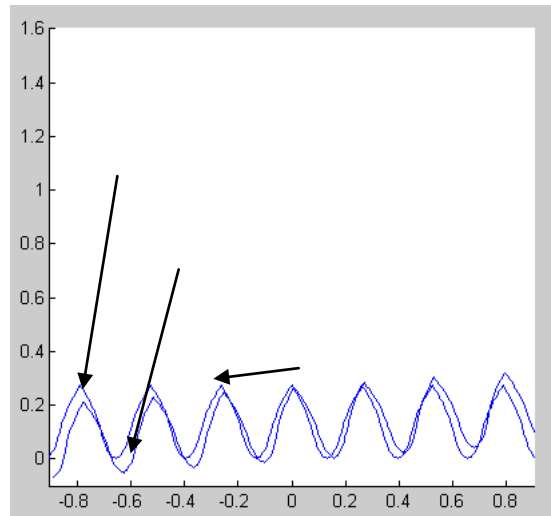


Fig. 3-12: Illustration of the hobbing process

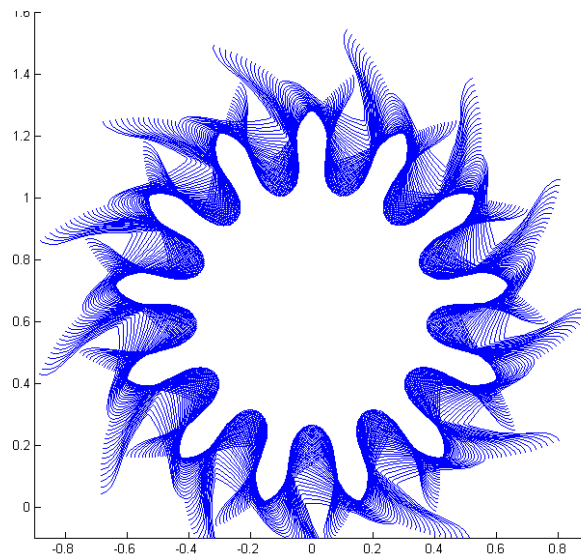


Fig. 3-13: Simulation result of Case 1

Figure 3-14 shows the zoom in views of the simulated gear. From the figure, it can be observed that the simulated gear profile is very much uniform and the gear teeth resemble one another. However, under real manufacturing environments, process defects such as spindle asynchronization, helix pitch error of the cutter and the tool spindle run-out will generally be unavoidable.

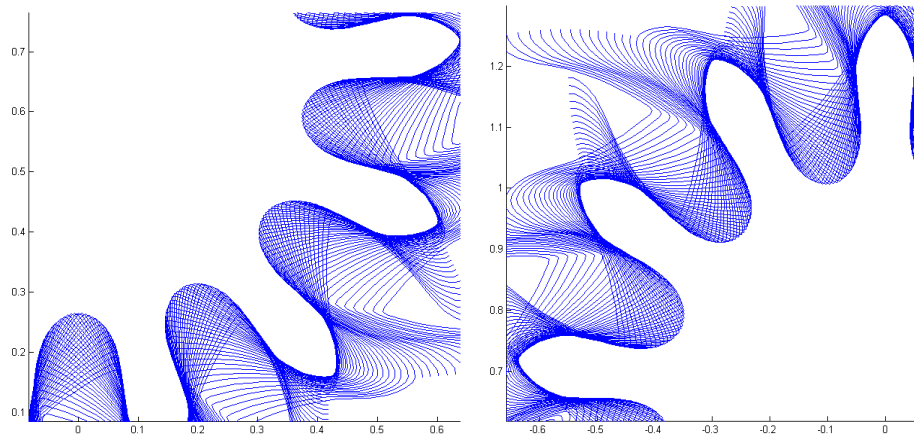
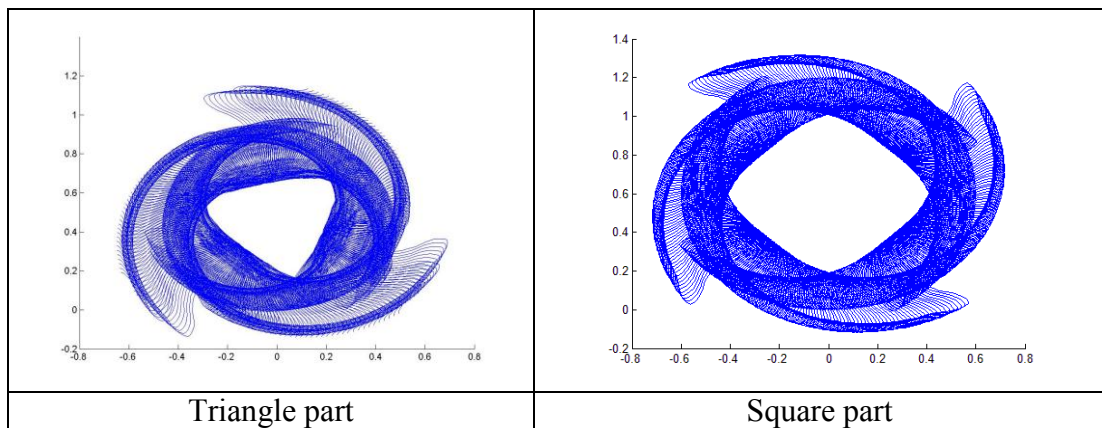


Fig. 3-14: Zoom up views of the simulated gear profile

Besides, we also can also machine other polygon parts except gear by using the same tool, as shown in Figure 3-15.



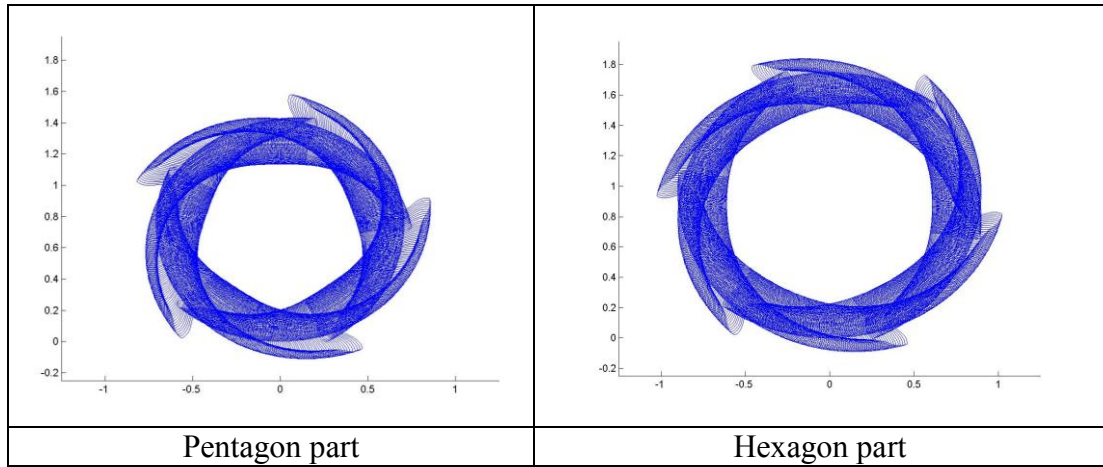


Fig. 3-15: Some polygon parts

Case 2: An Eccentric Part

Figure 3-16 shows an eccentric part. To cut this part, we used three cut as listed in Table 3-2. Note that among the three cuts, the helix pitch remains the same. The simulation result, as shown in Figure 3-17.

Table 3-2: The parameters for cutting an eccentric part

The first cut:	
Synchronization ratio, γ	2
Helix pitch, λ	0.0015
Center distance, a	2
The second cut:	
Synchronization ratio, γ	2
Helix pitch, λ	0.0015
Center distance, a	0.925
The third cut:	
Synchronization ratio, γ	2
Helix pitch, λ	0.0015
Center distance, a	0.825

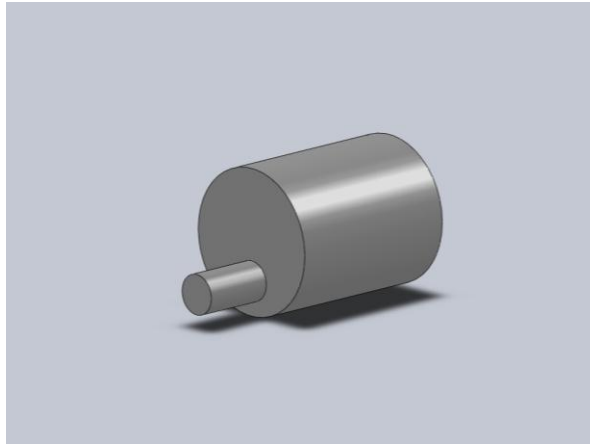


Fig. 3-16: An ecentric part

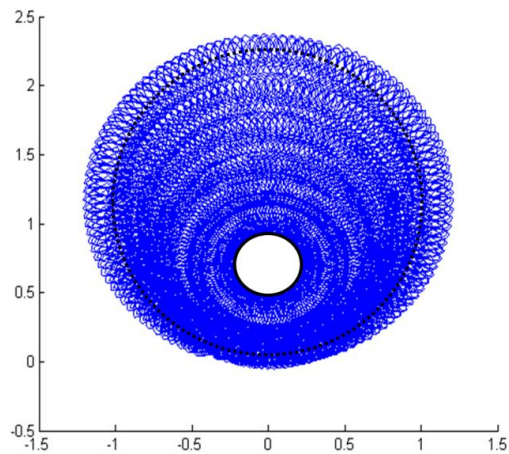


Fig. 3-17: Simulation result of Case 2

Case 3: A Continuous Changing Part

Figure 3-18 shows a continuous changing asymmetric part: One side of the part is elliptic, while the other side is angle, the cross-section of the part changes continuously. Conventionally, it will have to be machined by milling, which is difficult and inefficient. The new method can do it efficiently.

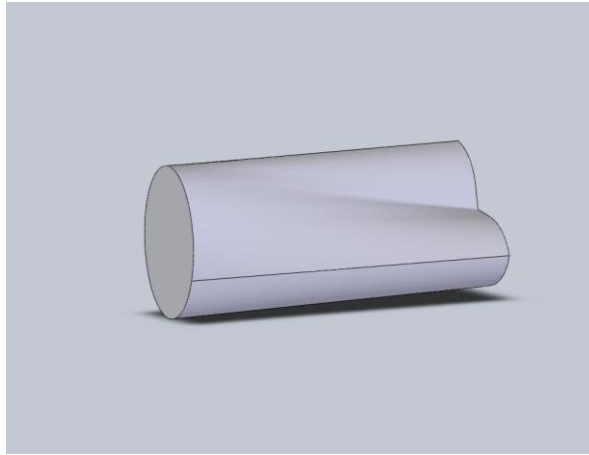


Fig. 3-18: A continuously changing axial asymmetric part

First, the part is decomposed into a number of sections. The left most section is elliptic and the right most section is angular. For the elliptic section, the machining parameters are listed in Table 3-3. The simulation result is shown in Figure 3-19.

Table 3-3: The parameters of cutting the elliptic section

Synchronization ratio, γ	2
Helix pitch, λ	0.0015
Center distance, a	0.43

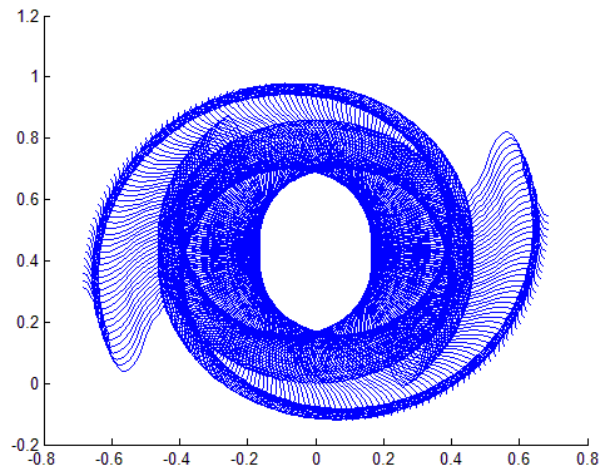


Fig. 3-19: Simulation of cutting the elliptic section

For cutting the angular section, two cuts are used as shown in Table 3-4. The simulation result is shown in Figure 3-20.

Table 3-4: The parameters of cutting the angular section

The first cut	
Synchronization ratio, γ	4
Helix pitch, λ	0.0030
Center distance, a	0.43
The second cut	
Synchronization ratio, γ	2
Helix pitch, λ	0.0030
Center distance, a	0.12

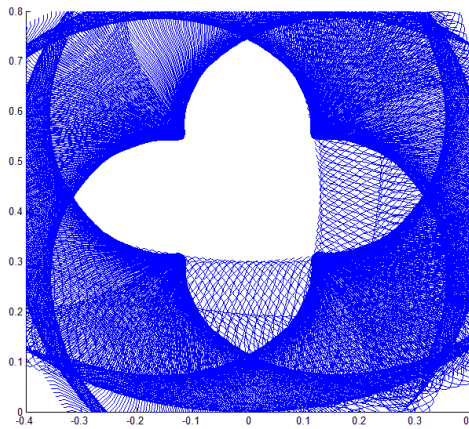


Fig. 3-20: Simulation of cutting the angular section

Finally, stitching the sections together, the entire machining plan is generated. Figure 3-21 shows the simulation results.

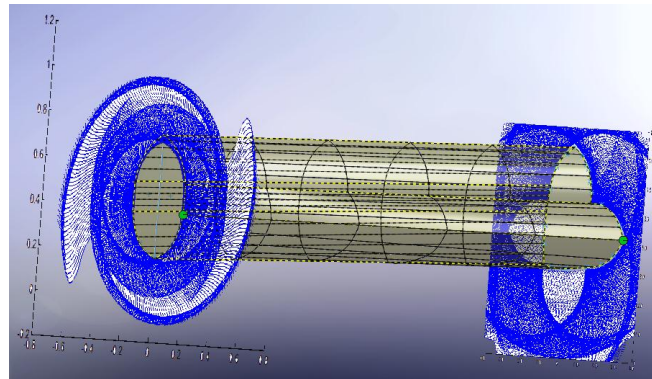


Fig. 3-21: Simulation result of Case 3

Through the parameters of simulation, above essence is based on the line in the equation to calculate several points, then using the curve or straight line segments connect them, such as literature [82, 83], but it cannot make a three-dimensional graphics, such as the

root cutting teeth of the transition, etc. The method of Literature [84] is that using cutting teeth drawn out to simulate the actually teeth, but this method also draws a two-dimensional graphic.

This section thought the generation method and the process of cutting, a three-dimensional model can be made, as shown in Figure 3-22. This method can improve the speed of the gear simulation. As a right transition with the root cutting curve, this method can be used for defect analysis and design of a knife. It not only may be used in standards gear simulation, but also can be used for a drive gear, modified gear and other available parts by using generation method as shown in Figure 3-23.

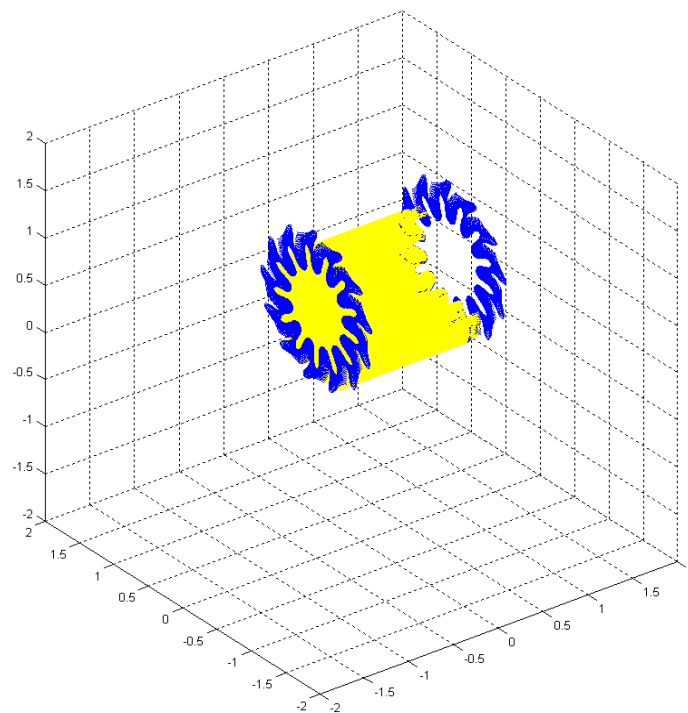


Fig. 3-22: 3D Simulation result of master gear

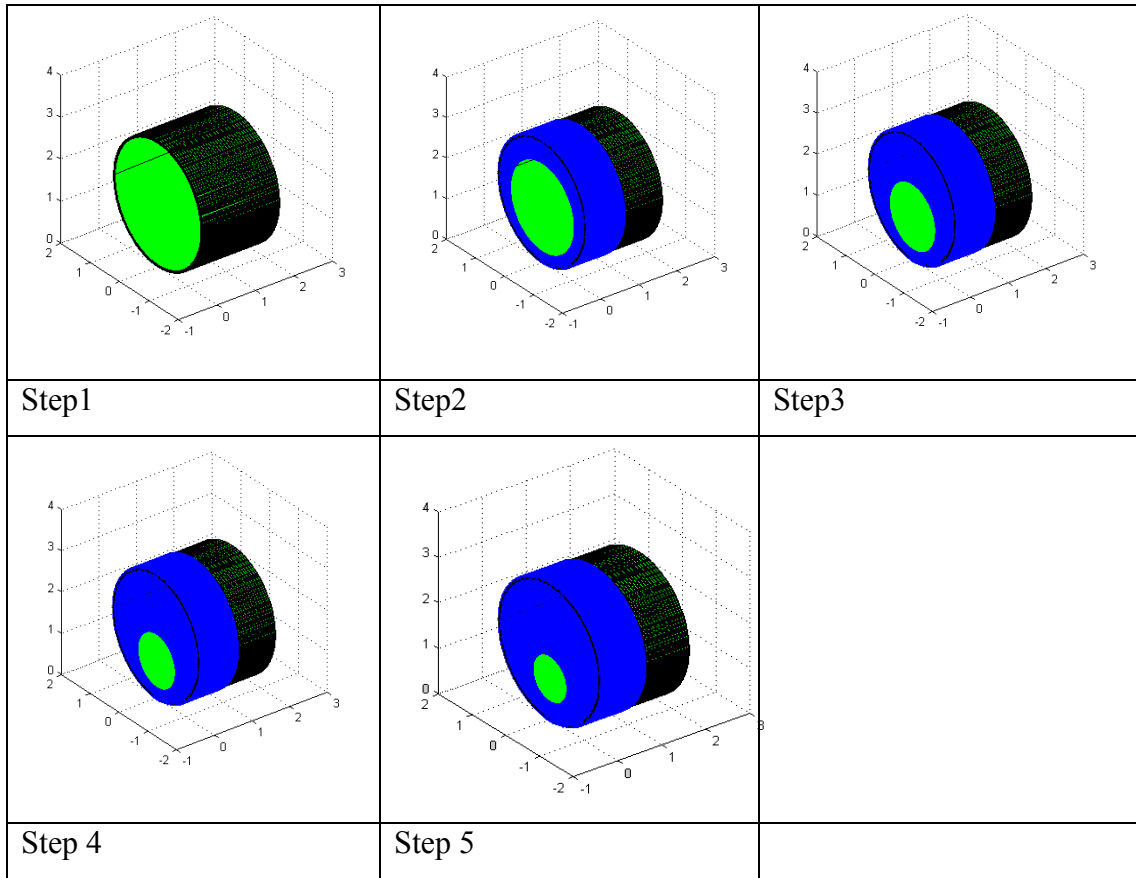


Fig. 3-23: Simulation process of eccentric part

3.4 Cutting Tests

The experiments were conducted on our Multi-Axes CNC Turn-Mill-Hob Machining Centre [74]. And, we use the same hob (Figure 3-10) for below cutting test. Four cases are studied in this chapter: (1) a 13 teeth gear; (2) A pentagon part; (3) An elliptical part and (4) A star part.

Case 1: A 13 teeth gear

With the synchronization accuracy measured, the gear hobbing performance of our system can be evaluated. We use the same tool for hobbing experiment; the tool is

shown in Figure 2-20. The corresponding gear profile of this cutter by simulation is shown in Figure 3-13 [53].

Using brass as workpiece material, a gear sample is machined and it is magnified using a CMM system, namely, Mitutoyo's Quick Vision Pro. [64]. Figure 3-24 is the magnified image of the sample gear, which is machined by our machine.



Fig. 3-24: The magnified sample gear machined by our machine

In order to compare the machined profile with the design profile, the machined profile is extracted using the CMM system and 3600 sample points are generated along the gear profile with an extraction accuracy of $\pm 3 \mu\text{m}$. Furthermore, the extracted gear profile is compared to the design profile and this comparison is shown in Figure 3-25. It can be observed in this figure that the machined profile is very close to the design profile. In order to quantify the machining error, an offset envelope will be generated around the design profile to fully enclose the machined gear profile. Figure 3-26 shows the machined gear profile enclosed by a $\pm 7.5 \mu\text{m}$ error bound.

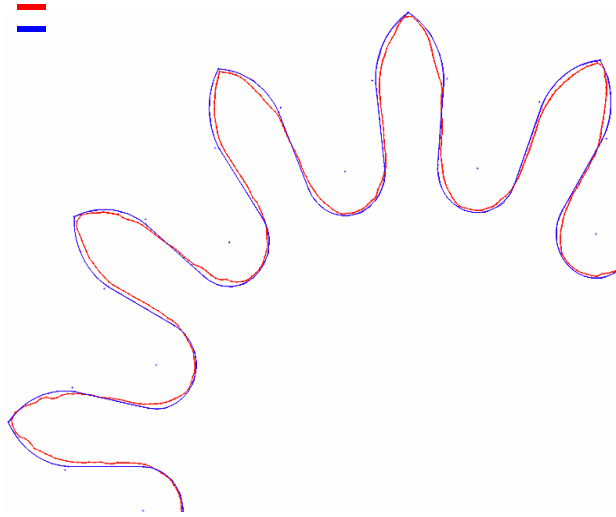


Fig. 3-25: Comparison between the machined profile and the design profile

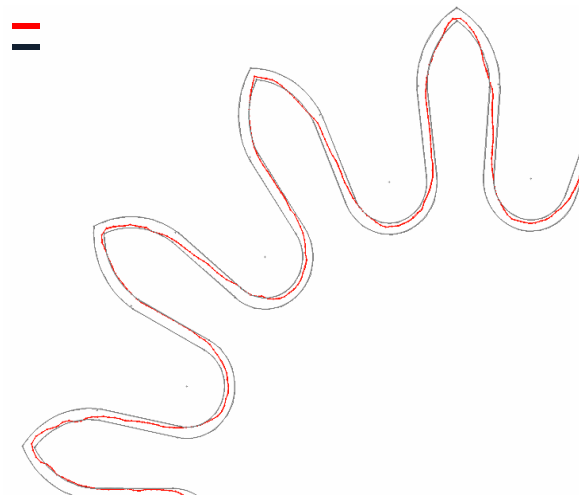


Fig. 3-26: The machined profile enclosed by the error $\pm 7.5 \mu\text{m}$ bound

Case 2: A pentagon part

Figure 3-27 shows the CAD model of the pentagon part. The exo-park radius of the part is 0.5 mm and the length of the part is 3 mm. The hobbing parameters are as follows: the synchronization ratio $\gamma = 4.8$, the helix angle $\lambda = 0.0045$ and the center distance $a = 0.7$. The tool path is shown in Figure 3-28. The experiment result is shown in Figure 3-29.

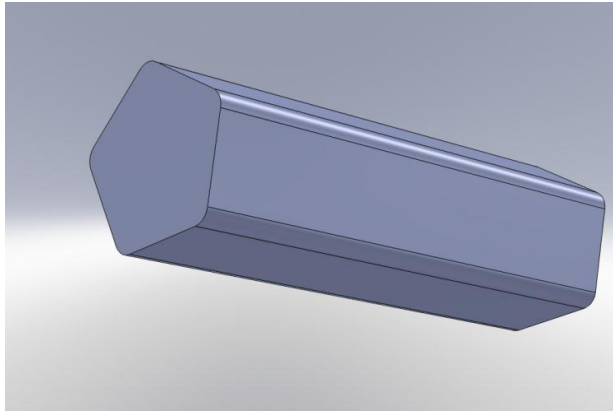


Fig. 3-27: The CAD model of Case 2

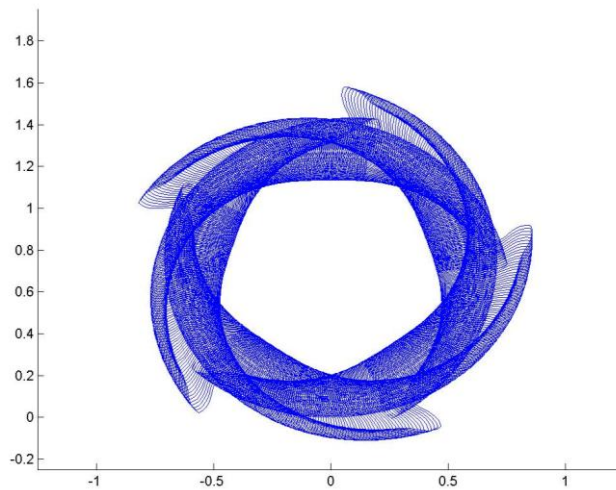


Fig. 3-28: The tool path of part



Fig. 3-29: A sample experiment result

The machined part is measured using a Mitutoyo CMM system Quick Vision Pro. Figure 3-30 shows the measurement result. The exo-park radius of the part is 0.50457 mm. For comparison purpose, Figure 3-31 shows the 2D profile of the CAD drawing in comparison to the simulation and experiment results. The sum-of-squares error between the design and the experiment is 0.0032 mm, less than 1%.

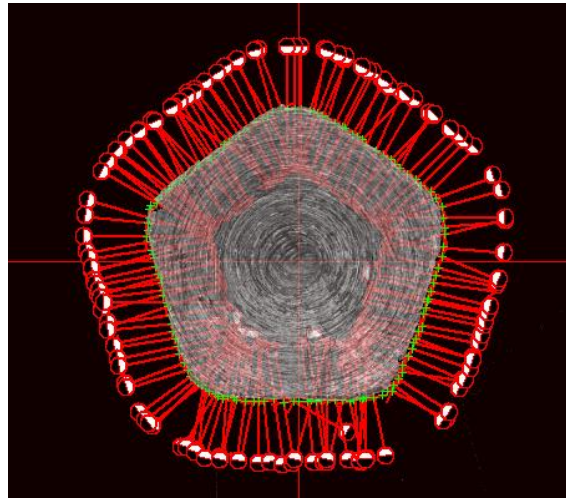


Fig. 3-30: The CMM measurement result

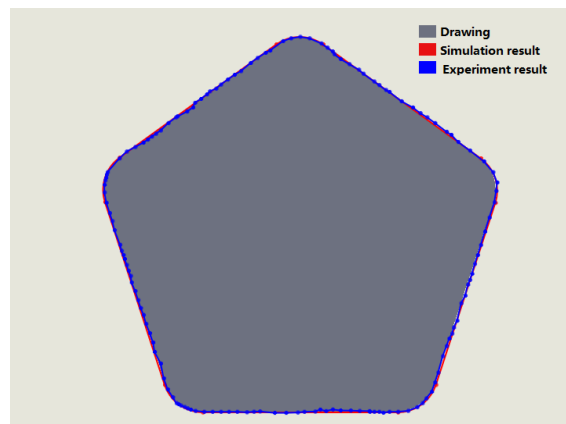


Fig. 3-31: The comparison in 2D

Case 3: An elliptical part

Figure 3-32 shows the 3D CAD model of the part. The major and minor axes of the part are 0.54 mm and 0.34 mm respectively. The length of the part is 3 mm. The hobbing

parameters are as follows: the synchronization ratio $\gamma = 12$, the helix angle $\lambda = 0.0030$ and the center distance $a = 0.43$. Figure 3-33 shows the tool path. Figure 3-34 shows a sample experiment result.

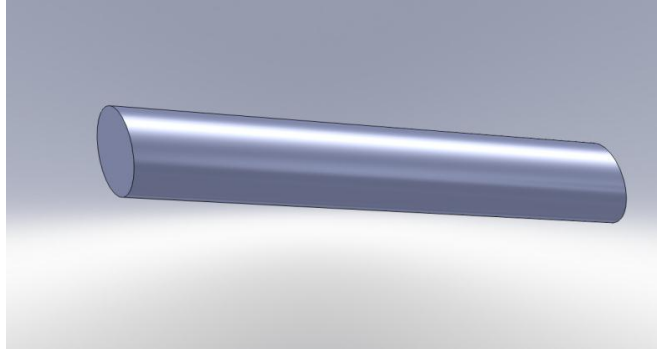


Fig. 3-32: The CAD model of the elliptical part

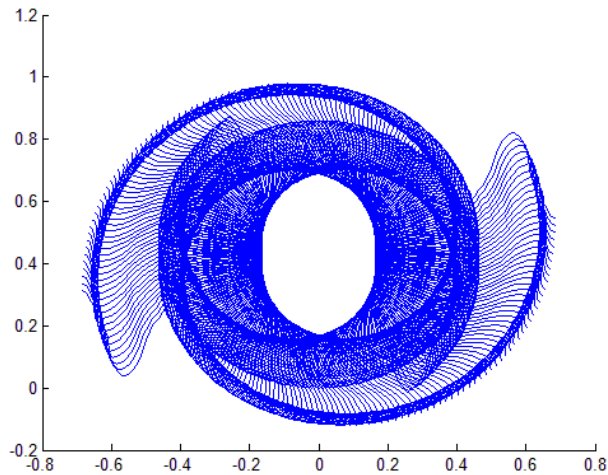


Fig. 3-33: The tool path of the part



Fig. 3-34: A sample experiment result

Figure 3-35 shows the CMM measurement result. The major axis is 0.5363 mm and the minor axis is 0.3384 mm. Figure 3-36 shows the 2D profile of the CAD drawing in comparison to the simulation and experiment result. The sum-of-squares error is 0.003 mm, again very small.

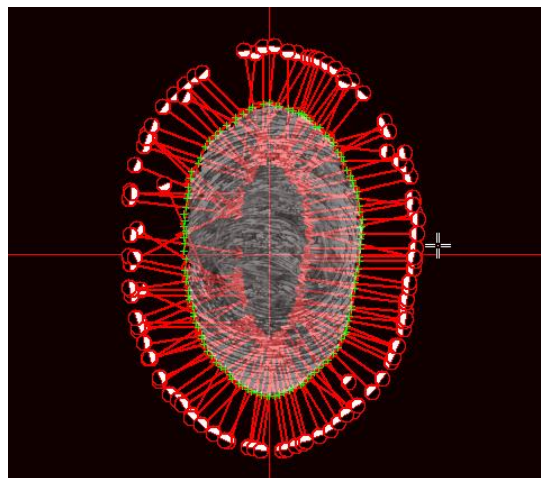


Fig. 3-35: The CMM measurement result

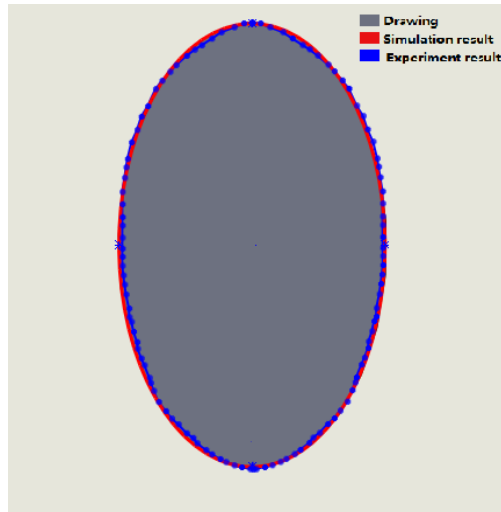


Fig. 3-36: The comparison in 2D

Case 4: A star part

Figure 3-37 shows the 3D CAD model of the part. The exo-park diameter of the part is 0.6 mm and the length is 3 mm. The hobbing parameters are as follows: the synchronization ratio $\gamma = 6$, the helix angle $\lambda = 0.0048$ and the center distance $a = 0.4$. Figure 3-38 shows the tooth path and Figure 3-39 shows the experiment result.

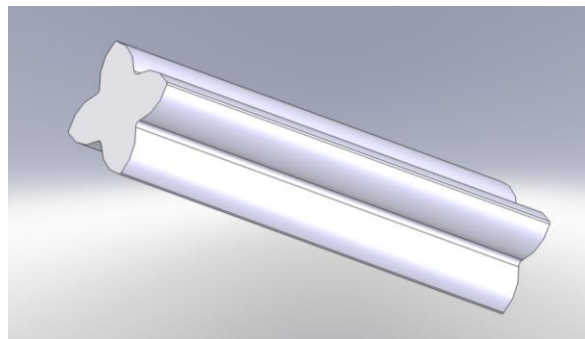


Fig. 3-37: The CAD model of the part

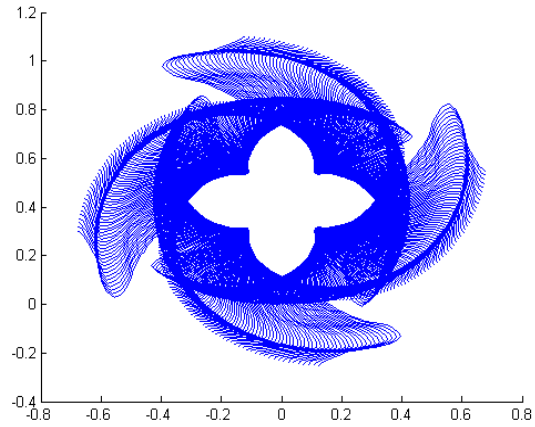


Fig. 3-38: The tool path of the part



Fig. 3-39: An experiment result

Figure 3-40 shows the CMM measurement result. Figure 3-41 shows the 2D CAD profile of the part with a comparison to the simulation and experiment result. The sum-of-squares error is 0.0028.

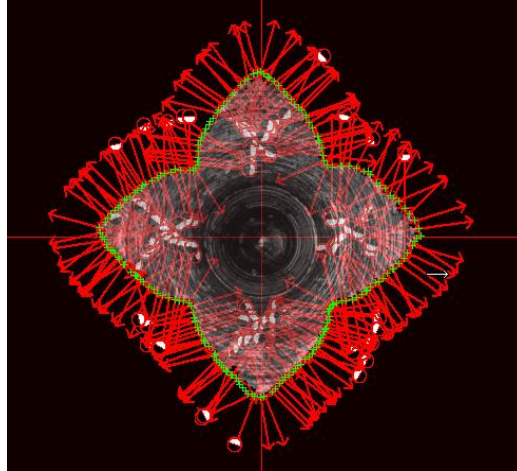


Fig. 3-40: The CMM measurement of the part

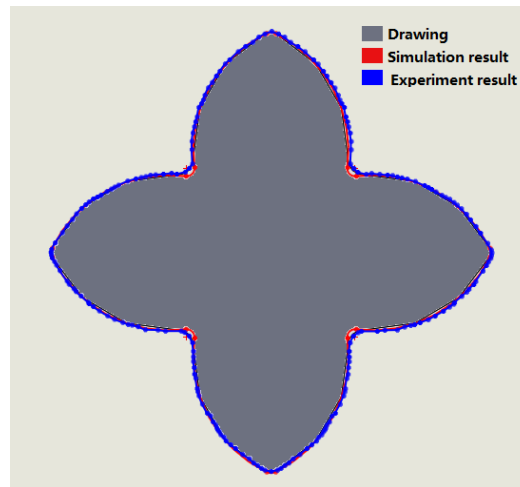


Fig. 3-41: The comparison in 2D

It is interesting to note that the part can also be cut using conventional turning - milling. We use the Material Removal Rate (MRR) to compare the efficiency between traditional machining method and our new method to machine this part. There are two assumptions for this comparison experiment: 1) machining this concave part; 2) each method only can use one machining tool.

At this time, the milling cutter must be able to get into the smallest concave corner, which is $d = 0.1$ mm. As a result, with standard cutting condition $S = 40,000$ RPM, $f = 420$ mm/min, and $a_p = 0.002$ mm, the Material Removal Rate (MRR) is:

$$MRR = a_p \times d \times f = 0.084 \text{ mm}^3/\text{min}$$

Using the presented method, on the other hand, the standard cutting condition is $S = 2700$ RPM, $f = 7$ mm/min, and hence the MRR is:

$$MRR = Lf \frac{B_w B_h}{2} = 0.7585 \text{ mm}^3/\text{min}$$

Where, L is the length of hob, f is the feed, B_w and B_h are the width and height of the teeth respectively. In other words, the presented method is about 9 times more efficient than that of the conventional milling method.

3.5 Summary

Based on the study above, following conclusions can be drawn:

- (a) By controlling the helix angle, λ , the synchronization ratio, γ , and the center distance, a , it is possible to hob many axial symmetric / asymmetric parts.
- (b) The presented method is efficient. In some cases, the Material Removal Rate (MRR) could be many times higher than the conventional method.
- (c) Our Multi-Axes CNC Turn-Mill-Hob Machining Center is capable for hobbing complex precision parts.
- (d) Not all the parts can be machined in this presented method.

Comparing to the existing technologies, the presented method has a number of advantages, including:

- It is simple and efficient, since it needs only one setup and just a few tools;
- It is reliable, since the multi-teeth hob is strong against tool breakage;
- It is precise, since the multi-teeth hob tool cuts only a small chip at a time and hence, will not induce excessive vibration and chatter;

- It is inexpensive, since it does not require complex tools and fixtures.

With these advantages, it is expected that the new method will find many applications in the near future.

Chapter 4:

Milling Axial Asymmetric Parts

4.1 A Brief Review

It is known that CNC machines are usually based on Cartesian coordinate system. In order to achieve a curved movement in Cartesian coordinate, the curve needs to be interpolated, either by a linear interpolator, or a circular interpolator, or a B-Spline interpolator, or a NURBS interpolator [85-87]. There are also other methods, such as the three L1 spline method proposed by Ming-Jun Lai [88], but their applications are limited. Among the aforementioned interpolators, the linear interpolator and the circular interpolator are the most popular and have been used as basic functional modules of CNC systems [89, 90]. Based on these modules, many complex contours may be generated. For example, Qiu and et al [91] used sequential circular arc interpolations to generate spiral curves.

Recently, the use of polar coordinate system in CNC machines has attracted some attention. In [92], Maeda and Ohno used polar coordinate and polar interpolation to construct multidimensional surfaces. In [93], Heap and Hogg extended the point distribution model in polar coordinate system. Comparing to Cartesian coordinate system, the polar coordinate system may have several advantages, especially for rotational axes. For example, in the polar coordinate system a circle can be generated by simply rotating the rotational axis. In this case, the interpolation error is zero, much better than that of the circular interpolation in Cartesian coordinate system [94]. Though, for complex curves, the interpolation in polar coordinate system is rather complex and is still a challenge for CNC programming.

For a complex contour, to plan the interpolation points based on polar coordinate are not an easy work. Traditionally, it is done by some aided CAM softwares, for example, MasterCAM [95], SolidWorks [96] and *et al.* But for the watch parts, few complex

contours are used, so the above softwares are not necessary to be used considering the machining cost.

4.2 The Theory

Figure 4-1 shows the difference between using Polar coordinate interpolation and Cartesian coordinate interpolation to machine parts. From this figure, we can get the characteristic by using Polar coordinate interpolation: 1) It is effective for machining centers that have rotational axes; 2) It is effective for machining rotational parts.

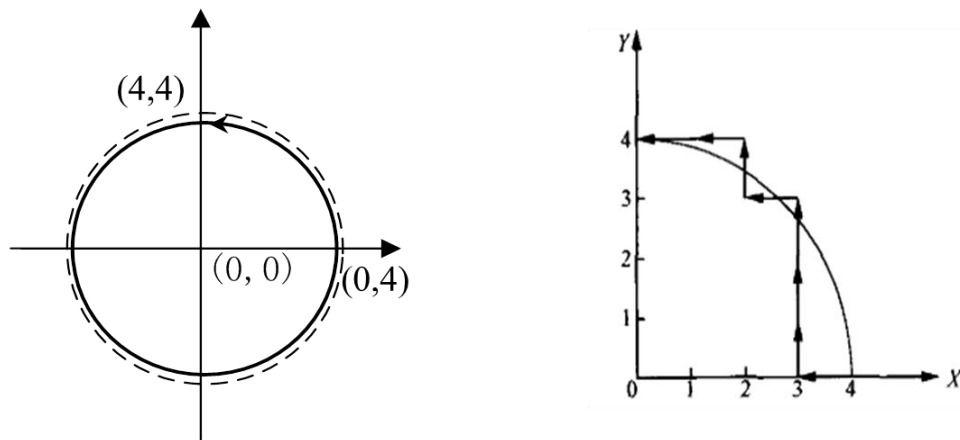


Fig. 4-1: the difference between using Polar coordinate interpolation and Cartesian coordinate interpolation to machine parts

Figure 4-2 shows the configuration for milling and grinding operations. As shown in the figure, $C2$ is the milling or grinding spindle. It is mounted on a table with linear axes $X1$ and $Z1$. $C1$ is the turning spindle that holds the workpiece. It is also a rotational axis. This configuration requires the control of two linear axes and a rotation axis. Therefore, the polar coordinate system is preferred.

This section presents a new CNC programming module using polar coordinate system. The module has been integrated into our CNC turn-mill-hob machining center.

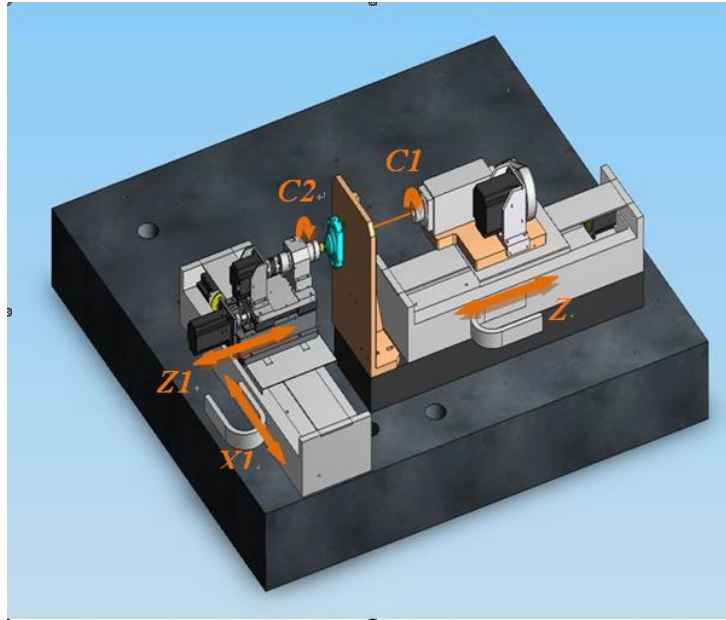


Fig. 4-2: The architecture for milling and grinding

The motion control in a polar coordinate system has two key parameters: the radius, r , and the angle, θ . The function relationship between these two parameters are as follows:

$$r = f(\theta), \quad \dot{r} = \frac{\partial}{\partial \theta} f(\dot{\theta}) \quad (4-1)$$

or

$$\theta = f^{-1}(r), \quad \dot{\theta} = \frac{\partial}{\partial r} f^{-1}(\dot{r}) \quad (4-2)$$

Similar to that of the Cartesian coordinate system, a curve in the polar coordinate system can be approximated by a sequence of linear, circular and/or other types of curves. In this chapter, we developed two basic interpolation functions: one is linear interpolation and the other is circular interpolation, as detailed below.

4.2.1 The expression of curves in polar coordinate system

In polar coordinate system, the expressions of a circle and a line are as follows:

Circle

If the center of a circle is at the origin of the coordinate system, the function of the circle is:

$$r = a \quad (4-3)$$

where, a is a constant. Note that only the angle moves and its velocity is $\dot{\theta}$. The positioning error in the angular direction is the main source of trajectory errors.

If the center of a circle is not at the origin, then the circle can be expressed as follows:

$$\theta = \arccos \frac{r^2 - a^2 + r_0^2}{2rr_0} + \theta_0 \quad (4-4)$$

where (r_0, θ_0) is the center of the circle. The velocity relationship is

$$\dot{r} = r_0 \sin(\theta - \theta_0) \cdot \dot{\theta} + \frac{r_0}{r} \cos(\theta - \theta_0) \quad (4-5)$$

Line

In polar coordinate system, line needs to be interpolated. Suppose the beginning and the ending points of a line are (r_1, θ_1) and (r_2, θ_2) , respectively, then the function of the line can be expressed as follow:

$$r = \frac{r_1 r_2 \sin(\theta_1 - \theta_2)}{r_1 \sin(\theta_1 - \theta) + r_2 \sin(\theta - \theta_2)} \quad (4-6)$$

In particularly, if θ_1 is zero, Equation (6) is simplified as

$$r = \frac{r_1 r_2 \sin \theta_2}{r_1 \sin \theta + r_2 \sin(\theta_2 - \theta)} \quad (4-7)$$

Moreover, its velocity relationship is

$$\dot{r} = \frac{r_1 r_2 \sin \theta_2 \cdot \dot{\theta} \cdot [r_1 \cos \theta - r_2 \sin(\theta_2 - \theta)]}{[r_1 \cos \theta + r_2 \sin(\theta_2 - \theta)]^2} \quad (4-8)$$

It shall be pointed out that in the polar coordinate system, every interpolation segment of a line is Archimedean spiral, therefore the accuracy is a little worse than that of Cartesian coordinate system.

4.2.2 Interpolation in polar coordinate system

In the polar coordinate system, a curve can be approximated by a sequence of linear and / or circular segments. Each segment is described by $(\Delta\theta, \Delta r)$, where $\Delta\theta$ and Δr denote the incremental values in angle and radius, respectively. From Equations (3), (4) and (7), the position of each circular segment can be expressed based on some rules such as Digital Differential Analyzer (DDA).

Moreover, the velocity of a segment is:

$$v = \pm \sqrt{\dot{r}^2 + \dot{\theta}^2} \quad (4-9)$$

According to Equations (5) and (8), the velocities in radial and angular directions can be also derived.

The interpolation processes are given below:

Circular interpolation

If the center of a circle is at the origin of the polar coordinate system, then according to Equation (3) the interpolated positions are $(r_0, \theta_0 + \Delta\theta \cdot i)$, where $i = 1, 2, \dots, n$, and n is the number of interpolation points. Moreover, the velocities are 0 and $\dot{\theta}$ respectively.

If the center of a circle is not at the origin of the polar coordinate system, then the interpolation positions can be determined using Equation (4). Suppose the i^{th} interpolation point is (r_i, θ_i) and the movement increments are:

$$\Delta\theta_i = \theta_i - \theta_{i-1} \quad (4-10)$$

$$\Delta r_i = r_i - r_{i-1} \quad (4-11)$$

Then the interpolation points are $(r_0 + \sum_{j=1}^i \Delta r_j, \theta_0 + \sum_{j=1}^i \Delta\theta_j)$, where $i = 1, 2, \dots, n$, and n is the number of interpolation points.

Linear interpolation

If $\theta_1 = 0$, then the interpolation points can be calculated using Equation (7). Suppose the i^{th} interpolation point is (r_i, θ_i) and the i^{th} increment position is $(\Delta r_i, \Delta\theta_i)$, then the

interpolation point can be described as $(r_1 + \sum_{i=1}^n \Delta r_i, \theta_1 + \sum_{i=1}^n \Delta\theta_i)$.

4.2.3 The Interpolation programming module

Based on the interpolation methods above, two programming modules are developed. For the purpose of easy operation, the center is set at the origin and θ_1 is set for 0 while

calculating the interpolation positions of a line. In case the center is not at the origin and θ_1 is 0, a simple shift is needed.

Circle interpolation

For a circular contour, only the rotation axis moves, so the motion control is as follows:

Step 1: get the beginning position (r_0, θ_0) and the ending position (r_0, θ_1) ,

Step 2: get the increment of the rotation axis $\Delta\theta_i$

Step 3: move to $(r_0, \Delta\theta_i)$

Then the interpolation positions can be achieved by DDA. The program module is a simple G code:

```
G20 C theta2 X r2
```

where, C and X are the rotation and the linear axes respectively, theta2 and r2 denote the ending angle the rotation axis and the ending position of the linear axis, respectively. Note that the initial position is the current position.

Figure 4-3 illustrates the circular interpolation module. Note that the beginning position is $(r_0, 0)$.

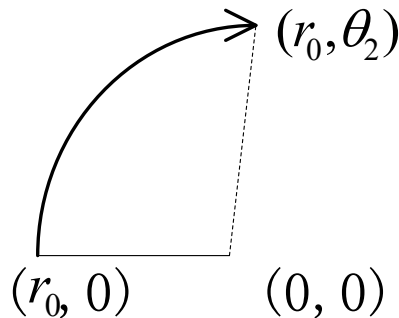


Fig. 4-3: The circular interpolation principle

Line interpolation

For line interpolation, the motions from both the rotation axis and the linear axis are needed. The procedure of the motion control system is as follows:

Step 1: get the beginning position (r_1, θ_1) and the ending position (r_2, θ_2)

Step 2: get the incremental step $\Delta\theta_i$

Step 3: calculate the interpolation positions $(\Delta r_i, \Delta\theta_i)$

Step 4: move to $(r_1 + \Delta r_i, \theta_1 + \Delta\theta_i)$

The program module is a simple G code:

```
G21 C theta2 X r2
```

where, theta2 and r2 denote the ending angle of the rotation axis and the ending position of the linear axis, respectively. Figure 4-4 illustrates the linear interpolation module. Note that before executing the G code, the beginning position is $(r_1, 0)$, and the ending position is $(r_2, \theta_2 - \theta_1)$.

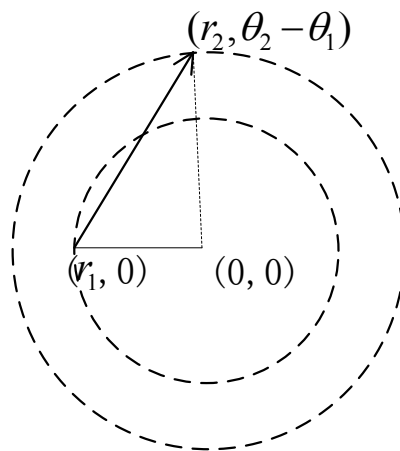


Fig. 4-4: The linear interpolation principle

4.2.4 Analysis of interpolation errors

The interpolation errors in polar coordinate system can be calculated based on geometry. If the center of a circle is at the pole, the movement of the linear axis is 0, then the interpolation error is 0.

After a curve is interpolated in the polar coordinate, the movement segmentation can be described as a two-dimensional increment $(\Delta\theta, \Delta r)$. Usually, the increment is executed by a numerical control system by commercial Corps., then the interpolation errors can be analyzed.

With a linear interpolator, the velocity relationship of $C1$ and $X1$ axes is:

$$\Delta r = b \cdot \Delta\theta \quad (4-12)$$

When $\Delta\theta$ is small enough, Equation (12) can be written as

$$\dot{r} = b\dot{\theta} \quad (4-13)$$

From Equation (4-13), the position relation can be achieved

$$r = a + b\theta \quad (4-14)$$

where a and b are constants. This equation shows an Archimedean spiral and the parameters in Equation (4-14) are

$$a = r_1 - \frac{r_1 - r_2}{\theta_1 - \theta_2} \theta_1 \quad (4-15)$$

$$b = \frac{r_1 - r_2}{\theta_1 - \theta_2} \quad (4-16)$$

Changing the parameter a will turn the spiral, while b controls the distance between

the arms.

Then the maximum absolute contour error can be estimated by

$$E_{\max} = \max\{|r_i(n) - r(n)|\} \quad (4-17)$$

In polar coordinate system, Archimedean spiral is generated when radial and angular coordinates are proportionally increasing. When generating an Archimedean spiral, the error will be very small. This will be very useful to generate accurate curve contour according to Ref [91].

4.3 Cutting Tests

The interpolation module based on polar coordinate is integrated into the developed machine center. Figure 4-5 shows the hardware Architecture of the control system.

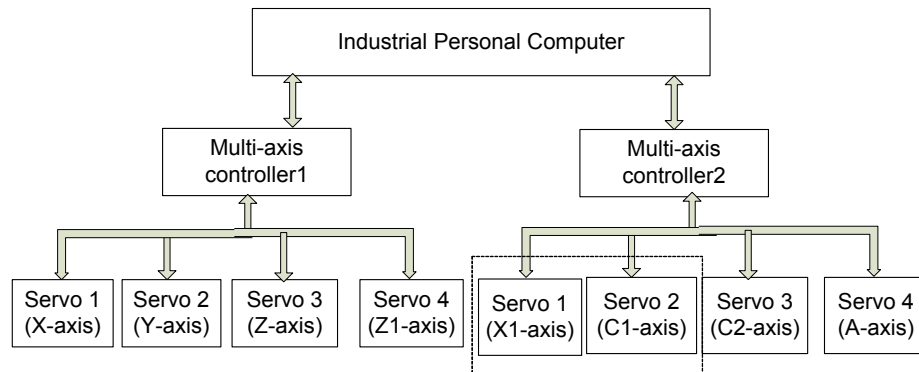


Fig. 4-5: Hardware Architecture of the control system

The system is controlled by two multi-axis controllers which are manufactured by Googoltech Technology Ltd with the model type GT-400-SV [55]. X1- and C1- axes interpolated in polar coordinate are controlled by Multi-axis controller2. And the multi-

axis controllers are inserted into an Industrial Personal Computer (IPC) through a Peripheral Component Interconnection (PCI) slot. All motion control programs including the polar coordinate programming module are developed in the IPC.

The typical application of the developed polar coordinate programming module is to machine a part called by Date Corrector Pinion which is a critical component in a mechanical watch. Usually, the part is difficult to be machined because of its complex contours and small size. Figure 4-6 shows its drawing.

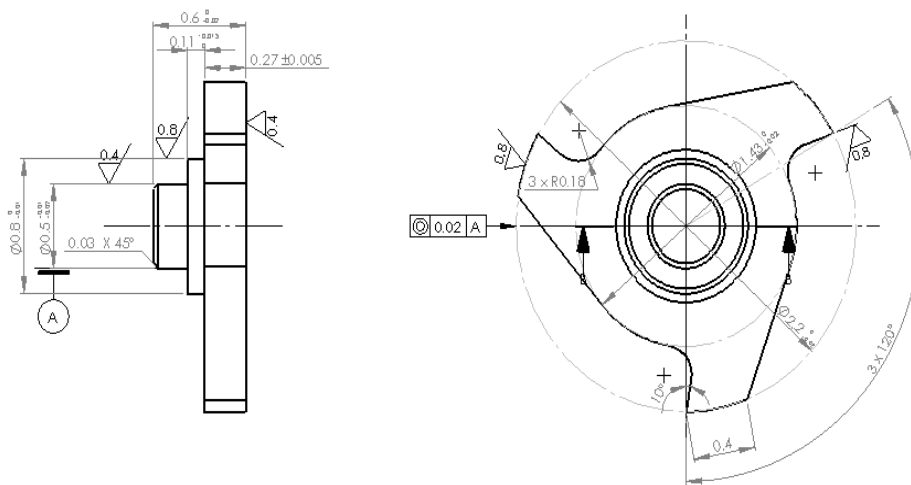


Fig. 4-6: The drawing of the Date Corrector Pinion

4.3.1 The machining process of Date Corrector Pinion

The machining process of Date Corrector Pinion includes turning and milling. The part can be machined by the developed machine center with only one time of fixture operation.

Before milling operations, the rough turning and the finish turning operations are used to machine cylindrical surfaces. In these machining processes, C1 axis is used as a spindle axis and worked in velocity mode.

In order to machine the contours shown in the right view of Figure 4-5, C1 axis should be changed as position mode to generate a rotational movement.

Using a milling tool with the diameter of 0.36mm, the contour can be generated by G20 and G21. The following G codes show one third of the machining process

F0.5

G20 C0.69 X1.28

G21 C1.486 X0.895

G20 C2.269 X0.895

G21 C2.094 X1.28

The other two thirds of the machining process are two iterations of the above process.

4.3.2 Simulation and experimental results

Simulation is made to verify the effectiveness of the designed interpolation module and the interpolation result is shown in Figure 4-7. It displays a good profile of Date Corrector Pinion.

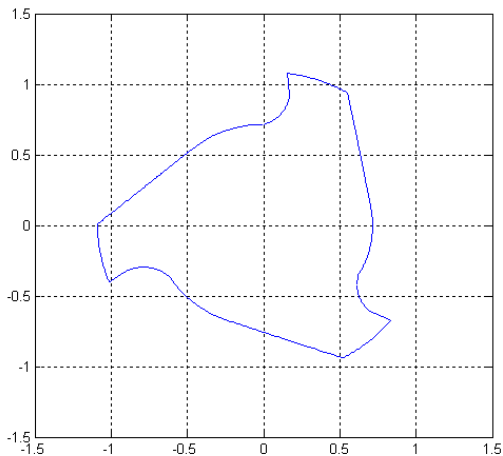


Fig. 4-7: Simulation result

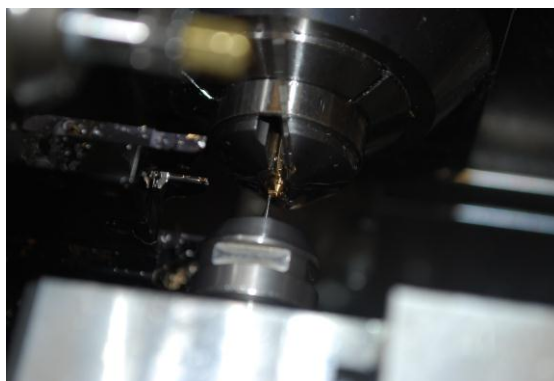


Fig. 4-8: The milling operation



Fig. 4-9: The machined Date Corrector Pinions

The milling operation of the developed gear hobbing machine center is shown in Figure 4-8 and the Date Corrector Pinion machined by the machine center and Deco10a are shown in Figure 4-9. From Figure 4-9, it can be concluded that the profile is in accordance with that in Figure 4-7. Several key dimensions of 10 random samples are measured to analyze the contour errors of the workpieces and the results are shown in Table 4-1. From the table it can be concluded that the developed programming module can help to machine qualified workpieces with linear and circular contours.

Table 4-1: Measurement results of the machined Date Corrector Pinions
(Material: AP20, Machining time: 5 minutes/piece, in mm)

	A	B	C	D	E
Nominal value	Φ2.200	Φ1.43	0.270	0.110	0.500
Tolerance	0	0	+0.005	+0.015	-0.010
	-0.020	-0.020	-0.005	0	-0.020
1	2.190	1.418	0.271	0.120	0.488
2	2.188	1.417	0.273	0.118	0.485
3	2.187	1.421	0.270	0.122	0.488
4	2.188	1.418	0.271	0.116	0.486
5	2.190	1.418	0.274	0.118	0.486
6	2.192	1.420	0.272	0.120	0.490
7	2.192	1.418	0.272	0.121	0.486
8	2.190	1.416	0.271	0.120	0.488
9	2.188	1.416	0.273	0.118	0.489
10	2.190	1.418	0.272	0.120	0.488
Max	2.192	1.420	0.274	0.122	0.490
Min	2.187	1.416	0.270	0.116	0.485
Mean	2.1895	1.418	0.2719	0.1193	0.4874
STD	0.001716	0.001563	0.001197	0.001767	0.001578

Also the developed programming module is easy to be used with only a little G codes. But by using Deco 10a the G codes are very long and must be generated by CAM software.

Table 4-2 lists the detailed comparison of our Multi-Axes CNC Turn-Mill-Hob Machining Center and Deco10a. From the comparison, it can be concluded that the developed interpolation module has high performance and easy to be used in our machine center.

Table 4-2: The comparison of our machining center and Deco10a in program module

	our machining center	Deco10a
Contouring accuracy	High	Low
How to generate G Code	By writing G code	By commercial CAM software
G code format	Special	Standard
Cost	Low	High

4.4 Summary

In the chapter, the basic interpolation principles of polar coordinate are described. Based on interpolation principles, a polar coordinate programming module is proposed and developed. The developed module presents as two special G codes and is integrated into the programming system of the developed Multi-Axes CNC Turn-Mill-Hob Machining Center.

Comparing with the commercial programming methods, the special programming module is easier to be used by CNC programmers.

Chapter 5:

Machining Dental Implants

5.1 A Brief Review

Dental implant has been attracting more and more attention due to their advantages of reliable and comfortable [97-99]. It is estimated that 10% of the people will need dental implants in their life time [100]. Owing to its reliable functional and aesthetic results, dental rehabilitation with implants has been widely accepted by doctors and patients in recent decades [101]. In long-term clinical application, the survival rate for dental implants is over 90% [102]. In the mid-1960s, orthopedic research by Branemark demonstrated the phenomenon of osseointegration, whereby a biocompatible metal could be structurally integrated into living bone at a biochemical level [103]. The application of this theory to dental implants reduced the dependence on mechanical interlocking and allowed the development of implant systems in a more versatile endosseous design [104]. Subsequently, it was realized that subtle changes in shape, length, and width of endosseous implants could influence success rates, [105] and implant manufacturers began providing implants in varying designs. The size and shape of implants have evolved to fit current surgical concepts and prosthetic design.

Now, companies offer a system for customer to choice. For example, the diameter of implant are 1 mm、1.2 mm、1.4 mm、3.75 mm and 4.2mm, the length are from 2 to 14 mm in products on the market [106]. But, no one research on and product the custom-made dental implants. A list of manufacturers of dental implants is shown in Table 5-1. Traditional implants have their limitation and they are not better fit due to the difference of patient's oral condition. In implant surgery, dentist needs to drill a hole in patient's alveolar bone, as shown in Figure 5-1[107]. Owing to there is only some model implants in market and everyone's oral condition is different, traditional implants have some problem in the surgery: one the one hand, as the requirement of fix model implant, the drilling hole must be bigger than actual teeth-root, which will lead to excess bone

loss; on the other hand, in some special case, you cannot drill the fix hole of model implant due to the special space and bone mass of patient.

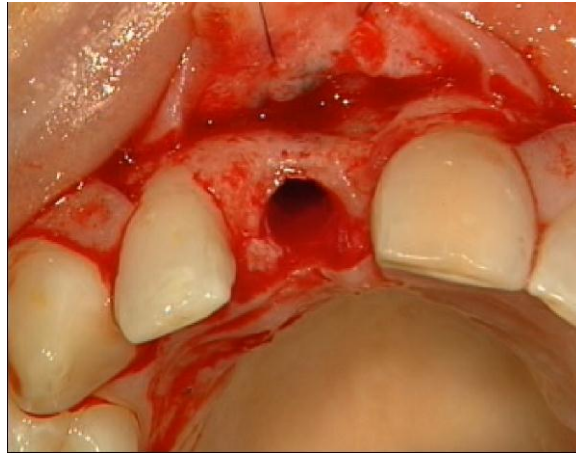



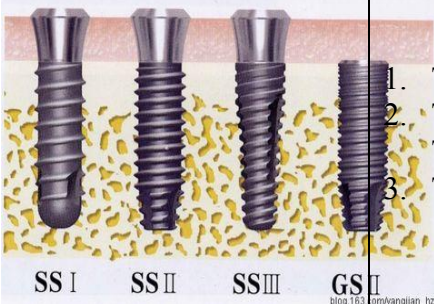
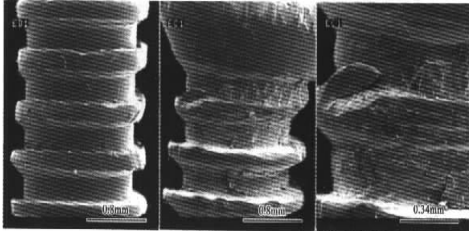


Fig. 5-1: Drilling hole in patient’s alveolar bone [107]

Table 5-1: A list of manufacturers of dental implants

Brand	Features
<p data-bbox="370 1024 665 1129">Branemark, (Nobelpharma system) England</p> 	<ol data-bbox="722 1165 1388 1312" style="list-style-type: none"> 1. Titanium purity is 99.75%; 2. Precise thread structure in surface; 3. Easily screwed into position and assigned stress by the thread
<p data-bbox="414 1455 625 1497">ITI, Switzerland</p> 	<ol data-bbox="722 1512 1388 1837" style="list-style-type: none"> 1. Quaternary titanium is machined by pure business titanium (ISO5832/1); 2. Microscopic porous Ti-plasma coating on surface; 3. Transgingival cervical is calathiform structure and it has smooth machined surface; 4. Conducive to cervical soft-tissues accreted and prevention the infection in periodontal soft-tissues.

<p>IMZ, Germany</p> 	<ol style="list-style-type: none"> 1. The material is medical pure titanium and the shape is like natural root of tooth; 2. 3 surface modification method: TPS, HA and SLA; 3. Less damage to root of tooth, especially applied to immediate restoration implant technique.
<p>OSSTEM, Korea</p> 	<ol style="list-style-type: none"> 1. The market share is the first in Korea; 2. Two methods: submerged method (GS) and Transgingival method (SS); 3. Taper connection design.
<p>CDIC, Mainland China</p>	<ol style="list-style-type: none"> 1. Hua Xi Implant Center, the first company has production license and registration license in China; 2. Pure titanium, thread structure. 3. The disadvantages of this implant: <ul style="list-style-type: none"> a. The machining precision is low and the surface is roughness; b. A large amount of impurities existed in implant, which decreased material strength and corrosion resistant property; c. Easily crumbled due to it is lower intensity. 

Besides, in posterior jaw regions with bones of poor texture, the survival rate is lower, ranging from 50 to 80% [108]. It is often hard to estimate the optimal primary stability in the posterior jaw, which leads to higher implant failure rates [109]. In general, the success of the success of dental implants is related to the quality and quantity of local bones, implant design and surgical technique [110]. Implant diameter and length are

accepted as key factors [111] [112]. Especially, in patients with a compromised medical condition (e.g. due to irradiation therapy or bone metabolic disorders, such as osteoporosis), implant failure rates are still substantially higher compared to those in healthy patients [113] [114]. Although some researchers begin to realize that thread geometry of implant has significant effects on the biomechanics of implant [115], there are only limited studies focusing on using different geometrical thread of the same implant to fit different bone quality. From above mentioned, we know that implant diameter, length, and shape is so important and they should be designed according to different patient's oral condition. The understanding of how these variables may affect implant success in varying qualities and quantities of bone allows the clinician to more accurately assess the potential success of an implant in a particular situation [97]. So, design a custom-made dental implant system is desirable and practical.

Another key problem of custom-made dental implant is manufacturing. Dental implant is difficult to machine due to its complex features and its material (titanium) [116]. With the ever increasing demand for tight tolerance and increased complexity and accuracy, traditional machine tools have become ineffective for machining them [117]. Fortunately, our Multi-Axes CNC Turn-Mill-Hob Machining Center can machine our custom-made dental implants accurately and efficiently [118].

5.2 The Database of Custom-made Dental Implant

Our technology is based on biomechanics. After patient's CT scan, we build the custom model by using our database of custom-made dental implant. Then, we use FEA and RP prototype for dentists analyze and modify. Finally, the automatic programming machining is used by our machining center. The design and production process is shown in Figure 5-2. This system will not only fill the Chinese domestic gaps, but also improve dental implantation and promote the process of immediate implantation theory in the world.

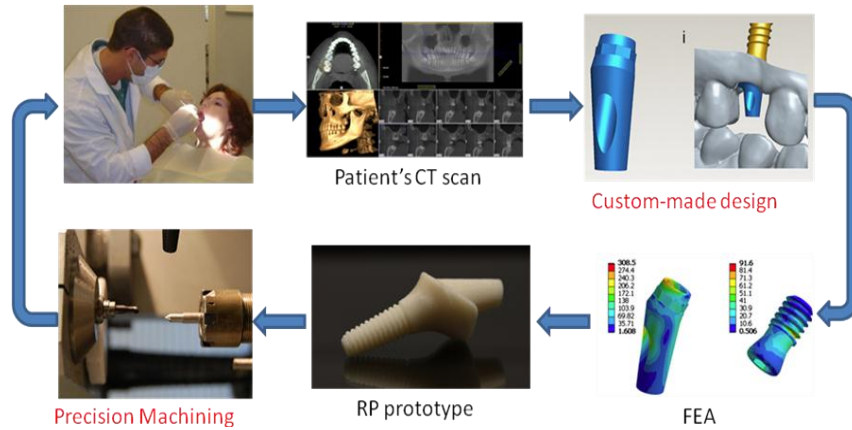


Fig. 5-2: The design and production process

Dental implant consists of three parts: implant (screw), abutment and connected component. Implant diameter is the dimension measured from the peak of the widest thread to the same point on the opposite side of the implant. The diameter measures the outside dimension of the thread. Implant diameter is not synonymous with the implant platform, which is measured at the interface of the implant connected with the abutment [97]. Because a variety of implant widths and platforms are available, a wide-platform implant is not always coincidental with an increased diameter of the implant thread. The length and diameter of implants were originally designed to allow the use of these implants in the average alveolar processes. Currently available implants vary in diameter from 3 to 7 mm [119]. The requirements for implant diameter are based on both surgical and prosthetic requirements. To gain maximum stability from the cortical plates of alveolar bone, the width of implants is designed to engage as much of the buccal and lingual plates as possible. Implants used for partially edentulous or single tooth spaces should also fit into the constraints [120]. The implant parameters and its optimization are shown in Figure 5-3 and Figure 5-4.

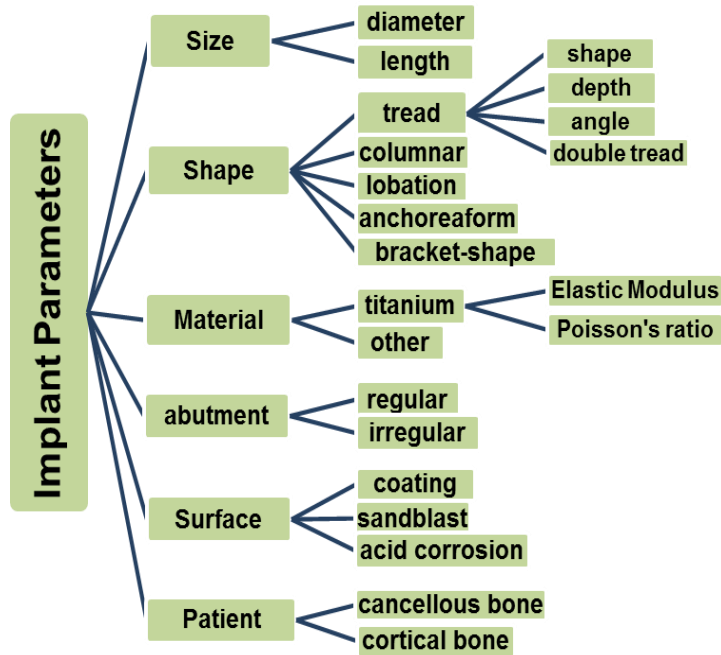


Fig. 5-3: The parameters of implant

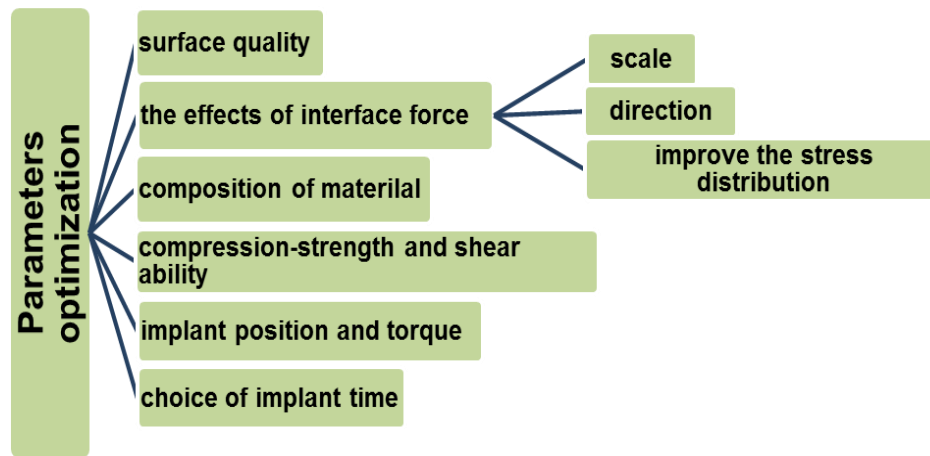


Fig. 5-4: Parameter optimization

Our custom-made database is based on the geometrical parameters of the implant, the patient's bone tissue, surface conditions and other parameters, as shown in Figure 5-5. We resolve the geometry of the implant as its diameter, length, pitch, abutment's angle, shape of screw, taper of screw and others. Using this method, we can build the database of custom-made dental implant (shown in Figure 5-6) [121] and find the best implant's parameters according to patient's oral space, gum and alveolar bone.

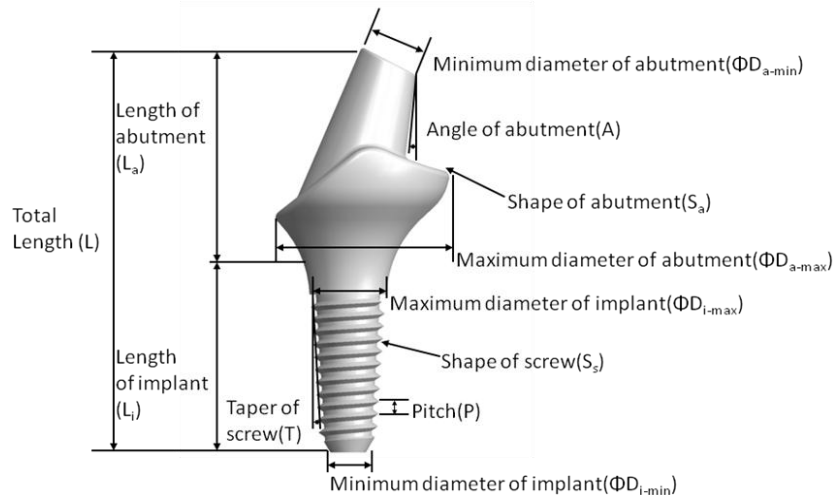


Fig. 5-5: Feature-based design of dental implant



Fig. 5-6: The database of custom-made dental implant [121]

The shapes of dental implants have varied from traditional root forms to blade and subperiosteal designs. The shape of dental implants has been one of the most contested aspects of design among the endosseous systems and may have an effect on implant biomechanics. We can design the “best-fit” dental implant for patients after calculating by our database. Figure 5-7 shows one example of “best-fit” condition.

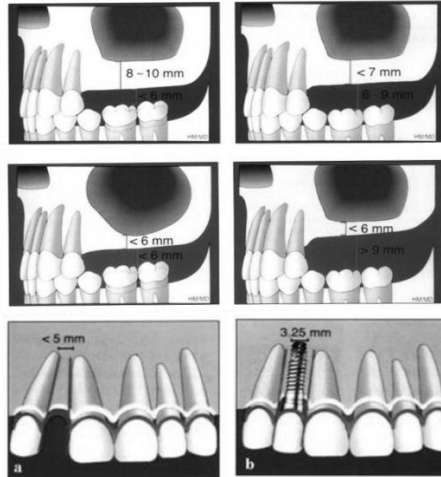


Fig. 5-7: One example of ‘best-fit’ condition

Most current implants systems are available as solid or hollow screws or cylinders. Some implant manufacturers provide implants in both shapes and recommend their use in different types of bone. In one study, screw-shaped implants provided the greatest retention immediately after implant placement. To enhance initial stability and increase surface contact, most implant forms have been developed as a serrated thread. It is believed that thread geometry has a significant, positive effect on implant biomechanics. Pitch, the number of threads per unit length, is an important factor in implant design [122]. Increased pitch and increased depth between individual threads allows for improved contact area between bone and implant, and may modify the biomechanical properties of screw-shaped implants [123]. But unfortunately, in some special case, single-thread is not enough for the earliest stability of implant. Because there are two type bones: cortical and cancellous. Different geometrical thread of implant can be employed to different bone quality, such as cortical or cancellous bone, which undoubtedly can decrease the stress around the implant. So, in our database, we consider this problem and using dual-tread design to solve special or difficult cases, as shown in Figure 5-8.

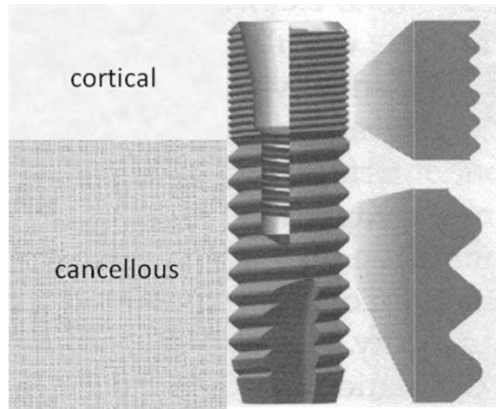


Fig. 5-8: Dual-tread design

5.3 The Design and FEA

From Figure 5-2: our design and production process, we can do the experiment validation. In according to patient's actual oral condition (shown in Figure 1), we build a plastic model, as shown in Figure 5-9.



Fig. 5-9: The plastic model

Using custom-made database, we get the best-fit implant as its diameter, length, pitch, abutment's angle, shape of screw, taper of screw and other parameters in this case, as shown in Table 5-2.

Table 5-2: The best-fit parameters in this case

Name	Value
Total length	11mm
Length of abutment	4mm
Length of implant	7mm
Angle of abutment	12°
Minimum diameter of abutment	2.5mm
Maximum diameter of abutment	5.5mm
Minimum diameter of implant	3mm
Maximum diameter of implant	4mm
Taper of screw	4°
Shape of screw	Single-Tapered thread
Pitch	0.5mm

Figure 5-10 shows the 3D drawing by using these parameters. To compare the biomechanical behaviors of this dental implant by dimensional finite element analyses, the FEA model set up in Figure 5-11 and its material properties and boundary conditions shown in Figure 5-12.

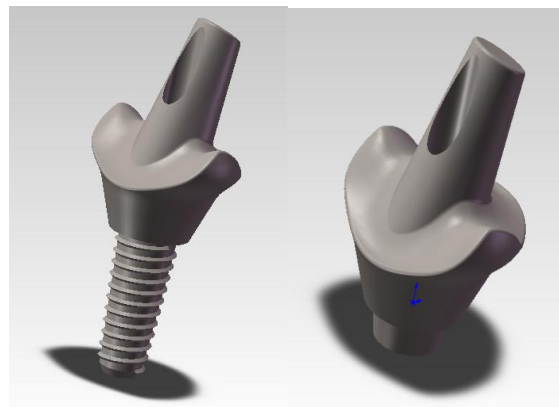


Fig. 5-10: The 3D drawing of this custom-made dental implant

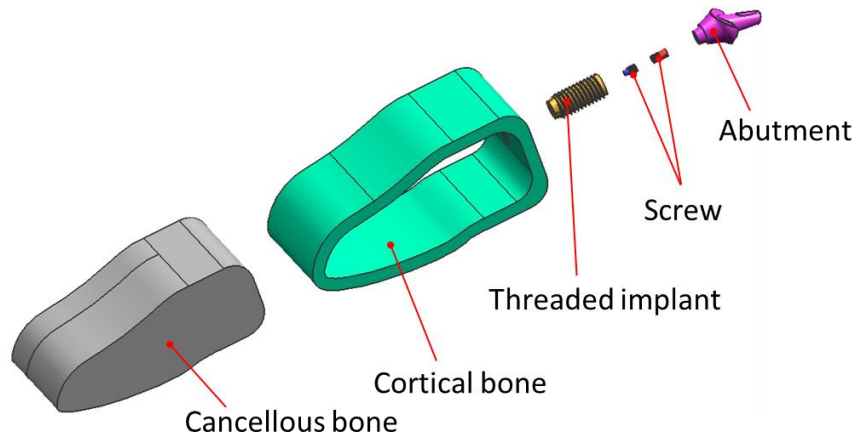


Fig. 5-11: The model of FEA

Material	E (GPa)	ν	ρ (kg/m ³)	Reference
Abutment	110	0.35	4500	Ma et al. (2006)
Screw	110	0.35	4500	Ma et al. (2006)
Cortical bone	14	0.30	1700	Rho et al. (1993)
Trabecular bone	3	0.30	270	Rho et al. (1993)
Titanium (Ti)	110	0.35	4500	Lin et al. (2006)

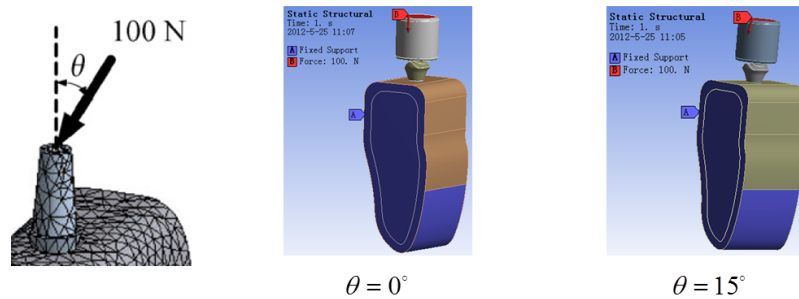


Fig. 5-12: The material properties and boundary conditions

From Figure 5-12, we can know that 100 N loads were applied along the implant axial ($\theta = 0^\circ$) and buccolingual directions ($\theta = 15^\circ$) respectively. The Max EQV stresses in jaw bones and the Max displacement in implant-abutment complex were evaluated. The average Poisson's ratio of this patient's alveolar bone is 0.3 and Yield strength of our implant's material is about 800Mpa. Figure 5-13 to Figure 5-16 show the result as equivalent Stress and total Deformation in two types respectively.

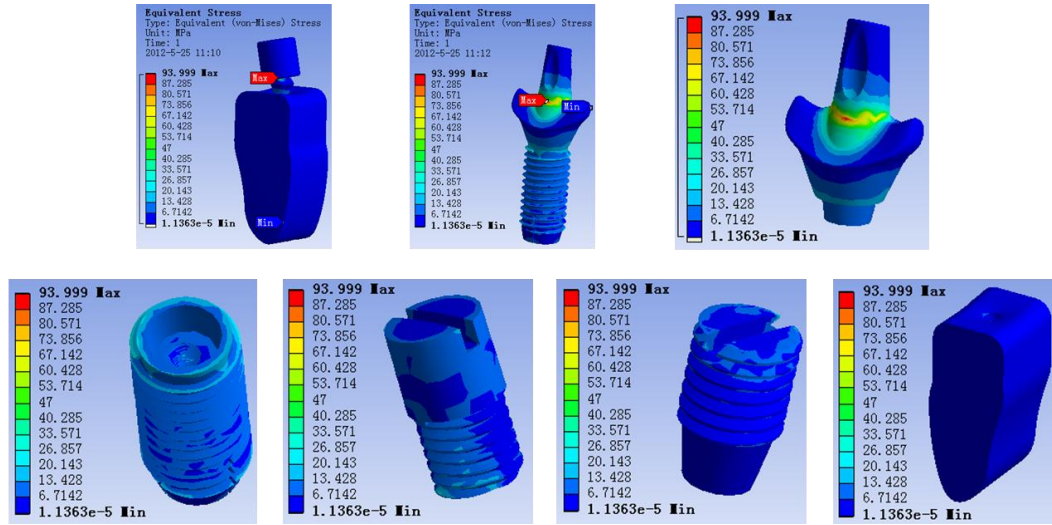


Fig. 5-13: $\theta = 0$, Max. Equivalent Stress = 93.999MPa

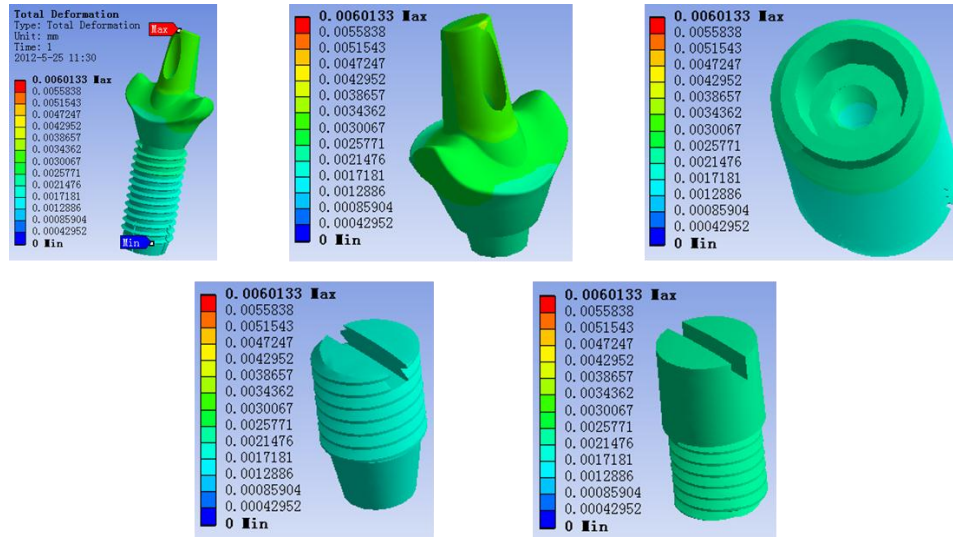


Fig. 5-14: $\theta = 0$, Max. Total Deformation = 0.0060133mm

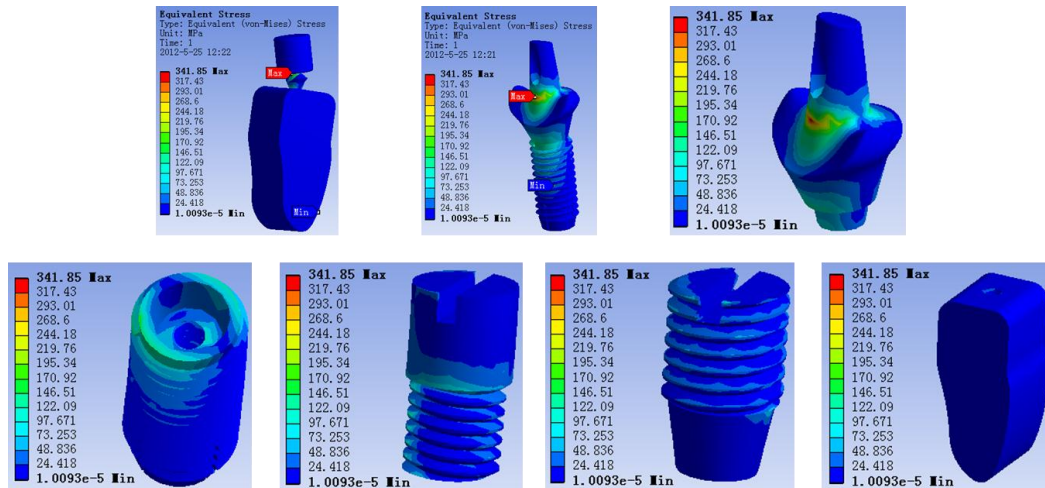


Fig. 5-15: $\theta = 15^\circ$, Max. Equivalent Stress = 341.85MPa

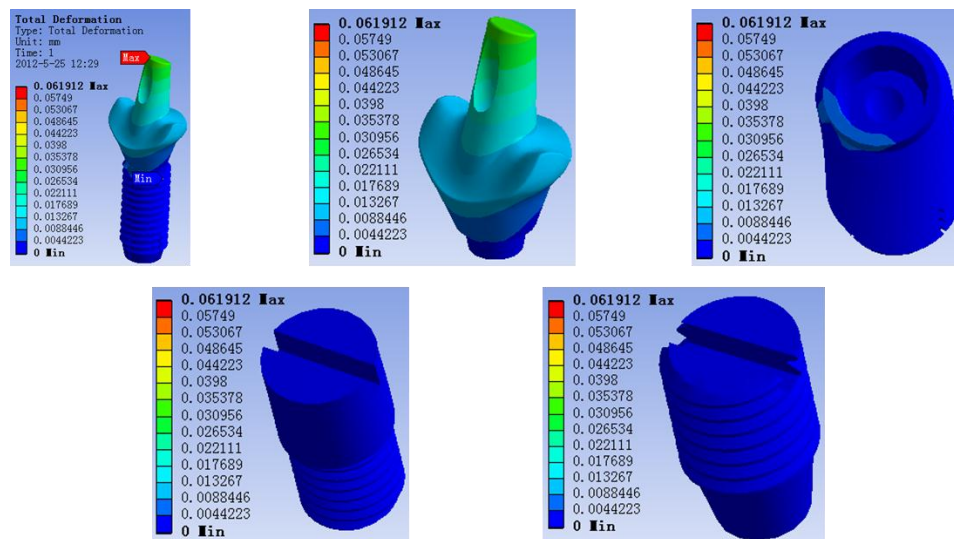


Fig. 5-16: $\theta = 15^\circ$, Max. Total Deformation = 0.061912mm

So, the result shows that: a) the Max. Equivalent Stress is 93.999MPa and 341.85MPa respectively. These stresses are less than material Yield strength. b) the Max. Total Deformation are so small, there are 0.0060133mm and 0.061912mm respectively. So, this custom-made implant meets the strength requirements of dental implant and has moderate pressure in patient's alveolar bone, which will shorten the bone integration time.

5.4 Cutting test

And then, dentist can use this FEA result and RP prototype (shown in Figure 5-17) to check and modify the design. Finally, the automatic programming is used by our machining center for machining this custom-made dental implant, as shown in Figure 5-18. Figure 5-19 shows samples machined by Selected Laser Machine (SLM) [127] (non surface treatment).



Fig. 5-17: The RP prototype



Fig. 5-18: Machined sample by using our machining center



Fig. 5-19: Machined sample by SLM

From Figure 5-18 and Figure 5-19, we can know that the profile of parts machined by our machining center is better than SLM. Especially, the surface and the thread of screw are smoother.

Table 5-3 shows the measurement results of our machining dental implant. From this table, we can find the maximum STD is only 0.002983 mm.

Table 5-3: The measurement results of our machining dental implant
(Material: pure titanium, Machining time: 16 minutes/piece, in mm)

	A	B	C	D	E
Nominal value	Φ2.500	Φ 5.500	4.000	7.000	11.000
Tolerance	+0.005	+0.005	+0.005	+0.005	+0.010
	-0.005	-0.005	-0.005	-0.005	-0.010
1	2.498	5.495	4.001	7.002	11.002
2	2.496	5.497	4.002	7.003	11.001
3	2.499	5.500	3.998	7.001	11.004
4	2.501	5.496	3.998	7.002	10.998
5	2.498	5.502	4.004	6.998	10.997
6	2.503	5.502	4.002	6.999	10.996
7	2.497	5.501	4.000	6.997	10.997

8	2.498	5.499	3.997	7.003	11.003
9	2.501	5.504	3.998	7.001	11.002
10	2.498	5.502	4.001	6.999	10.997
Max	2.503	5.504	4.004	7.003	11.004
Min	2.496	5.495	3.997	6.997	10.996
Mean	2.4989	5.4998	4.0001	7.0005	10.9997
STD	0.002132	0.002974	0.002283	0.002121	0.002983

5.5 Summary

Comparing to the existing technologies, the new method has a number of advantages:

- a) Custom-made implant is best fit possible, especially for incisors;
- b) Custom-made implant is best beautiful and decreased unnecessary bone loss;
- c) The database of dental implant is simple and easy to use for dentist diagnosis;
- d) The machining center has capability of machining dental implant, due to its multi-functions and its high accuracy;
- e) The efficiency of machining dental implant by our machine is high, due to the multi- function and automatic programming.
- f) Set automatic 3-D computer graphics, FEA, rapid prototyping and precision machining as a whole, which will improve production efficiency and reduce the costs

With these advantages, it is expected that the new method will have a significant impact to biomechanics and manufacturing industry for years to come.

The method provides a chance for further research activities in the field of dental implant.

Chapter 6:

Concluding Remarks and Future Work

6.1 Concluding Remarks

This thesis is devoted to design, build and use a Multi-Axes CNC Turn-Mill-Hob Machining Center, including mechanical design, control system design, choices of components, prototype building, machine calibration, performance testing, and applications. Following is the summary.

- **Building a Multi-Axes CNC Turn-Mill-Hob Machining Center:** As the demand for miniature components becomes higher as a consequence of the emerging trend of product miniaturization, the ability to manufacture these components accurately, swiftly and cost effectively becomes inevitable. In this thesis, our machine developed by our institute is introduced. The machine has 8 axes, which can achieve turning, milling, grinding, hobbing and so on. With a flexible tool spindle and multiple cutting tools, the machine is able to machine parts with complex features such as gear profile and non-circular section in one single setup. Then, the machine uses the electronic gearing method for gear hobbing control; this gives not only higher accuracy but also ease of use. Finally, the machine uses advanced motion control technology for multi-axes synchronized motion; this ensures the accuracy.

Based on experiments, the performance of the machine is found that: the machining error is $\pm 3 \mu\text{m}$ in turning, $\pm 7 \mu\text{m}$ in milling, and the maximum profile error is less than $\pm 7.5 \mu\text{m}$ in gear hobbing with excellent surface finish. The accurate is almost as the same as the precision machines in the market, but our machine is only cost \$350,000 HK dollar. It is seen that our machine is very competitive.

- **Developing a new for hobbing axial asymmetric parts:** Based on the computer modelling and experiment testing, following conclusions can be drawn:

- (a) By controlling the helix angle, λ , the synchronization ratio, γ , and the center distance, a , it is possible to hob many axial symmetric / asymmetric parts.
- (b) The presented method is efficient. In some cases, the Material Removal Rate (MRR) could be many times higher than the conventional method.
- (c) Our Multi-Axes CNC Turn-Mill-Hob Machining Center is capable for hobbing complex precision parts.
- (d) Not all the parts can be machined in this presented method.

Comparing to the existing technologies, the presented method has a number of advantages, including:

- It is simple and efficient, since it needs only one setup and just a few tools;
- It is reliable, since the multi-teeth hob is strong against tool breakage;
- It is precise, since the multi-teeth hob tool cuts only a small chip at a time and hence, will not induce excessive vibration and chatter;
- It is inexpensive, since it does not require complex tools and fixtures.

With these advantages, it is expected that the new method will find many applications in the near future.

- **Developing a new CNC module based on polar coordinate interpolation:** The basic interpolation principles of polar coordinate are investigated. Based on interpolation principles, a polar coordinate programming module is developed. The module can be activated using two special G codes and is tested in our Multi-Axes CNC Turn-Mill-Hob Machining Center.

Comparing to the commercial programming methods, the module is more accurate and easier to use.

- **Machining custom-made dental implants:** Comparing to the existing technologies, the new method has a number of advantages:
 - (a) Custom-made implant is best fit possible, especially for incisors;

- (b) Custom-made implant is best beautiful and decreased unnecessary bone loss;
- (c) The database of dental implant is simple and easy to use for dentist diagnosis;
- (d) The machining center has capability of machining dental implant, due to its multi-functions and its high accuracy;
- (e) The efficiency of machining dental implant by our machine is high, due to the multi- function and automatic programming.
- (f) Set automatic 3-D computer graphics, FEA, rapid prototyping and precision machining as a whole, which will improve production efficiency and reduce the costs

With these advantages, it is expected that the new method will have a significant impact to biomechanics and manufacturing industry for years to come.

6.2 Future Work

It believed that our machining center and new machining method will find many practical applications in the near future. Though, it should be pointed out that the new system is still in its infancy and further research and development are needed. The future research includes:

- **Multi-Axes CNC Turn-Mill-Hob Machining Center:** The machine provides an experimental platform for further research activities in the field of machining of miniature components with complicated features. Other research activities we are conducting are: simulation of process defects in machining complex parts, friction control. At the time where this thesis is written, a new and product-quality Multi-Axes machining center is actually being designed and manufactured, as shown in Figure 6-1.

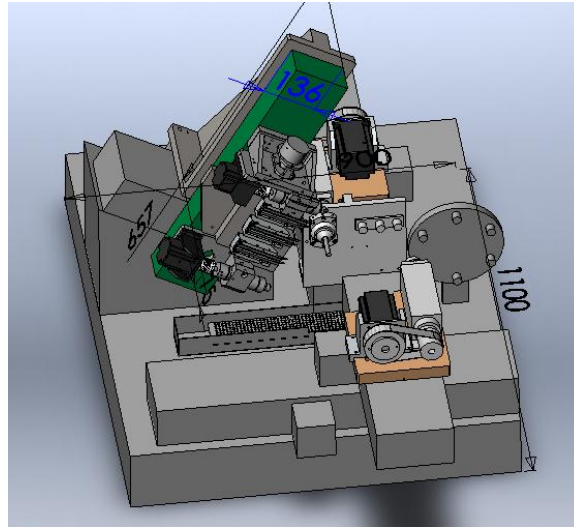


Fig. 6-1: The CAD drawing of the new machining center

In this new design, we improve: a) Under assurance functions, the structure is more compact and the volume is smaller; b) Increase a servo motor into auxiliary axis θ to achieve time varying of helix angle; c) Increase a new axis (sub-spindle) for back machining of parts, as shown in Figure 6-2.

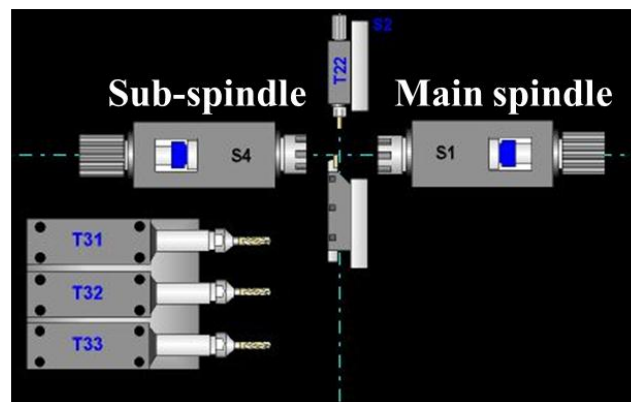


Fig. 6-2: The design of main spindle and sub-spindle

- **Hobbing axial asymmetric parts:** The presented study is however just the beginning, as many issues are yet to be investigated. In fact, the examples presented above are the “forward” problems: given the hob and the control parameter to find the shape of the part. In practice, the “backward” problem is much more important, in which the final shape of the part is given and the objective is to find the hob and

the control parameters. In addition, in the examples presented above, the three control parameters are all set as constants. In practice, they could be time varying resulting many complex shapes

- **Study on the application in Biomedical Engineering:** Improved the design of our custom-made dental implant and make more biomedical samples by using our machining center. The detail comparison of our machined biomedical parts and the product in market.

Bibliography

- [1] Okazaki Y. and Kitahara T., “NC Micro-lathe to Machine Micro-parts.” *Proceedings of ASPE’s 15th Annual Meeting*, v22 (2000), pp.575-578.
- [2] <http://unit.aist.go.jp/amri/group/finemfg/English/research/micro-lathe-e2.htm>
- [3] Lu Z., Yoneyama T.. “Micro cutting in the micro lathe turning system.” *International Journal of Machine Tools and Manufacture*, v39 (1999), pp. 1171-1183.
- [4] Ito S., Iijima D., Hayashi A., Aoyama H., Yamanaka M.. “Micro Turning System: A Super Small CNC Precision Lathe for Microfactories.” *Proceedings of ASPE’s 16 Annual Meeting*, v27 (2002), pp. 295-298.
- [5] Loffler F.. “Design of a Small Precision Lathe.” *Proceedings of the EUSPEN International Topical Conference*, Aachen, Germany, May 19th-20th, 2003, pp. 81-84.
- [6] Bae Y.H., Ko J.K., Chung B.M., Kim H.S.. “Micro Machining with Micro Turning Lathe.” *Proceedings of ASPE’s 16th Annual Meeting*, 2001, pp.157-160.
- [7] Kussul E., Baidyk T., Ruiz-Huerta L., Caballero-Ruiz A., Velasco G. and Kasatkina L. “Development of micromachine tool prototypes for microfactories.” *Journal of Micromechanics and Microengineering*, 2002, pp. 795-812.
- [8] Kussul E., Baidyk T., Ruiz-Huerta L., Caballero-Ruiz A. and Velasco G. “Development of Low-Cost Microequipment.” *Proceedings of International Symposium on Micromechatronics and Human Science*, 2002, pp. 125-134.
- [9] Campus Santiago. “Machinability study on precision turning of PA66 polyamide with and without glass fiber reinforcing”, *Materials & Design*, 2009.
- [10] Yuichi Okazaki, Yuichi Okazaki, Noboru Morita. “Desk-Top NC Milling Machine with 200 krpm Spindle”, *Proc. ASPE Annual Meeting*, 2001.
- [11] Vogler M., Liu X., Kapoor S., DeVor R. and Ehman K.. “Development of Meso-scale machine tool (mMT) systems.” *Transaction of NAMRI/SME*, v30 (2002), pp. 653-661.
- [12] Kurita T., Watanabe S., Hattori M.. “Development of hybrid micro machine tool.”

- Proceedings EcoDesign 2001: Second International Symposium on Environmentally Conscious Design and Inverse Manufacturing*, 2001, pp. 797-802.
- [13] Takeuchi Y., Sakaida Y., Sawada K. and Sata T., “Development of a 5-Axis Control Ultraprecision Milling Machine for Micromachining Based on Non-Friction Servomechanisms.” *Annals of the CIRP*, v49 (2000), pp.295-298.
- [14] Takeuchi Y., Sawada K. and Sata T.. “Computer Aided Ultra-Precision Micro-Machining.” *Proceedings of IEEE Conference on Robotics and Automation*, 1995, pp. 67-72.
- [15] D.A. Axinte, S. A. Shukor, A. T. Bozdana, “An Analysis of the Functional Capability of an In-House Developed Miniature 4-Axis Machine Tool”, *Int. J. of Machine Tools and Manufacture*, Vol. 50, pp. 191-203, 2010.
- [16] Okazaki Y., Mishima N. and Ashida K.. “Microfactory – Concept, History, and Developments.” *Journal of Manufacturing Science and Engineering*, v126 (2004), pp.837-844.
- [17] Tanaka M. “Development of desktop machining microfactory.” *RIKEN Review, Advances on Micro-mechanical Fabrication Techniques*, v34 (2001), pp. 46-49.
- [18] Mishima N., Tanikawa T., Ashida K. and Maekawa H.. “Design of a Microfactory.” *Proceedings of DETC’ 02*, 2002, pp. 103-110.
- [19] Tanikawa T. and Arai Tatsuo. “Development of a Micro-Manipulation System Having a Two-Fingered Micro-Hand.” *IEEE Transactions on Robotics and Automation*, v15 (1), 1999, pp. 152-162.
- [20] Maekawa H. and Komoriya K.. “Development of a Micro Transfer Arm for a Microfactory.” *Proceedings of IEEE International Conference on Robotics and Automation*, 2001, pp. 1444-1451.
- [21] Ehman K., DeVor R. and Kapoor S.. “Micro/Meso-scale Mechanical Manufacturing – Opportunities and Challenges.” *Proceedings of JSME/ASME International Conference on Materials and Processing*, 2002, pp.6-13.
- [22] Subrahmanian R. and Ehman K.. “Development of a Meso-scale machine tool (MMT) for Micro-machining.” *Proceedings of the 2002 Japan-USA Symposium on Flexible Automation Hiroshima*, Japan (2002).
- [23] Ishikawa Y. and Kitahara T., “Present and Future of Micromechatronics.”

Proceedings of International Symposium on Micromechatronics and Human Science, 1997, pp. 13-20.

- [24] Masuzawa, “State of the Art of Micromachining.” *Annals of the CIRP*, v49 (2), 2000, pp.473-488.
- [25] <http://www.koepfer.com/>
- [26] www.tornos.com/prd-e.html
- [27] <http://www.mazak.com>
- [28] www.liebherr.com
- [29] www.strasuak-mikro.ch
- [30] www.adlee.com
- [31] www.mini-lathe.com
- [32] Claudin and J. Rech, “Development of a new rapid characterization method of hob’s wear resistance in gear manufacturing: Application to the evaluation of various cutting edge preparations in high speed dry gear hobbing”. *Journal of Materials Processing Technology*, 2009 (209): 5152–5160.
- [33] Hua Qiu, Kai Chengt and Yan Li, “Optimal circular arc interpolation for NC tool path generation in curve contour manufacturing”, *Computer-Aided Design*, Vol. 29, No. 11, 1997, pp. 751-760.
- [34] Min-Yang Yang, Won-Pyo Hong. “A PC–NC milling machine with new simultaneous 3-axis control algorithm”, *International Journal of Machine Tools & Manufacture*, 41 (2001),2001, pp. 555–566
- [35] Xingui Guo, Yadong Liu, Daoshan Du, Kazuo Yamazaki, Makoto Fujishima. “A universal NC program processor design and prototype implementation for CNC systems”, *Int. J. of Advance Manufacturing Technology*, Published on line 27 September, 2011.
- [36] Young Joon Ahn, Christoph Hoffmann, Yeon Soo Kim. “Curvature continuous offset approximation based on circle approximation using quadratic Bézier biarcs”, *Computer-Aided Design*, 43 (2011), 2011, pp. 1011–1017.
- [37] M. C. Shaw, “Metal Cutting Principle, Oxford Series on Advanced Manufacturing”, in London, England, 2004.
- [38] J. Tlustý, S. Smith, and C. Zamudio, “New NC Routines for Quality in Milling”,

- CIRP Annals – Manufacturing Technology*, Vol. 39, Issue 1, Pages 517-521, 1990.
- [39] D. Dragomatz, and S. Mann, “A Classified Bibliography of Literature on NC Milling Path Generation”, *Computer-Aided Design*, Vol. 29, No.3, pp. 239–247, 1997.
- [40] N. Mishima, T. Tanikawa, K. Ashida, et al. “Design of a Microfactory”. *Proceedings of DETC’02 ASME 2002 Design Engineering Technical Conferences*, pp. 103~110, Sept. 29-Oct. 2, 2002, Montreal, Canada.
- [41] Jean-Marc Breguet, Carl Schmitt, Reymond Clavel. “Micro / Nanofactory: Concept and State of the Art”. *Proc. of SPIE. 2000*, pp. 4194:1~11,.
- [42] I. Verettas, R. Clavel. A. Codourey. “Microfactory: Desktop Cleanrooms for the Production of Microsystems”. *Proc. of the 5th IEEE International Symposium on Assembly and Task Planning*, pp. 18~23, July 10-11, 2003, Besancon, France.
- [43] K. Dutta, P. Dev, P. Dewilde, and et al. “Integrated Micromoter Concepts”, *Proceedings of ICMCST*, pp. 36~37, Aug. 18~21, 1970.
- [44] T. Kitahare, Y. Ishikawa, T. Terada, and et al. “Development of Micro-lathe”, *Journal of Mechanical Engineering Laboratory*, Vol. 50, No. 5, pp. 117~123, 1996.
- [45] Y. Okazaki, and T. Kitahara “NC Micro-lathe to Machine Micro-parts.” *Proceedings of ASPE’s 15th Annual Meeting*, Vol. 22, pp.575-578, 2000, Scottsdale, America.
- [46] Z. Lu and T. Yoneyama, “Micro Cutting in the Micro Lathe Turning System.” *Int. J. of Machine Tools and Manufacture*, Vol. 39, pp. 1171-1183, 1999.
- [47] Yazhou Sun, Yingchun Liang and Ruxu Du, “Experimental Study of Surface Roughness in a Micro-milling Process,” *Proceedings of the 6th WSEAS International Conference on Robotics, Control and Manufacturing Technology*, pp. 30-35, April 16-18, 2006, Hangzhou, China.
- [48] J. P. Davim, L. R. Silva, A. Festas, and A. M. Abrão, “Machinability Study on Precision Turning of PA66 Polyamide With and Without Glass Fiber Reinforcing”, *J. of Materials and Design*, Vol. 30, pp. 228-234, 2009.
- [49] J. S. Mecombera, D. Hurdb and P. A. Limbacha, “Enhanced Machining of Micron-Scale Features in Microchip Molding Masters by CNC Milling”, *Int. J. of*

Machine Tools and Manufacture, Vol. 45, Issues 12-13, pp. 1542-1550, 2005.

- [50] www.applitec.com
- [51] P. H. Daryani. *The Art of Gear Fabrication*, Industrial Press, Inc., in New York, 2002.
- [52] C. Claudin, and J. Rech, “Development of a new rapid characterization method of hob’s wear resistance in gear manufacturing: Application to the evaluation of various cutting edge preparations in high speed dry gear hobbing”. *Journal of Materials Processing Technology*, 2009 (209): 5152–5160
- [53] www.dimetal.com
- [54] <http://www.advantech.com/>
- [55] www.googoltech.com
- [56] www.mitsubishi-automation.com/products/servomotion_mr_j3_html
- [57] Bleuter H., Clavel R., Breguet J.M., Langen H. and Pernette E.. “Issues in Precision Motion Control and Microhandling.” *Proceedings of IEEE International Conference on Robotics and Automation*, 2000, pp. 959-964
- [58] W. Y. Chan, W. J. Xu and R. Du, “A Study on Cycloidal Gears,” *Proceeding of CAD’07*, June 25-29, 2007. Honolulu, Hawaii, USA.
- [59] Chen C.L., Jang M.J. and Lin K.C.. “Modelling and high-precision control of a ball-screw-driven stage.” *Precision Engineering*, v28, 2004, pp. 483-495.
- [60] W. J. Xu, Daton Qin, Y. Fu and R. Du, “A New Approach for Reducing the Cycloid Gear’s Sensitivity to Misalignment Errors in Precision Transmission,” *Proceedings of MNC2007, MicroNanoChina07*, Jan. 10-12, 2007, Sanya, Hainan, China.
- [61] www.renishaw.com
- [62] F. L. Litvin, and A. Fuentes: *Gear Geometry and Applied Theory*, 2nd ed. in New York, Cambridge University Press, 2004.
- [63] Feng Xianying, Wang Aiqun, and Linda Lee, “Mathematical Description of Spatial Hob-Generating Motion for an Arbitrary Gear Tooth Profile”, *Materials Science Forum*, Vol. 471. pp. 409-413 3, 2004.
- [64] MITUTOYO QV Apex 302 CNC Vision Measuring System
- [65] George T.-C. Chiu, Jaydev P. Desai, Jason Gu, Guillaume Morel, “Inreoduction to

The Focused Section on Healthcare Mechatronics”, *IEEE/ASME Transactions on Mechatronics*, Vol.1, No.2, April. 2010.

- [66] Iwasaki M., Takei H. and Matsui N., “GMDH-Based Modeling and Feedforward Compensation for Nonlinear Friction in Table Drive Systems.” *IEEE Transactions on Industrial Electronics*, Vol.50 (6), 2003, pp. 1172-1178.
- [67] J. Tlustý, S. Smith, and C. Zamudio, “New NC Routines for Quality in Milling”, *CIRP Annals – Manufacturing Technology*, Vol. 39, Issue 1, Pages 517-521, 1990.
- [68] D. Dragomatz, and S. Mann, “A Classified Bibliography of Literature on NC Milling Path Generation”, *Computer-Aided Design*, Vol. 29, No.3, pp. 239–247, 1997.
- [69] P. H. Daryani: *The Art of Gear Fabrication*, Industrial Press, Inc., New York, 2002.
- [70] K. Yanagimoto, T. Otsubo, K. Nakayama, K. Sakai, “Method of Manufacturing Asymmetric Gear, Non-circular and Asymmetric gear, Gear mechanism, and Barrel Finishing Machine,” *US Patent 6991522*, 2006.
- [71] A. Ishibashi and H. Yoshino, “Design and Manufacture of Gear Cutting Teeth and Gears with an Arbitrary Profile,” *J. of JSME*, Series 3, Vol. 30, pp. 265, 1987.
- [72] K. D. Bouzakis, S. Kombogiannis, A. Antoniadis and N. Vidakis, “Gear Hobbing Cutting Process Simulation and Tool Wear Prediction Models,” *Trans. of ASME, J. of Manufacturing Science and Engineering*, Vol. 124, pp.42-51, 2002.
- [73] S. Uematsu, “Effect of Variation of Angular Velocity in Gear Rolling Process on Profile Error,” *J. of the International Societies for Precision Engineering and Nanotechnology*, Vol. 26, pp. 425-429, 2002.
- [74] N. S. Chan, “Millimeter-scale Turning Centre: Theory and Implementation,” *Master Thesis*, The Chinese University of Hong Kong, 2007.
- [75] Xianying Feng, Aiqun Wang, and Linda Lee, “Mathematical Description of Spatial Hob-Generating Motion for an Arbitrary Gear Tooth Profile”, *Materials Science Forum*, Vol. 471. pp. 409-413 3, 2004.
- [76] W. Y. Chan, W. J. Xu and R. Du, “A Study on Cycloidal Gears,” *Proceeding of CAD’07*, June 25-29, 2007. Honolulu, Hawaii, USA.
- [77] W. J. Xu, Daton Qin, Y. Fu and R. Du, “A New Approach for Reducing the Cycloid Gear’s Sensitivity to Misalignment Errors in Precision Transmission,”

Proceedings of MNC2007, MicroNanoChina07, Jan. 10-12, 2007, Sanya, Hainan, China.

- [78] R.K. Jing, S.W. Wang, X.Y. Yu, “Involute Cylinder Gear Modeling Based on Pro/E,” *Modern Manufacturing Engineering*, (11)43-45, 2004.
- [79] F. L. Litvin, and A. Fuentes: *Gear Geometry and Applied Theory*, 2nd ed. New York: Cambridge University Press, 2004.
- [80] Chan W.Y., Xu W.J. and Du R., “A Study on Cycloidal Gears,” *accepted for publication in CAD’07*, June 25-29, 2007. Honolulu, Hawaii, USA.
- [81] 景仁坤，王三武，余旭阳。基于Pro/E的渐开线圆柱齿轮建模。《*现代制造工程*》，2004（11）：43-45。
- [82] 张志森，李世国，张裕中。基于Solid Edge的渐开线斜齿轮三维造型技术研究。《*机械设计与研究*》。2002，18（3）：22-23。
- [83] 马秋成，罗益宁，等。基于UG的齿轮三维建模和消除齿轮投影的方法。《*机械设计与研究*》。2001，3（1）：27-28。
- [84] 徐武彬，高中庸。采用模拟切削法绘制精确的齿轮轮廓线。《*机械工程师*》，2001（5）：20-22。
- [85] Seon-Hong Kim and Young Joon Ahn. “An approximation of circular arcs by quartic B’ezier curves”, *Computer-Aided Design*, 39 (2007) 490–493.
- [86] Meng-Shiun Tsai, Hao-Wei Nien and Hong-Tzong Yau. “Development of a real-time look-ahead interpolation methodology with spline-fitting technique for high-speed machining”, *The International Journal of Advanced Manufacturing Technology*, (2010) 47:621–638
- [87] Hua Qiu, Kai Cheng, Yanbin Li, Yan Li and Jian Wang. “An approach to form deviation evaluation for CMM measurement of 2D curve contours, International”, *Journal of Machine Tools & Manufacture*, vol.41, pp.119-126, 2000
- [88] Ming-Jun Lai. “The convergence of three L1 spline methods for scattered data interpolation and fitting”, *Journal of Approximation Theory*, 145 (2007) 196 – 211
- [89] Young Joon Ahn, Christoph Hoffmann, Yeon Soo Kim. “Curvature continuous offset approximation based on circle approximation using quadratic Bézier biarcs”,

Computer-Aided Design , 43 (2011) 1011–1017

- [90] <http://www.fanuc.co.jp/eindex.htm>
- [91] Hua Qiu, Kai Cheng, Yan Li, “Optimal circular arc interpolation for NC tool path generation in curve contour manufacturing”, *Computer-Aided Design*, vol.29, pp 751-760 ,1997
- [92] Satoshi Maeda, Koichi Ohno. “A new method for constructing multidimensional potential energy surfaces by a polar coordinate interpolation technique”, *Chemical Physics Letters* , 381 (2003) 177–186
- [93] Tony Heap and David Hogg. “Extending the Point Distribution Model using polar coordinates”, *Image and Vision Computing* , 14 (1996) 589-599
- [94] Bugra Kilic, Juan A. Aguirre-Cruz, Shivakumar Raman. “Inspection of the cylindrical surface feature after turning using coordinate metrology”, *International Journal of Machine Tools & Manufacture* , 47 (2007) 1893–1903
- [95] <http://www.mastercam.com.cn>
- [96] <http://www.solidworks.com/>
- [97] Jae-Hoon Lee, Val Frias, Keun-Woo Lee, and Robert F.Wright, “Effect of Implant Size and Shape on Implant Success Rates: A Literature Review.”, *The journal of prosthetic dentistry*, 4(4) 2004 377-381.
- [98] Binon PP, “Implants and Components: Entering the New Millennium”, *Int Journal of Oral Maxillofac Implants*, 15(2000) 76-94.
- [99] ZHOU Lei, “Progress of Dental Implantology”, *West China Journal of Stomatology*, 27(1) (2009) 8-12.
- [100] Eckert SE, Koka S, Wplfinger G, Choi YG, “Survey of Implant Experience by Prosthodontists in the United States”, *J of Prosher Dent*, 11 (2002) 194-201.
- [101] Friberg B, Raghoobar GM, Grunert I, Hobkirk JA, Tepper G. “A 5-Year Prospective Multicenter Study on 1-Stage Smooth-Surface Bra°Nemark System Implants with Early Loading in Edentulous Mandibles”, *Int J Oral Maxillofac Implants*, 2008: 23: 481–486.
- [102] Turkyilmaz I. “Influence of Bone Density on Implant Stability Parameters and Implant Success: A Retrospective Clinical Study”, *BMC Oral Health* , 2008: 8: 32.
- [103] Branemark PI, Adell R, Breine U, Hansson BO, Lindstrom J, Ohlsson A. “Intra-

- Osseous Anchorage of Dental Prostheses. I. Experimental studies”, *Scand J Plast Reconstr Surg* , 1969;3:81-100.
- [104] Adell R, Hansson BO, Branemark PI, Breine U. “Intra-Osseous Anchorage of Dental Prostheses. II. Review of Clinical Approaches”, *Scand J Plast Reconstr Surg* , 1970;4:19-34.
- [105] Misch CE. Contemporary Implant Dentistry. 2nd ed. St. Louis: Elsevier;1999. p. 54.
- [106] Brogini N, Mcmanus LM, Hermann JS, et al. “Persistent Acute Inflammation”, *The Implant-Abutment Interface [J]*, *J Dent Res*, 82(3) (2003) 232-237.
- [107] CT scan figure, Guanghua School of Stomatology, Sun Yat-sen University, Guangzhou, China.
- [108] Martinez H, Davarpanah M, Missika P, Celletti R, Lazzara R. “Optimal Implant Stabilization in Low Density Bone”, *Clin Oral Implants Res*, 2001: 12: 423–432.
- [109] Miyamoto I, Tsuboi Y, Wada E, Suwa H, Iizuka T. “Influence of Cortical Bone Thickness and Implant Length on Implant Stability at the Time of Surgery–Clinical, Prospective”, *Biomechanical, and Imaging Study*, *Bone* 2005: 37:776–780.
- [110] Dilek O, Tezulas E, Dincel M. Required “Minimum Primary Stability and Torque Values for Immediate Loading of Mini Dental Implants: An Experimental Study in Nonviable Bovine Femoral Bone”. *Oral Surg Oral Med Oral Pathol Oral Radiol Endod* , 2008: 105: e20–e27.
- [111] Kong L, Sun Y, Hu K, Li D, Hou R, Yang J, Liu B. Bivariate “Evaluation of Cylinder Implant Diameter and Length: A Three-Dimensional Finite Element Analysis”, *J Prosthodont* 2008: 17: 286–293.
- [112] Ochi S, Morris HF, Winkler S. “The Influence of Implant Type, Material, Coating, Diameter, and Length on Periotest Values at Second-Stage Surgery: DICRG Interim Report No. 4. Dental Implant Clinical Research Group”, *Implant Dent*, 1994: 3: 159–162.
- [113] [Esposito M, Hirsch JM, Lekholm U, Thomsen P. “Biological Factors Contributing to Failures Of Osseointegrated Oral Implants (I): Success Criteria and Epidemiology”, *European Journal of Oral Sciences*, 1998;106(1):527–51.

- [114] Marco F, Milena F, Gianluca G, Vittoria O. “Peri-Implant Osteogenesis in Health and Osteoporosis”, *Micron*, 2005;36(7–8):630–44.
- [115] Jianhua Ao, Tao Li, Yanou Liu, Yin Ding, Guofeng Wu, Kaijin Hu, Liang Kong. “Optimal Design of Thread Height and Width on An Immediately Loaded Cylinder Implant: A Finite Element Analysis”, *Computers in Biology and Medicine*, 40(2010):681-686.
- [116] Y.B. An, N.H. Oh, Y.W. Chun, Y.H. Kim, D.K. Kim, J.S. Park, “Mechanical Properties of Environmental-Electro-Discharge-Sintered Porous Ti Implants”, *Materials Letters*, 59 (2005) :2178– 2182.
- [117] M.C. Shaw, *Metal Cutting Principle*, Oxford Series on Advanced Manufacturing, London, England (2004).
- [118] Yazhou Sun, Yingchun Liang and Ruxu Du, “Experimental Study of Surface Roughness in a Micro-milling Process” Proceedings of the 6th WSEAS International Conference on Robotics, *Control and Manufacturing Technology*, Hangzhou, China (2006) 30-35.
- [119] Ivanoff CJ, Sennerby L, Johansson C, Rangert B, Lekholm U. “Influence of Implant Diameters on The Integration of Screw Implants. An Experimental Study in Rabbits”, *Int J Oral Maxillofac Surg*, 1997;26:141-8.
- [120] Holmgren EP, Seckinger RJ, Kilgren LM, Mante F. “Evaluating Parameters of Osseointegrated Dental Implants using Finite Element Analysis—A Two-dimensional Comparative Study Examining The Effects of Implant Diameter, Implant Shape, and Load Direction”, *J Oral Implantol*, 1998;24:80-8.
- [121] www.ipe.cuhk.edu.hk
- [122] Hansson S, Werke M. “The Implant Thread as A Retention Element in Cortical Bone: The Effect of Thread Size and Thread Profile: A Finite Element Study”, *J Biomech* 2003; 36:1247-58.
- [123] Lin S, Shi S, LeGeros RZ, LeGeros JP. “Three-Dimensional Finite Element Analyses of Four Designs of A High-Strength Silicon Nitride Implant”, *Implant Dent*, 2000; 9:53-60.
- [124] Chen C.L., Jang M.J. and Lin K.C. “Modelling and High-Precision Control of A Ball-Screw-Driven Stage”, *Precision Engineering*, 28 (2004) 483-495.

- [125] Iwasaki M., Takei H. and Matsui N.. “GMDH-Based Modeling and Feedforward Compensation for Nonlinear Friction in Table Drive Systems” *IEEE Transactions on Industrial Electronics*, Vol.50(6), 2003, pp. 1172-1178
- [126] Bleuter H., Clavel R., Breguet J.M., Langen H. and Pernette E.. “Issues in Precision Motion Control and Microhandling” *Proceedings of IEEE International Conference on Robotics and Automation*, 2000, pp. 959-964
- [127] www.slm-solutions.com

Publication Record

- [1] Xianshuai Chen, Longhan Xie, Jianyu Chen, R. Du and Feilong Deng, “Design and Fabrication of Custom-made Dental Implants”, *Journal of Mechanical Science and Technology*, 26 (7) (2012) 1~6.
- [2] Xianshuai Chen, Dailin Zhang, Songmei Yuan, and Ruxu Du, “A Precision CNC Turn-Mill Machining Center with Gear Hobbing Capability”, Submitted to *Precision Engineering*, 2012.
- [3] Dailin Zhang, Xianshuai Chen (correspond author) and Ruxu Du. “A CNC Program Module Based on Polar Coordinate System” Submitted to *Computer-Aided Design*.
- [4] Xianshuai Chen, Longhan Xie, Jianyu Chen, R. Du and Feilong Deng, “Design and Fabrication of Custom-made Dental Implants”, *Proceedings of Intl. Conf. on Materials and Reliability 2011*, Busan, Korea, Nov. 20-22, 2011.
- [5] Xianshuai Chen and R. Du, “A Precision CNC Turn-Mill Machining Center with Gear Hobbing Capability” *Proceedings of IRGTM Summer School 2011*, German, 2011.
- [6] Xianshuai Chen and R. Du, “A New Method for Machining Axial Symmetric/Asymmetric Parts with Experiment Validation”, *Proceedings of International Forum on Micro Manufacturing 2010*, 2010.
- [7] Xianshuai Chen and R. Du, “A New Method for Machining Axial Symmetric/Asymmetric Parts”, *Proceedings of The 8th Cross-strait Advanced Manufacturing Technologies Workshop*, 2010.
- [8] Xianshuai Chen, Chan N.S and R. Du, “A New Theory for CNC Micro Hobbing”, published by *Watch and Clock (The core Journal of China)*, the second phase, 2010.
- [9] Gong Zhang, Zhangong Xie, Xianshuai Chen (correspond author) and Xuefeng Zhou, “Permanent Magnets Design and Magnetic Field Analysis of a Novel Permanent Magnet Linear Motor”, *Proceedings of 2012 International Conference on Advance Materials Design and Mechanics (ICAMDM 2012)*, 2012.